Aus dem

Lübecker Institut für Ernährungsmedizin

Direktor: Prof. Dr. Christian Sina

INHIBITING DNA SENSING PATHWAY TO CONTROL STEROID RESISTANT LUNG INFLAMMATION

Inauguraldissertation

Zum Erwerb des Doktorgrades

der Universität zu Lübeck

-Aus der Sektion Medizin-

vorgelegt von

Bushra Ahmed Mdkhana

aus Ländliches Damaskus, Syrien

Lübeck 2023

1. Berichterstatterin/Berichterstatter: PD Dr. rer. nat. Yves Laumonnier

2. Berichterstatterin/Berichterstatter: Prof. Dr. med. Saleh Ibrahim

Tag der mündlichen Prüfung: 06.07.2023

Zum Druck genehmigt. Lübeck, den 13.06.2023

-Promotionskommission der Sektion Medizin-

Table of Contents

LIST OF ABBREVIATIONS

AHR	Airway hyperresponsiveness
cdiGMP	cyclic-di-guanosine monophosphate (cyclic-di-GMP)
cGAMP	2′,3′-cyclic guanosine monophosphate–adenosine monophosphate (2′,3′-cyclic GMP-AMP)
cGAS	cyclic guanosine monophosphate–adenosine monophosphate (GMP-AMP) synthase
AMs	Alveolar macrophages
CRDs	Chronic respiratory diseases
GINA	Global Initiative for Asthma
COPD	Chronic obstructive pulmonary disease
Dex	Dexamethasone
DLS	Dynamic Light Scattering
dsDNA	Double Stranded-Deoxyribonucleic acid
EE	Entrapment efficiency
GR	Glucocorticoid receptor
HDAC2	Histone deacetylase 2
HDM	House dust mite
IFN-I	Type I interferon
IL-6	Interlukin-6
IRF3	Interferon regulatory factor 3
LPS	Lipopolysaccharide
MCh	Methacholine
PDI	Polydispersity Index
PLGA	Poly (Lactic-co-Glycolic Acid)
STING	Stimulator of interferon genes
TBK1	TANK-binding kinase 1
TGF-β1	Transforming growth factor beta
Th1	Type 1 inflammation
Th2	Type 2 inflammation

List of Figures

List of Table

Chapter I.
Introduction

Chronic respiratory diseases (CRDs) are chronic diseases that affect the airways and other structures of the lungs causing breathing abnormalities (WHO, 2007). Globally, CRDs are one of the leading causes of mortality and morbidity. Because of their prevalence and economic impact, CRDs present a public health challenge in both developed and developing countries (Ait-Khaled et al., 2001). Asthma is one of the largest contributors to chronic respiratory disease burden worldwide (GBD, 2020). United Arab Emirates (UAE) has the highest incidence and prevalence of CRDs among 21 countries in North Africa and Middle East (Fallahzadeh et al., 2022).

1.1. Asthma

1.1.1. Definition

Asthma originally was considered as a single disease that manifested with respiratory symptoms, such as wheezing, cough, shortness of breath, and chest tightness (Kuruvilla et al., 2019; Wenzel, 2012). The three main key features of asthma are chronic inflammation, hyperresponsiveness, and remodeling of the airways (Wenzel, 2012).

Asthma was recently defined by Global Initiative for Asthma (GINA) in the 2022 update of the Global Strategy for Asthma Management and Prevention as: “Asthma is a heterogeneous disease, usually characterized by chronic airway inflammation. It is defined by the history of respiratory symptoms such as wheeze, shortness of breath, chest tightness and cough that vary over time and in intensity, together with variable expiratory airflow limitation (GINA, 2022).” Asthma being a heterogenous disease has presented with variable degree of airway inflammation, severity, natural history, and treatment responsiveness (Kuruvilla et al., 2019).

1.1.2. Epidemiology

Asthma is one of the major chronic respiratory diseases (CRDs) globally. It affects all aged groups with relatively low mortality and high morbidity compared to other CRDs (Dharmage et al., 2019). Around 262 million people suffered from asthma worldwide in 2019 (WHO, 2022a), and this is suspected to increase by 100 million in 2025 (Dharmage et al., 2019). Asthma was ranked as the 16th leading cause of years lived with disability and the 28th leading cause of disease burden (Dharmage et al., 2019). Asthma has higher prevalence in high socio-income countries, and higher death rates in low-to-middle socio-income countries (Dharmage et al., 2019; GBD, 2020). In line, Global Burden of Diseases, Injuries, and Risk Factors Study (GBD) recently reported from 204 countries in 2019 that asthma was responsible for almost 22 million total disability-adjusted life years (DALYs) and upto 21% of DALYs from chronic respiratory disease (**Fig. 1.1**).

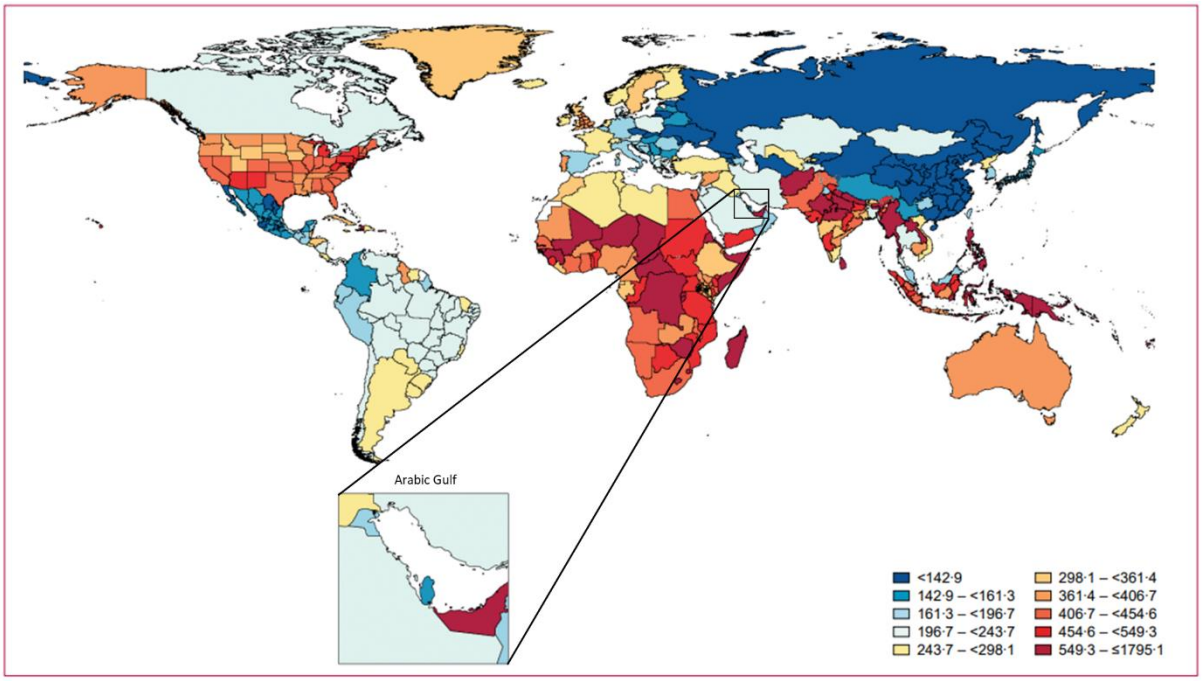

Figure 1.1. Asthma age-standardized DALYs rates (per 100000) by location, both sexes combined, 2019 (GBD, 2020).

Asthma has a different pattern of incidence and prevalence between age groups; with higher incidence and prevalence among children and higher mortality rate among adults (Dharmage et al., 2019). One of the largest epidemiological studies among the young is International Study of Asthma and Allergies in Childhood (Mallol et al., 2013). In its phase

three, more than million children were surveyed from 233 centers in 98 countries. The prevalence of asthma among the 6-7 years old group is the highest among the other studied groups. Recently, asthma was ranked as the 19th leading cause of disease burden in children aged below 10 years old (GBD, 2020).

In the UAE, epidemiological studies were conducted to study asthma incidence, prevalence, and mortality rates. Approximately 5-12% of the UAE population suffers from asthma (Alsowaidi et al., 2010a; Alsowaidi et al., 2010b; Mahboub et al., 2012), while the rates among UAE children range between 13 and 16% (Al-Hammadi et al., 2013; Al-Maskari et al., 2000; Alsowaidi et al., 2010a; Behandy et al., 2015; Bener et al., 1994; Hussein et al., 2018), depending on the geographical prevalence of asthma in different Emirates of UAE. The SNAPSHOT program was conducted to find the updated prevalence of asthma among 33,486 adult participants from July 2014 to February 2016 in five Middle Eastern countries: UAE, Saudi Arabia, Kuwait, Egypt, and Turkey (Tarraf et al., 2018). It indicates a consistent prevalence of asthma across the UAE, significantly higher in females compared to males, specifically in the elderly group, above 50 years old (Tarraf et al., 2018). A recent epidemiological study recruited 3436 children from Dubai and the Northern Emirates in March to June 2019 (Ibrahim et al., 2021). The prevalence of asthma was higher among 6-7 years old group compared to 13-14 years old group, and in boys more than girls in both age groups. The highest prevalence in 6-7 years old group was observed in Dubai while 13-14 years old was in Ras Al Khaimah. Overall, the prevalence was lowest in Ajman and the highest prevalence was in Ras Al Khaimah, followed by Dubai. Further, UAE has the highest estimated prevalence and mortality rate of asthma among the six Gulf Cooperation Council countries; with an estimated mortality rate of 6.0 deaths per 100,000 population, while 6.8% was the estimated prevalence (Finkelstein et al., 2021).

The economic burden of asthma in UAE is relatively high. In Abu Dhabi, the estimated total direct treatment cost was 105 million - UAE Dirhams (29 million US dollars) (Alzaabi et al., 2014). Recently, asthma showed to be the second leading cause of estimated annual direct medical costs among the Gulf Cooperation Council countries, which was 251 million US dollars (Finkelstein et al., 2021).

1.1.3. Phenotypes and Endotypes

Asthma pathophysiology is dominated by chronic airway inflammatory response resulting from inflammation causing mediators released from inflammatory cells including B lymphocytes, T lymphocytes, eosinophils, macrophages, mast cells, neutrophils, and some airway structural cells, as well as through triggering remodeling of the airway wall (Holgate, 2012). Although it is generally known that the large airways are site of chronic airway inflammation and remodeling, it is now largely acknowledged that inflammation also involves the small airways (Cottini et al., 2015).

The term "asthma" represents an umbrella for a variety of mechanistic pathways (endotypes) and clinical manifestations (phenotypes), which all manifest as common asthma symptoms (Kuruvilla et al., 2019). Asthma is classified into two major phenotypes, non-atopic or "intrinsic" asthma, and atopic or "extrinsic" asthma. The non-atopic form is most prevalent among older patients, while the atopic asthma predominates during childhood and is triggered by allergens. While asthma endotypes include two major groups: Type 2 immune response (Th2)-high, and non-Th2-high (Th2-Low) groups.

1.1.3.1. Th2-high

Type 2 immune responses are described by Th2 cells, immunoglobulin E (IgE) and eosinophils (Iwasaki et al., 2017; Kubo, 2017). Type 2 immune responses are considered the central molecular mechanism driving asthma (Woodruff et al., 2009). Based on the allergic response, asthma is classified into atopic and non-atopic asthma (**Fig. 1.2**).

The development of atopic asthma is mainly associated with the sensitization to aeroallergens (Holgate, 2012; Kubo, 2017). In atopic lung inflammation, airway epithelial cells are perturbated with allergens, and infections providing the initial danger signal resulting in the secretion of cytokines and chemokines (such as interleukin (IL)-33, TSLP and IL-25), as well as trafficking and maturation of dendritic cells (DCs) to the mucosal epithelium. DCs uptake the allergens and then migrate to the draining lymph node where naive T cells are sensitized with the DC-presented allergen peptides. The naive T cells differentiate into adaptive Th2 cells; and IL-4 induces GATA3 to activate these Th2 cells via the signal transducer and activator of transcription 6 (STAT6) signal (Ohta et al., 2017). These primed Th2 cells migrate to the site of lung inflammation and produce Th2 cytokines (including IL-4, IL-5, IL-9, and IL-13) (Caminati et al., 2018; de Groot et al., 2015). IL-4 is responsible for Th2 cell development and B-cell isotype switching to IgE. IL-5 regulates the migration, maturation, and survival of eosinophils; because of that eosinophils and eosinophilic inflammation is more prominent in

the Th2 asthma subtype. The eosinophil's degranulation causes the release of eosinophil peroxidase, major basic protein, eosinophil cationic protein, cytokines (IL-4, IL-13, and IL-6) and chemokines (CCL-17, CCL-22, CXCL-9, and CXCL-10) (McBrien et al., 2017). Eosinophil peroxidase and major basic protein stimulate neutrophils, mast cells and epithelial cells. IL-4 and IL-13 simulate the IgE production and B cells proliferation, whereas IL-6 enhances plasma cells survival. CCL-17 and CCL-22 recruit Th2 cells, while CXCL-9 and CXCL-10 recruit Th1 cells. Mast cell hyperplasia and its degranulation is regulated by IL-9. At the same time, the crosslinking of allergen-specific IgE antibodies to the high-affinity FcεRI causes the mast cells to release mast cell-derived proteases (tryptase and chymase), biogenic amines (serotonin and histamine), and lipid mediators (sphingolipids, platelet-activating factor, leukotrienes, and prostaglandins). IL-13 is responsible for mucous hypersecretion, subepithelial fibrosis, eotaxin production, and airway hyperresponsiveness.

In contrast, non-atopic asthma is characterized by the absence of allergen specific IgE antibodies in the serum and the involvement of innate immune cells, specifically innate lymphoid cells 2 (ILC2) (Kubo, 2017). Proteases, and pollutants can cause airway epithelial cell injury and barrier disruption leading to IL-33 and TSLP cytokine secretion, which in turn activate basophils and ILC2s to produce Th2 cytokines (IL-4, IL-5, and IL-13). Also, the basophil-derived IL-4 activates ILC2s to release the chemoattractant CCL11 or eotaxin-1, that attracts eosinophils to the lung. The activated ILC2s also produce IL-5 and IL-13.

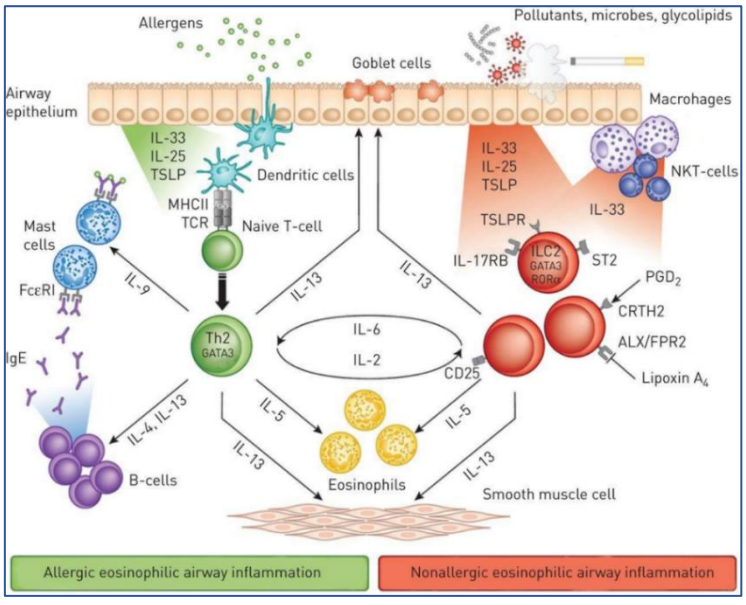

Figure 1.2. Two different pathways lead to eosinophilic airway inflammation in asthma, allergic (atopic) and non-allergic (non-atopic) airway inflammation (de Groot et al., 2015).

1.1.3.2. Non-Th2-high (Th2-Low)

While mild to moderate asthmatics cater more towards Th2 inflammatory response, Th2 low phenotype is frequently encounter in severe form of asthma (Woodruff et al., 2009). Therefore, based on the severity of asthma, the principal cells involved in the immune response have been observed to change. For instance, Th17 immune response have been reported in steroid resistant severe asthma (Poon et al., 2016; Ramakrishnan et al., 2019). A Th1 immune response with neutrophil recruitment has been noted in some cases of chronic and severe asthma, specifically in bacterial infections (Gauthier et al., 2017; Hamzaoui et al., 2005; Raundhal et al., 2015; Truyen et al., 2006).

1.2. Pathophysiology of severe asthma

According to the National Asthma Education and Prevention program, asthma can be classified into four severity levels based on its severity: intermittent, mild persistent, moderate persistent, and severe persistent (National Asthma et al., 2002). The terms “severe asthma,” “uncontrolled asthma,” “difficult-to-treat asthma,” or “refractory asthma” are usually interchangeable (Poon et al., 2016); are defined in the European Respiratory Society /American Thoracic Society Task Force as: ‘‘Asthma which requires treatment with high dose inhaled corticosteroids plus a second controller (Long acting β-agonist or leukotriene receptor antagonist/theophylline) for pervious year or daily oral ICs for ≥ 50% of previous 12 months to prevent it from becoming ‘uncontrolled’ or which remains ‘uncontrolled’ despite this therapy (Chung et al., 2014).’’

The prevalence of severe asthma is approximately 5-10% of asthmatic subjects worldwide (Poon et al., 2016), but it accounts for high mortality rate and significant socioeconomic burden related to asthma. These patients usually encounter persistent and aggressive asthma symptoms despite the high dosage of treatments (Lommatzsch et al., 2014). Treating this category of patients represent the majority of disease burden in the health care system. Collectively, finding effective treatment for severe asthma is a major unmet need for these patents, mandating the need to understand better the underlying mechanisms.

Following exposure to allergens, the activated DCs migrates towards the lymph node secreting IL-23 and IL-6 (Holgate, 2012; Kubo, 2017). The naive T cells are differentiated into Th17. Transforming growth factor β (TGF-β) and IL-6 induce Th17 cells through Rorγt-STAT3 signal (Ohta et al., 2017) (**Fig. 1.3**). Upon repetitive allergen exposures, the memory cells get activated resulting in robust and sustained release of cytokines (Hamid et al., 2009; Lambrecht et al., 2019).

Increased IL-17A and IL-17F levels have been reported to positively correlate with asthma severity (Halwani et al., 2013; Ohta et al., 2017). IL-17 cytokines contribute to airway smooth muscle remodeling (Chang et al., 2012; Evasovic et al., 2019; Halwani et al., 2013; Ramakrishnan et al., 2019), recruiting and activating both neutrophils (Halwani et al., 2013; Ramakrishnan et al., 2019; Ramirez-Velazquez et al., 2013) and B cells (Halwani et al., 2014; Ramakrishnan et al., 2019), and promoting fibrosis and mitochondrial dysfunction in bronchial fibroblasts (Halwani et al., 2013; Ramakrishnan et al., 2019; Ramakrishnan et al., 2020a). As a result, neutrophils are more prominent in Th17 high asthma subtype and neutrophil-rich Th17-cell-driven airway inflammation may represent steroid-resistant asthma. Neutrophils has a specific pattern of cell death called NETosis, wherein neutrophil extracellular traps resulted from the release of their DNA outside cells in presence of excessive reactive oxygen species production. Recently, NETosis has been shown to be involved in severe asthmatic airway inflammation (Nabe, 2020). The expression of IL-17A and IL-17F cytokines in airway biopsies of severe asthmatic patients is elevated when compared to patients without asthma (Ramakrishnan et al., 2019). Specifically, IL-17A was detected in the serum and airways of asthmatic individuals while IL-17F was elevated in airway tissues, specifically in the epithelium and submucosa (Poon et al., 2016).

Crosstalk between the immune cells has been documented in previous literature; with evidence of Th2/Th17-high endotype with a mixed pattern of neutrophilic-eosinophilic inflammation which is a feature of steroid resistant severe asthma phenotype (Ramakrishnan et al., 2019).

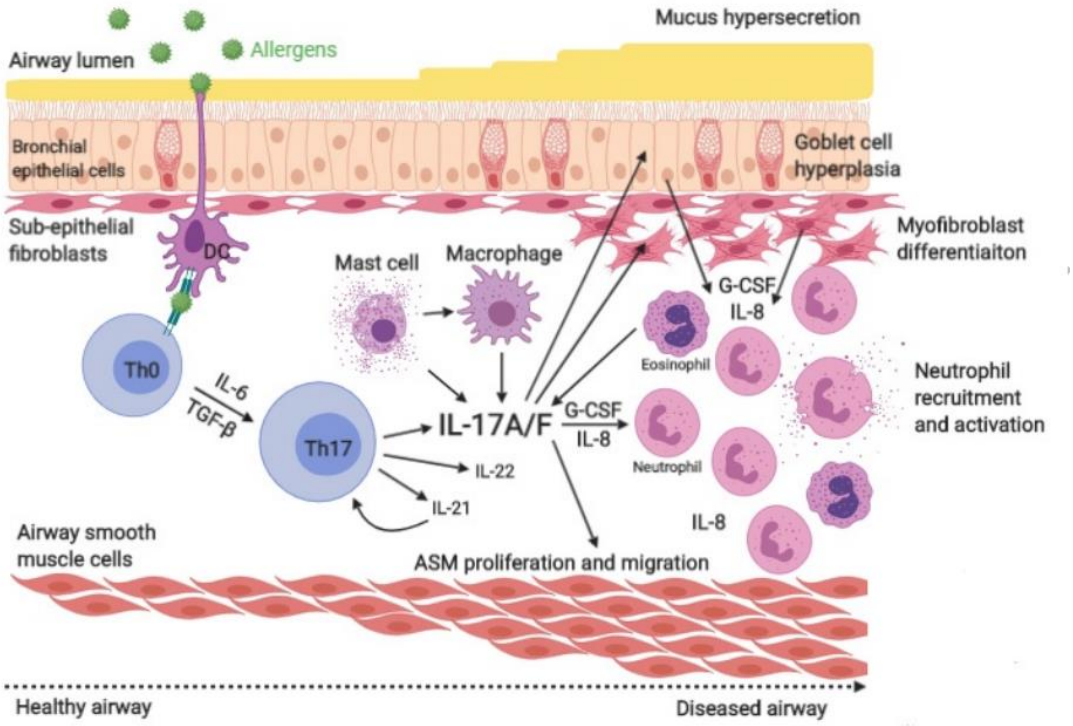

Figure 1.3. The role of IL-17 in asthma pathogenesis, particularly severe asthma (Ramakrishnan et al., 2019).

Moreover, type 1 inflammation (Th1) is associated with corticosteroid-resistant severe asthma in 50% of severe asthmatic patients (Gauthier et al., 2017; Raundhal et al., 2015). Type 1 immune responses are characterized by the presence of Th1, and neutrophils. Different factors are involved in the development of type 1 inflammation, including cigarette smoke, pollutants, and viruses (Iwasaki et al., 2017). These factors can activate both innate immune pathways, and Th1/Th17 inflammation.

These factors disrupt airway epithelial cell barrier leading to the secretion of interferon-γ (IFN-γ) and activation of both macrophages and DCs which in turn leads to IFNα/β production (Iwasaki et al., 2017). These IFNs help induce an antiviral state. Furthermore, the activated macrophages and DCs secrete cytokines, IL-12, IL-23, TNF-α and IL-6, and chemokines, CXCL-10 and IL-8. IL-12 and IFN-γ induce T-bet to stimulate Th1 cells through the STAT4 signal (Ohta et al., 2017). This microenvironment aids in differentiating the naive T cells into Th1 and Th17 cells and recruiting neutrophils; which are the key features of type 1 inflammation. In type 1 immunity, ILC1 is activated by IL-12 and secreted IFN-γ, ILC3 is

activated by IL-23 and secreted IL-17, and IL-22 (Iwasaki et al., 2017). IFN- γ acts as a proinflammatory mediator and enhances the expression of downstream genes such as CXCL10 that could explain airflow hyperresponsiveness and steroid hyporesponsiveness in asthma (Gauthier et al., 2017; Lambrecht et al., 2019).

Collectively, chronic inflammation is the causative mechanism that underline asthma, particularly, severe asthma.

1.2.1. Airway remodeling during asthma

The remodeling of the airway wall resulted from chronic injury and inflammation that altering airway structure and function (Fehrenbach et al., 2017). In asthma, airway structural alterations encompass enlargement of glands, increased smooth muscle mass, subepithelial fibrosis, and epithelial alterations (Bergeron et al., 2009) (**Fig. 1.4**). These structural changes consequently lead to thickening of airway walls, airway narrowing, airway edema, bronchial hyperresponsiveness, and mucous hypersecretion (Bergeron et al., 2009). In mild asthma, airway remodeling is partially reversible, however it is mostly irreversible in chronic severe asthma (Halwani et al., 2010).

Airway remodeling involves the dysregulation of a repeated injury-repair process. The injury is usually initiated by environmental (pathogens, allergens, pollutants, and cigarette smoke), or mechanical stress factors (Al-Muhsen et al., 2011), or inflammation (Fehrenbach et al., 2017). Chronic airway inflammation is the major force driving airway remodeling. Airway remodeling driven by the complex interaction between inflammatory and structural cells through the release of multiple cytokines, chemokines, and growth factors leading to complex signaling environment (Al-Muhsen et al., 2011).

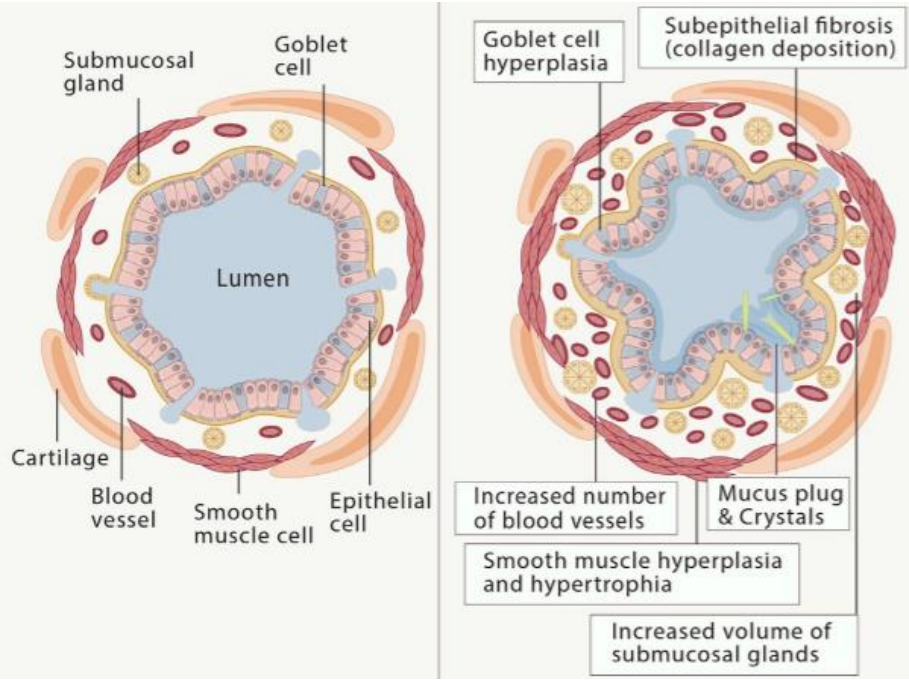

Figure 1.4. The airway remodeling in severe asthma (Lambrecht et al., 2019).

1.2.1.1. Epithelial alteration

Shedding of the bronchial epithelium is the major epithelial alteration that has been detected in sputum and bronchoalveolar lavage fluid from severe asthmatic patients and in autopsy lungs of fatal asthma (Trejo Bittar et al., 2015). Loss of ciliated cells has been reported for severe asthmatic epithelia, which were replaced partially by goblet cells, and/or impaired ciliary function (Trejo Bittar et al., 2015). This has a negative impact on mucociliary clearance. It has been suggested either that the epithelium of asthmatics is more prone to turnover than epithelium of healthy control subjects, or that the epithelial basement membrane is weakened in the asthmatic airways (Bergeron et al., 2009). This process is mediated with high rate of apoptosis which is mainly driven by tumor necrosis factor-α (TNF- α) and TGF-β (Halwani et al., 2011; Halwani et al., 2010).

1.2.1.2. Goblet and mucous gland hyperplasia

Goblet cell and submucosal gland hyperplasia/metaplasia is more prominent in severe and fatal asthma. It mainly causes increased mucus production, particularly the mucin glycoprotein, contributing to airway narrowing (Trejo Bittar et al., 2015). Type-2 inflammation is the main trigger for mucus hyper-secretion, likely through IL-9 and IL-13 signalling (Halwani et al., 2010).

1.2.1.3. Subepithelial fibrosis.

Reticular basement membrane thickening is one of major histological changes in severe asthma. It involves the deposition of collagen-I, collagen-III, immunoglobulins, fibronectin, and tenascin; mainly due to Type-2 inflammation through TGF-β pathway (Halwani et al., 2011; Trejo Bittar et al., 2015). The tissue resident fibroblasts differentiate into apoptosis-resistant myofibroblasts resulting in their overactivation paving way to increased extracellular matrix deposition in the submucosal space below the basement membrane (Kis et al., 2011). This differentiation is due to the epithelial mesenchymal transition which is influenced by the complex environment, cytokines, growth factors, extracellular matrix composition (Kis et al., 2011). Subepithelial fibrosis is thus, more prominent in severe asthma.

1.2.1.4. Increased smooth muscle mass.

Airway smooth muscle is responsible for adjusting the tone of the airway (Bergeron et al., 2009). Hypertrophic, hyperplastic, and migrated of airway smooth muscle towards the subepithelial layer are prominent histological indicators of asthmatic airway remodeling (Halwani et al., 2010). The smooth muscle remodeling has been positively correlated with asthma severity (Bergeron et al., 2009; Halwani et al., 2010). Also, smooth muscle cells participate in the inflammatory processes though their release of chemokines (IL-8 and eotaxin), proinflammatory cytokines (IL-5 and TGFβ) and extracellular matrix proteins (tissue inhibitors of metalloproteinases and metalloproteinases) (Bergeron et al., 2009; Halwani et al., 2010).

Furthermore, airway remodeling is defined clinically as airway obstruction that do not respond to anti-inflammatory treatment, particularly, inhaled corticosteroid (Halwani et al., 2013). Airway remodeling is therefore, associated with poor clinical outcome. Thus, early diagnosis and prevention of airway remodeling could subsequently reduce illness severity and enhance disease management.

1.2.2. Steroids Resistance

The most severe and difficult to treat form of asthma is known as steroid resistant asthma. In milder form of asthma, steroids reduce inflammation via both genomic and nongenomic mechanisms (Poon et al., 2016; Ramamoorthy et al., 2016). Genomic actions of steroids are through binding to the glucocorticoid receptor (GR) in cytoplasm which undergoes a conformational change exposing 2 nuclear localization signals, triggering a rapid translocation into the nucleus through nuclear pores. Subsequently, the complex of steroid -

GR binds to the promoter region of target genes to either stimulate or inhibit gene transcription. In contrast, the non-genomic effects of steroid occur within seconds to minutes of GR activation through utilizing different kinases, such as Protein kinase B (AKT), and mitogen-activated protein kinases (MAPKs) which resulted in regulating proliferation and apoptosis (Ramamoorthy et al., 2016; Samarasinghe et al., 2012). Thus, non-genomic GR signaling that adds greater complexity and diversity to the biological actions induced by glucocorticoids. However, in severe asthma, despite glucocorticoids treatment, the extracellular signal-regulated kinase (ERK1/ERK2) and p38 MAPK pathways are activated with increased protein phosphatase 1 expression (DUSP1), which in turn involved in neutrophil recruitment via stimulating CXCL8 synthesis (Robins et al., 2011).

Another major mechanism underlining severe asthma, is the dysregulation of the expression of the Glucocorticoid receptor altering the GRα/GRβ ratio (Al Heialy et al., 2020). Indeed, GR exists in 2 isoforms GRα (Steroid-binding isoform of GR) and GRβ (nonbinding isoform of GR) acting as negative regulator of the classical GRα. Mechanistically, type-2 inflammation, likely through IL-2/IL-4 cytokines, significantly decreased GRα expression without affecting GRβ (Vazquez-Tello et al., 2013), while IL-17 significantly increased GRβ expression (Ramakrishnan et al., 2019; Vazquez-Tello et al., 2013). Further, the binding affinity and nuclear translocation of steroid-bound GR is reduced in steroid resistant asthma as compared to the steroid sensitive asthma (Poon et al., 2016). Moreover, supplementation of vitamin D selectively favors the upregulation of GRα receptor and downregulation of IL-17 in peripheral blood of severe asthmatics deficient with vitamin D (Mahboub et al., 2021). Finally, histone acetylation is needed to initiate steroid–GR-induced gene repression as reduction in histone acetylation is associated with steroid resistance (Matthews et al., 2004). Specifically, histone deacetylase 2 (HDAC2) is selectively reduced by the upregulation of GRβ (Li et al., 2010) and by oxidative stress (Barnes, 2013).

1.3. DNA damage in asthma

Asthma is triggered by exposure to different allergens, the most common allergen worldwide is house dust mite (HDM) (Gregory et al., 2011). While HDM exerts various detrimental effects leading to asthma, it also significantly increases the oxidative DNA damage in lung tissue, which in turn induces proinflammatory cytokine production, including IL-4, IL-5, and IL-13, and cellular apoptosis (Chan et al., 2016). In line, the oxidative DNA damage

was also significantly increased in the lung of ovalbumin-induced asthmatic murine model (Wang et al., 2018a). In asthmatic patients, DNA damage was significantly increased relative to controls and correlated to disease severity (Gaballah et al., 2018; Saini et al., 2019). As DNA damage could induce the leakage of self-double-stranded DNA (dsDNA) into cytosol (Dhanwani et al., 2018), the release of self-dsDNA in nasal lavage by NETosis has been observed and is significantly correlated with the type-2 allergic inflammation exacerbation, IL-5 and IL-13 secretion in asthmatic patients (Toussaint et al., 2017), which has been associated with steroid resistant severe asthmatic airway inflammation (Nabe, 2020). Furthermore, DNA damage could also induce the formation of micronuclei (Fenech et al., 2020), which is an encapsulated chromosome fragments after failing to be a primary nucleus (Krupina et al., 2021). The frequency of micronuclei was higher in asthmatic patients compared to healthy controls (Saini et al., 2014), and significantly increased with disease severity (Lintsov et al., 2019). Interestingly, alveolar macrophages (AMs) in response to GM-CSF and IL-33 stimulation undergo DNA damage-induced stresses, thus exhibiting signs of polynucleation, polyploidy, and micronuclei formation (Quell et al., 2020).

Pulmonary inflammation observed in smoking patients is mainly driven by oxidative DNA damage and subsequent cell death (Paschalaki et al., 2013). Smoker COPD patients have elevated levels of oxidative DNA damage in their peripheral blood, which in fact was proposed to identify patients at high mortality risk (Ceylan et al., 2006; Maluf et al., 2007). Indeed, the cell death induced by cigarette smoke is mainly associated with the release of danger associated molecular patterns (DAMPs) as self-dsDNA, which strongly correlated with neutrophilic airway inflammation, a characteristic of COPD (Pouwels et al., 2017). The effect of cigarette smoke exposure in inducing the release of self-dsDNA in the bronchoalveolar space upon respiratory barrier damage has been illustrated in mice (Nascimento et al., 2019). Interestingly, the frequency of micronuclei, being a significant indicator of DNA damage, was also increased in smokers compared to non-smokers and to higher extent in smoking asthmatics (Rossnerova et al., 2011; Saini et al., 2019).

1.4. Immune signaling pathways activated in response to DNA damage.

The innate immune system recognizes the pathogen-associated molecular patterns (PAMPs) comprising of nucleic acids, protein, lipids, structural components via distinct pattern recognition receptors (PRRs). PRRs are cell-surface and intracellular receptors. These

receptors include RIG-I-like receptor (RLR), toll-like receptor (TLR), NOD-like receptor (NLR), C-type lectin-like receptors (CLmin) as well as certain cytoplasmic free-molecule receptors, such as stimulator of interferon genes (STING), cyclic GMP-AMP synthase (cGAS), gamma-interferon-inducible protein 16 (IFI16) and DNA-dependent activator of interferon-regulatory factors (DAI), to name a few (Barber, 2011; Jensen et al., 2012; Tan et al., 2018). These PRRs initiate a signaling cascade culminating in primarily type I interferon (IFN-α/β) and inflammatory cytokine production (Schneider et al., 2014). Although type I (IFN-α, IFN-β, IFN-ε, IFN-κ, IFN-ω in humans) and type III (IFN-γ) IFNs are key inflammatory cytokines, other pro-inflammatory cytokines such as tumor necrosis factor alpha (TNF-α), and interleukin-1 (IL-1), IL-6, and IL-18, also play a supporting role.

Toll-like receptors (TLRs) are widely expressed in various cellular compartments including plasma membranes, endosomes, lysosomes, cytosol and endocytolysosomes. The various TLRs recognize a variety of pathogen- and danger-associated molecular patterns (PAMP and DAMP), including nucleic acids (NA), lipids, proteins and lipoproteins (Akira et al., 2006). NA sensing TLR3, 7, 8 and 9, anchored on the intracellular membranes of endosomes (Fitzgerald et al., 2020); TLR3 detects dsRNA, TLR7 and 8 detect ssRNA and TLR9 detects unmethylated CpG containing ssDNA. Furthermore, previous studies showed that TLR9 can detect chromosomal and mitochondrial DNA, self-dsDNA, through fragmentation into short ssDNA by DNase II (Miyake et al., 2018). Mainly by this mechanism, TLR9 can sense cytosolic self-dsDNA. Different TLRs are equipped with distinct adaptor proteins, including myeloid differentiation primary response gene 88 (MyD88), toll-interleukin 1 receptor (TIR) domain-containing adaptor-inducing interferon-β (TRIF), and TIR domain-containing adaptor protein (TIRAP), that induces distinct immune responses (Kawai et al., 2010). For instance, TLR4, TLR7, TLR8 and TLR9 uses the MyD88 adaptor for downstream signaling, and TLR3 and TLR4 uses TRIF. MyD88 activates the transcription factors NF-κB and IRF7, while TRIF activates the transcription factors IRF-3 and NF-κB to induce the expression of type I interferon.

NOD-like receptors (NLRs) are a type of PRR that detect a wide range of both cytosolic PAMPs and DAMPs. NLRs such as NACHT, LRR, and PYD domains-containing protein 1 (NLRP1), NLRP3, NLR family CARD domain-containing protein 4 (NLRC4), and absent in melanoma 2 (AIM2), interact with apoptosis-associated speck-like protein (ASC) and caspase-1 forming a multiprotein complex called inflammasome (Swanson et al., 2019; Zhao et al., 2020). The main receptors that associate with self-dsDNA sensing are AIM2 (Hu et al., 2016;

Lian et al., 2017) and NLRP3 inflammasome (Wu et al., 2019; Zhong et al., 2018). The inflammasome causes the secretion of pro-inflammatory cytokines, IL-1β and IL-18, and induces a form of inflammatory cell death called pyroptosis (Swanson et al., 2019; Zhao et al., 2020). The activation of inflammasome requires two steps - priming and activation. Initially, the priming step involves the activation of PRRs (TLRs) via sensing PAMPs. This eventually leads to NF-κB activation and induce the expression of pro-caspase-1, pro-IL-1β and pro-IL-18. Then, the activation step is triggered by sensing intracellular DAMPs. The recruitment of pro-caspase-1 by ASC speck induces caspase-1 activation by self-cleavage which subsequently cleaves the pro-IL-1β, pro-IL-18 and inactive gasdermin D (GSDMD) into IL-1β, IL-18 and active GSDMD. Further, activated GSDMD induces pyroptosis by forming pores in cell membrane allowing pro-inflammatory cytokines, IL-1β and IL-18, to be secreted into the extracellular space (Swanson et al., 2019; Zhao et al., 2020).

STING pathway

In the last decade, STING was identified as an adapter protein involved in innate immune signaling triggering IFN-I expression in response to mislocalized nucleic acids in the cytosol. STING is well documented as a cytosolic DNA sensing pathway consequent to cytosolic self-DNA binding to cGAS dependent manner (Barber, 2015; Kumar, 2019; Uggenti et al., 2018). This cGAS activation upon dsDNA binding in the cytosol leads to the production of the second messenger cyclic GMP-AMP (cGAMP). Then, cGAMP binds to STING, located on the endoplasmic reticulum, resulting in its translocation to the Golgi apparatus where TBK1 is recruited and activated by autophosphorylation (Mdkhana et al., 2021a). Activated TBK1 cause the activation of the transcriptional factors, IRF-3, IRF-5, and NF-κB, via phosphorylation, which then translocate to the nucleus to induce transcription of type I interferon and other inflammatory genes, including IL-1, TNF-α, and IL-6, respectively (**Fig. 1.7**). Once released, type I IFNs bind to their cognate receptors (IFNAR), thereby activating the JAK-STAT signaling pathway leading to the transcription of interferon stimulated genes (ISGs). These have been reported to govern chemotaxis, cell migration, apoptosis, and cell proliferation, as well as to modulate immunological recognition and defend against viral infection (Li et al., 2017). Indeed, the dysregulation of type I interferon signaling can result in an overproduction of ISGs, which in turn over-activating the immune system (Li et al., 2017).

Interestingly, cGAS-STING pathway is activated by DNA leaking from rupture micronuclei which in turn stimulate the innate immune response (de Oliveira Mann et al., 2017;

Mackenzie et al., 2017), thus linking DNA damage to inflammatory mechanisms (de Oliveira Mann et al., 2017; Mackenzie et al., 2017).

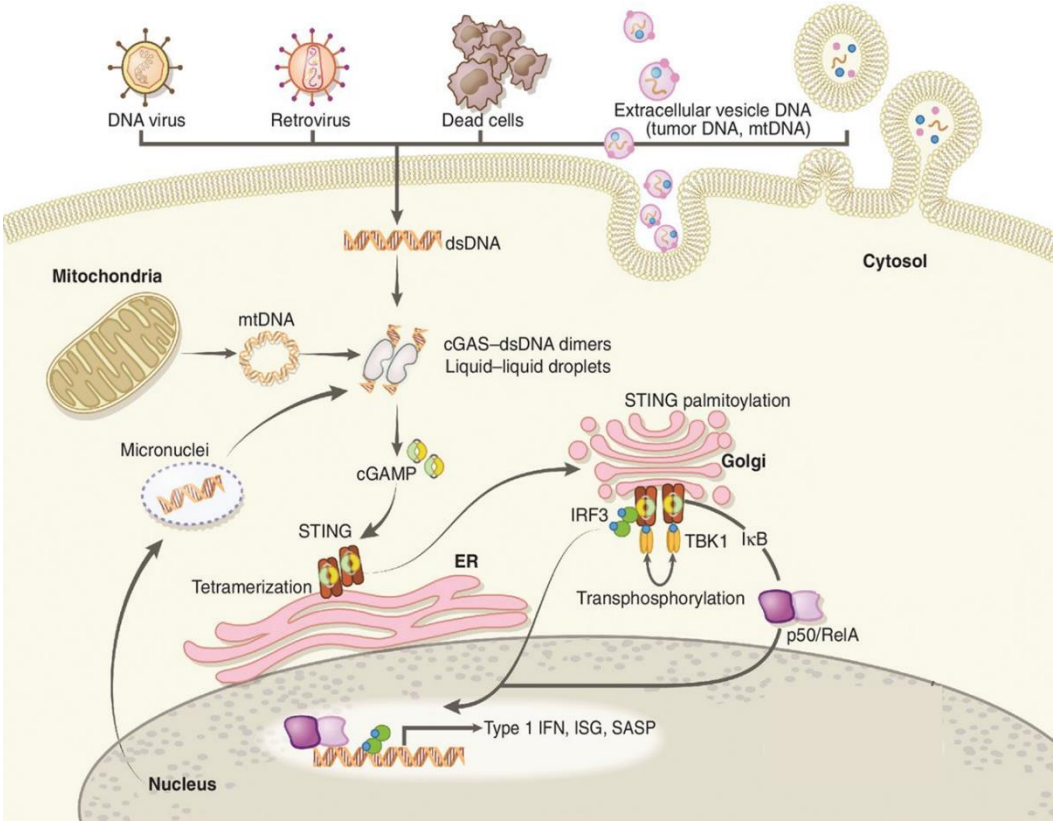

Figure 1.5. cGAS-STING signaling in immunity (Kwon et al., 2020).

Constitutive activation of STING, as a result of cytosolic DNA fragments or gene variation, and the subsequent excess production of IFNs and proinflammatory cytokines contribute to the pathogenesis of several inflammatory and autoimmune diseases, such as STING-associated vasculopathy with onset in infancy (SAVI) (Liu et al., 2014). The gain of function mutations in STING1 gene is the causative factor for constitutive STING activation. The main manifestations of this disease are systemic inflammation, severe vasculitis in the extremities and interstitial lung disease with mixed lymphocytic inflammatory infiltration and interstitial fibrosis (Liu et al., 2014). Most of the current information on STING pathway has been derived from cancer research attempting to stimulate immune responses by using STING agonists such as cGAMP (An et al., 2019; Deng et al., 2014; Liu et al., 2019). Interestingly,

metastatic lung cancer was controlled in both lungs upon administration of cGAMP encapsulated in liposomal nanoparticle via the stimulation of pro-inflammatory tumor microenvironment in lung metastases (Liu et al., 2019).

This pathway is also known to drive inflammation in different chronic inflammatory diseases, such as systemic lupus erythematosus (An et al., 2017; Kato et al., 2018; Thim-Uam et al., 2020), rheumatoid arthritis (Wang et al., 2019), acute lung injury (He et al., 2021; Ning et al., 2020; Wu et al., 2021), and silicosis (Benmerzoug et al., 2019; Benmerzoug et al., 2018). In synovial tissue from patients with rheumatoid arthritis, cytosolic dsDNA-cGAS-STING pathway was positively correlated with the severity of synovial inflammation of rheumatoid arthritis (Wang et al., 2019). Wherein the overexpression of DNaseII reduces the accumulation of cytosolic dsDNA, which in turn decreases the inflammatory cytokines and matrix metalloproteinases-13 secretion. Thus, DNaseII overexpression resulted in reducing the cytosolic dsDNA-induced synovial inflammation in rheumatoid arthritis.

Patients with silicosis and fibrotic interstitial lung disease have high levels of dsDNA in sputum and activated STING pathway from lung tissues, respectively (Benmerzoug et al., 2018). As lung cells undergo apoptosis due to silica exposure, self-dsDNA is released in the bronchoalveolar space, which activates STING pathway (Benmerzoug et al., 2019; Benmerzoug et al., 2018). Therefore, degrading extracellular self-dsDNA by DNaseI resulted in the inhibition of STING activation and type I IFN response (Benmerzoug et al., 2018). The activation of STING contributes to acute lung injury in a cytosolic DNA-dependent manner, while cGAS or STING deficiency attenuated murine acute lung injury (Ning et al., 2020). Interestingly, STING inhibitor alleviated acute lung injury via inhibiting inflammatory cytokines production, including TNF-α, IL-6, IL-12, and IL-1β, and adhesion molecule vascular cell adhesion protein-1 (VCAM-1) (Wu et al., 2022a).

Despite such critical functions, limited data on inhibition of the cGAS-STING axis are available. One STING inhibitor, H151, has recently been discovered and is a potent, irreversible and selective inhibitor (Haag et al., 2018). It binds covalently to STING at the transmembrane cysteine residue position 91, halts STING palmitoylation and clustering at Golgi apparatus, resulting in blockage of downstream type I IFN response, and hence reduces inflammation (Haag et al., 2018).

1.5. STING pathway in asthma

As has been stated earlier, self-dsDNA is significantly correlated with the type-2 allergic inflammation exacerbation in asthmatic patients (Toussaint et al., 2017), which potentially activates the STING pathway in asthmatic lung tissue. Interestingly, airway epithelial cGAS detects cytosolic dsDNA in IL-33 stimulated cells, and HDM- and OVA-induced asthmatic murine model; promoting Th2 immunity via regulating the production of airway epithelial GM-CSF (Han et al., 2020). Further, cGAMP, a STING ligand, promotes HDM allergic asthma, via significant increase in serum IgE levels (Nunokawa et al., 2021; Ozasa et al., 2019), percentage of B cell (Nunokawa et al., 2021), and eosinophil infiltration (Ozasa et al., 2019), in bronchoalveolar lavage fluid. The inhibition of TBK1 by Amloxanox decreased cGAMP-induced lung allergic inflammation (Ozasa et al., 2019). Interestingly, STING plays an important role in severe asthma through innate lymphoid cells (ILCs) plasticity (Doherty, 2020), since ILC2 function is inhibited and shifted toward ILC1 response which promote type 1 inflammation upon using fungal allergens, Aspergillus flavus and Alternaria, in combination with STING ligands, cGAMP and cyclic-di-GMP, respectively (Cavagnero et al., 2021; She et al., 2021). In addition, in sputum from asthmatic patients, the expression of IFN-β, and ISGs was positively correlated with neutrophilic asthma (da Silva et al., 2017), while the IFN-α was significantly associated with high lymphocytes level (Hastie et al., 2018). Further, airway epithelial and peripheral blood ISGs levels were significantly higher in asthmatic patients and associated with decreased lung function (Bhakta et al., 2018). Bronchoalveolar lavage cells from severe asthmatics had higher expression of the transcriptional factor IRF5, downstream of STING pathway, when compared to mild asthmatics or healthy controls (Oriss et al., 2017).

The release of self-dsDNA following cigarette smoke exposure activates the DNA sensor cGAS-STING pathway triggering IFN I-dependent lung inflammation (Nascimento et al., 2019). In addition, activated STING induced both pulmonary inflammation and fibrosis in a bleomycin mouse model (Sun et al., 2020). Interestingly, the gene expression signature from peripheral blood and bronchial brushings of COPD patients was associated with ISGs, which correlated with high airway wall thickness, decline in lung function, and frequent exacerbations (Yun et al., 2022).

1.6. STING pathway contribution to steroid resistance

The innate immune responses, specifically through the cytosolic DNA sensing pathways, are differentially regulated by glucocorticoids (Wang et al., 2017). The self-dsDNA

released in nasal lavage from asthmatic patients was unaffected by inhaled corticosteroid (Toussaint et al., 2017), while the peripheral blood ISG expression in severe asthmatic cases was not affected by using oral corticosteroid (Bhakta et al., 2018).

STING leads to the activation of downstream transcription factors IRF3 and IRF5 which are crucial for IFN-I induction (Andzinski et al., 2016). IRF-5 expressed by M1 macrophages induced IFN-γ– and IL-17–producing CD4+ T cells in co-cultured human T cells (Oriss et al., 2017). Further, IRF-$5^{-/-}$ mice subjected to HDM/cdiGMP sensitization had significantly lower Th1/Th17 response and increase in Th2 response. Thus HDM/cdiGMP sensitized IRF-$5^{-/-}$ mice were responsive to glucocorticoid treatment resulted in the suppression of the Th2 response (Oriss et al., 2017).

As has been stated earlier, STING pathway also leads to pro-inflammatory gene expression via NF-κB activation (Barber, 2015). The activated NF-κB pathway leads to glucocorticoid resistance through different mechanisms that has been summarized from (Enweasor et al., 2021). The activated NF-κB inhibits the expression and function of the GR, via a) inhibition of GR nuclear translocation, b) hindrance of GR binding to its promoter region, especially glucocorticoid response elements, in glucocorticoid-responsive genes, c) interference with transcription factors that interact with GR to form monomeric form in mechanism called “tethering”. NF-κB is activated further by decreased GR function, resulting in a vicious cycle of proinflammatory responses.

Class I HDAC, particularly HDAC1 and HDAC2, mediates ISG expression (Marie et al., 2018), supported by a functional redundancy between these two enzymes (Icardi et al., 2012). HDAC1 and 2 differentially regulated STAT activity in response to IFN-α (Icardi et al., 2012). Inhibition of HDAC1 induces dsDNA release into cytosol which in turn, activated the STING pathway in pseudorabies viral infection (Guo et al., 2021). Collectively, due to the functional redundancy between HDAC1 and HDAC2, the inhibition of HDAC2 may lead to STING pathway activation in context of steroid hyporesponsiveness respiratory diseases.

1.7. Rational and hypothesis

Anti-inflammatory drugs such as corticosteroids represent the main type of therapy for asthma. However, in addition to the side effects accompanying long-term usage of corticosteroids, many patients, especially those at a severe stage of the disease, develop resistance to corticosteroids (GINA, 2022). This fact has triggered intensive research into the

development of alternative medications that would decrease lung inflammation and tissue remodeling and therefore allow for better control of disease symptoms.

Cyclic GMP-AMP synthase (cGAS) and stimulator of interferon gene (STING) pathway has recently emerged as one of the key pathways regulating chronic inflammation (Kato et al., 2018). This pathway is mostly triggered by DNA damage, the level of which is upregulated in chronically inflamed tissue, including lung tissue during asthma (Chan et al., 2016), and triggers the production of pro-inflammatory mediators, mostly type I interferons. Type I interferons were shown to regulate glucocorticoid resistance by suppressing glucocorticoid-induced leucine zipper (GILZ) expression (Dankers et al., 2022). However, the contribution of this pathway to lung inflammation as well as steroid hyporesponsiveness in asthma is elusive.

1.8. Aims and objectives

Objective 1: Determine the activation level of STING pathway during chronic lung inflammation.

Aim 1: Analyze in-silico data to determine STING activation at baseline in severe asthmatic mouse model.

Aim 2: Examine STING activation in fibroblast of severe asthmatic patients at baseline.

Aim 3: Evaluate the baseline level of STING pathway in lung tissue of different asthmatic mouse models.

Objective 2: Determine the responsiveness of STING pathway to steroid treatment versus STING inhibitor.

Aim 1: Determine the activation level of STING pathway in lung tissue of severe asthmatic mouse model following steroid treatment using in-silico data.

Aim 2: Evaluate in severe asthmatic fibroblasts, the responsive of STING pathway to steroid versus a combination of steroid and STING inhibitor.

Aim 3: Evaluate the responsive of STING pathway to steroid versus a combination of steroid and STING inhibitor in lung tissue of severe asthmatic mouse model.

Objective 3: Study the ability of nanoparticles (NP) loaded with STING inhibitor to better controlled lung inflammation and steroid hyporesponsiveness more effectively than free drug.

Aim 1: Develop a novel NP loaded with STING inhibitor (H151).

Aim 2: Assess the ability of the developed NPs to control lung inflammation and improve response to steroid treatment in steroid resistant asthma mouse model.

Chapter II.
Methodology

2.1. In-silico analysis of publicly available datasets of lung inflammatory mouse models

We analyzed a publicly available study dataset of lung inflammatory mouse models obtained from the National Center for Biotechnology Information Gene Expression Omnibus (NCBI GEO, http://www.ncbi.nlm.nih.gov/geo). The expression of the STING was evaluated using transcriptomic datasets of alveolar macrophages and lungs obtained from HDM sensitized mice. For the alveolar macrophages data set (GSE148590), the authors used flow cytometry to sort the CD11c+ CD64+ Siglec F+ from the bronchoalveolar lavage of adult female C57BL/6J mice after 3 weeks of intranasal exposures to HDM (Branchett et al., 2020). The two data sets of GSE137324 and GSE132377 were used for lung samples. For the GSE137324 dataset, the lungs were isolated from adult female C57BL/6J mice after 4 and 15 weeks of intranasal exposure to HDM (Allinne et al., 2019). Whole lung tissue from unsensitized, HDM plus cyclic di-GMP, and HDM plus cyclic di-GMP plus dexamethasone were extracted and used for RNA expression studies for the GSE132377 dataset.

RNA-sequencing platforms were used in all three datasets. We processed the RNAseq raw count using the Bioconductor package limma-voom (Ritchie et al., 2015), and presented the results as log2 counts per million (log CPM). The normalized STING gene expression level was compared across the groups. Student t-test was used for two groups and ANOVA with post hoc Bonferroni was used for three groups comparison.

2.2. Fibroblast cell culture

Human primary bronchial fibroblasts were isolated from endobronchial tissue biopsies which was obtained from the Quebec Respiratory Health Research Network Tissue Bank (McGill University Health Centre (MUHC)/ Meakins-Christie Laboratories Tissue Bank, Montreal, Canada), as described previously (Panariti et al., 2018; Saheb Sharif-Askari et al., 2021). The original study was approved by the MUHC Research Ethics Board (2003–1879). The patient characteristics are summarized in **Table 1**. The cells were cultured in Dulbecco's modified Eagle's medium (DMEM) (Sigma-Aldrich, Germany) supplemented with 10% fetal bovine serum (FBS), and 1% penicillin/streptomycin (Sigma-Aldrich, Germany). All

incubations and cell maintenance were done in a humidified incubator at 37 °C in 5% CO_2. All the experiments were conducted at matched passages and a maximum of eight times.

Table 1. Demographic characteristics, spirometry values of the enrolled subjects.

	Healthy	**Severe Asthmatics**
	n=4	n=5
Age, years	47.3 ± 12.5	47.8 ± 8.6
Caucasian Ethnicity	4	5
Male Gender	2	3

2.3. Cell Treatments

The fibroblasts from healthy and severe asthmatic individuals were seeded in 6- or 12-well-plates for experiments, and cultured until reaching ~70% confluency. Then, they were serum-starved in 1% FBS supplemented DMEM for 16 hours (h) and stimulated with 10 µg/ml *dermatophagoides pteronyssinus* House Dust Mite (HDM) extract (low-endotoxin, Greer Laboratories, catalog XPB70D3A25) for 4 h, 8 h, or 24 h. For drug treatment, cells were stimulated with HDM (10 µg/ml) for 1 h then treated with dexamethasone (Dex, 10nM) and/or STING antagonist, H151 (1µM), for the rest of the incubation period.

2.4. Mice

Female BALB/c mice (weighting 18 g – 20 g) were obtained from the University of Sharjah, animal facility. Mice experiments were performed following approval from Animal Care and Use Committee of University of Sharjah (agreement number: ACUC-20–02-11–01); in accordance with the national guidelines for the care of laboratory animals.

For the experiment performed in Lübeck, female BALB/c mice (8 – 12 weeks of age) were obtained from internal breeding and maintained at the University of Lübeck specific pathogen-free facility. This study was approved by the Schleswig-Holstein state authorities (56-5/16, 86-7/17 and 44-5/18). Animal care was provided in accordance with German rights.

All mice were housed under pathogen- and ovalbumin (OVA)-free conditions and kept in sterile, individually ventilated-cages (TECNIPLAST). They were maintained on a 12-h light–dark cycle and fed a sterile, maintenance diet (Altromin 1324 TPF) and sterile-distilled

water. Environmental enrichment was provided by autoclaved dust-free aspen bedding (ABEDD).

2.5. Steroid resistant mouse model and study groups

The experimental protocol for allergen sensitization and challenge was described previously (Gauthier et al., 2017; Raundhal et al., 2015). Briefly, we sensitized mice intranasally to 25 μg HDM extract (low-endotoxin, Greer Laboratories, catalog XPB70D3A2.5) and 5 μg cyclic-di-GMP (cdiGMP, BIOLOG Life Science Institute, catalog C057-05) in 10 μL of phosphate buffered saline (PBS) on days 1, 3, and 5, then rested for 5 days. After the initial sensitization, we challenged mice intranasally with 3 challenge sets with 4 days of rest between each set. Each challenge set included 25 μg HDM and 0.5 μg cdiGMP on day 1, then 25 μg HDM on the following 2 days. Mice were then sacrificed on day 28, and lungs were collected for histology and lung homogenate as illustrated in **figure 3.3.A**.

Six groups of mice were used:

1. Control untreated (PBS),
2. HDM/cdiGMP untreated,
3. HDM/cdiGMP dexamethasone treated (HDM/cdiGMP - Dex),
4. HDM/cdiGMP treated with Dex and H151,
5. HDM/cdiGMP treated with Dex and NP-H151,
6. HDM/cdiGMP treated with Dex and NP.

For Dex treatment, intraperitoneal administration of 4 mg/kg Dex was performed on 1st day of each challenge set and repeated every 3 days until the mice were sacrificed (Gauthier et al., 2017; Raundhal et al., 2015).

For H151 or NP-H151 treatment, 523.8 ng/kg H151 was administered as intranasal drops on 2nd day of each challenge set and repeated every 3 days until the mice were sacrificed.

2.6. Pulmonary IL-33 challenge

Challenging mice with recombinant IL-33 was performed as previously described (Wiese et al., 2023). 500 ng of recombinant IL-33 was administered intratracheally to anesthetized mice on four consecutive days. After 24 h of the final recombinant IL-33

challenge, mice were sacrificed, and lungs were harvested for lung homogenate as illustrated in **figure 3.5.A**.

2.7. Assessment of airway function

Mice were anesthetized with 114.5 mg/kg ketamine and 6.9 mg/kg xylazine administered intraperitoneally and tracheostomized; airway mechanics was assessed using the forced oscillation technique using FlexiVent, a computer-controlled small animal ventilator (SCIREQ, Montreal, Quebec, Canada). Once artificial ventilation has started, mice were injected intraperitoneally with the paralytic rocuronium bromide (2.5 mg/kg). Airway hyperresponsiveness (AHR) was assessed by increasing doses of nebulized methacholine (MCh) challenge test (0, 12.5, 25, 50 mg/ml), as previously described (Quell et al., 2020; Wiese et al., 2023). Total airway, and small airway resistance was reported as calculated in cm H_20.s./mL, and cm H_20/mL, respectively, by using FlexiVent software, version 8.0.4.

2.8. Histological analyses

The lungs were fixed in 10 % formalin, and then embedded in paraffin blocks. The sections (5µm thick) were obtained using a microtome (SLEE Medical GmbH, Germany), then stained with hematoxylin and eosin (H&E) or periodic acid-Schiff (PAS) using a Periodic Acid-Schiff kit (Sigma Aldrich) according to the manufacturer's protocol. The level of perivascular and peribronchial inflammation was evaluated and scored through quantification of the inflammatory cells in different lung sections. According to our score system, score 0, was given when there is no evidence of peribronchial, perivascular, and parenchymal infiltration of inflammatory cells. Score 1 was given to sections that showed evidence of few peribronchial, perivascular, and parenchymal infiltration of inflammatory cells. Score 2: one layer of peribronchial, perivascular, and parenchymal infiltration of inflammatory cells. Score 3: 2-4 layers of inflammatory cells in peribronchial, perivascular, areas. Score 4: extensive inflammatory infiltration (>4 layers of cell rings) in peribronchial, perivascular, and parenchymal areas. PAS-positive mucus-containing cells percentage was used to evaluate goblet cells compared to the total number of the epithelial cells.

2.9. Quantitative Real Time-Polymerase Chain Reaction (qRT-PCR)

qRT-PCR assay was performed as previously described (Ramakrishnan et al., 2020a). The total RNA from fibroblasts or lung homogenates was extracted using Trizol (Invitrogen)

following manufacturer's instructions. RNA concentrations and purity were assessed using Nanodrop spectrophotometer (Thermo Scientific), followed with cDNA synthesis, which was carried out using High-Capacity cDNA Reverse Transcription Kit (Applied Biosystems) in the Veriti Thermal Cycler (Applied Biosystems). Then, qRT-PCR reactions were performed using 5x Hot FirePol EvaGreen qRT-PCR SuperMix (Solis Biodyne) in QuantStudio 3 Real-Time PCR System (Applied Biosystems). The primers are listed in **Table 2**. The Comparative CT (ΔΔCT) method was used to analyze the gene expression after normalization to the housekeeping gene 18s rRNA. All results were expressed as mRNA expression (fold change) relative to healthy non-smoker for baseline measurements or unstimulated controls for treatment.

Table 2. List of human (h) and mouse (m) primer sequences used in qRT-PCR.

Genes	Forward Primer Sequence (5′-3′)	Reverse Primer Sequence (5′-3′)
h-STING	GTACCTGGTGCTCCACCTAGCC	CCCGGTACCTGGAGTGGATGTG
h-TBK1	TTGCGAGATGTGGTGGGTGG	ACACAGACTGTCCATCTTCCCCT
h-IFN-β	CCTGTGGCAATTGAATGGGAGGC	AGATGGTCAATGCGGCGTCCTC
h-IL-6	GAAAGCAGCAAAGAGGCAC	GCACAGCTCTGGCTTGTTCC
h-18s	CTACCACATCCAAGGAAGCA	TTTTTCGTCACTACCTCCCCG
m-cGAS	TGTGGAGCAGCTGAACACTGGC	AGCTCAATCCTGGGGACTTCC
m-STING	CCTAGCCTCGCACGAACTTG	CGCACAGCCTTCCAGTAGC
m-TBK1	GCTCGAGAGCTGGAGGACGATG	CCACAGATCAACGGTAGCCCC
m-IRF3	TGGACGAGAGCCGAACGAGGTT	TGTAGGCACCACTGGCTTCTGC
m-IFN-α	TGCTTTCCTGATGGTCCTGGCG	TCAGGCAGGAGAGAGGGGAGAG
m-IFN-β	CCTCACCTACAGGGCGGACTTC	TCATTCCACCCAGTGCTGGAGA
m-IFN-γ	TCAACAACCCACAGGTCCAGCA	TCAGCAGCGACTCCTTTTCCG
m-IL-17A	ACCGCAATGAAGACCCTGAT	TCCCTCCGCATTGACACA
m-GRα*	AAAGAGCTAGGAAAAGCCATTGTC	TCAGCTAACATCTCTGGGAATTCA
m-GRβ*	AAAGAGCTAGGAAAAGCCATTGTC	CTGTCTTTGGGCTTTTGAGATAGG
m-βactin	CATTGCTGACAGGATGCAGAAGG	TGCTGGAAGGTGGACAGTGAGG

* Primer sequence has been used from (Hinds et al., 2010).

2.10. Western blot

Western blotting assay was performed as previously described (Ramakrishnan et al., 2020b). The proteins from lung cells from all the groups were stimulated or not with 10 μg/ml HDM overnight or fibroblasts were extracted using RIPA lysis buffer (50mM Tris, 150mM NaCl, 1% sodium deoxycholate, 0.1% sodium-dodecyl-sulphate (SDS), 1% Triton X-100, pH7.5), after supplementation with 1x Protease Inhibitor Cocktail (Sigma-Aldrich, Germany) and 1 mM phenylmethylsulfonyl fluoride (Sigma-Aldrich, Germany). The protein lysates were quantified using ThermoScientific Pierce BCA Protein Assay Kit (ThermoFisher Scientific, US). Proteins were resolved in 8.5% or 12.5% SDS polyacrylamide gel, then transferred onto nitrocellulose membranes using semi-dry transfer cell. Membranes were blocked with 5% bovine serum albumin (BSA) for 1 h, then incubated at 4 °C with the following primary antibodies, which are listed in **Table 3**. The membranes were then probed with horseradish peroxidase-conjugated secondary antibodies for 1 h. Sapphire™ NIR-Q Biomolecular Imager (Azure Biosystems, Dublin, US) was used to detect the protein bands, which were subsequently quantified using ImageJ software.

Table 3. List of human (H) and mouse (M) antibodies used in western blot.

Antibodies	Reactivity	Source	Dilution
anti-phospho-STING (Ser365) Rabbit mAb	H	CST (#72971)	1:500
anti-STING Rabbit mAb	H	CST (#13647)	1:1000
anti-phospho-STING (Ser365) Rabbit mAb	M	CST (#72971)	1:500
anti-STING Rabbit mAb	M	CST (#50494)	1:1000
anti-phospho-TBK1/NAK (Ser172) Rabbit mAb	H M	CST (#5483)	1:500
anti-TBK1/NAK Rabbit mAb	H M	CST (#3504)	1:1000
anti-phospho-IRF3 (Ser396) Rabbit mAb	H M	CST (#29047)	1:500
anti-IRF3 Rabbit mAb	H M	CST (#4302)	1:1000
anti-β-actin Rabbit mAb	H M	CST (#4970)	1:1000

2.11. Enzyme-linked immunosorbent assay (ELISA)

Supernatants from fibroblast cell culture after 24 h of stimulation and from mouse lung tissues homogenates were collected to determine the levels of IFN-β using standard ELISA kits according to the manufacturer's instructions (Abcam).

2.12. Lung single cell suspension and alveolar macrophages isolation

Lung harvesting and cell isolation were performed as previously described (Quell et al., 2020). Briefly, whole lung lobes were taken out, cut into small pieces, and incubated under gentle agitation with 0.25 mg/mL liberase TL (Roche, Rotkreuz, Switzerland) and 0.5 mg/mL DNAse I (Sigma-Aldrich, Steinheim, Germany) in RPMI media (Life Technology, Carlsbad, CA, USA) for 45 min at 37 °C. Lungs pieces and cell suspension were passed through 40 µm strainer upon pressing with a syringe plunger, then washed with 10 mL media supplemented with 10% fetal bovine serum (FBS), and 1% penicillin/streptomycin (Sigma-Aldrich, Germany) before centrifugation (500 rcf for 5 min). The excess of red blood cells present in the isolation was removed by red blood cell lysis. After washing, pulmonary cell suspension blocked with an anti-CD16/32 antibody (eBioscience, Darmstadt, Germany) and then CD11c+ cells were sorted using EasySep™ Mouse Pan-DC Enrichment Kit II (StemCell Technologies, Canada; catalog no. 19803).

2.13. Flow cytometry analysis

To evaluate the frequency of high DNA content alveolar macrophages (AMs), and to determine ability of high DNA content AMs subsets to express STING, the sorted $CD11c^{hi}$ cells were rested for 24 h and incubated with Brefeldin A at the last 4 h to inhibit the cytokines secretion. 1 µg/mL of Hoechst 33342 fluorescent nucleic acid stain (ImmunoChemistry Technologies, USA; catalog no. 639) was used to stain DNA. The cells were collected, washed with PBS, and incubated with fixation/permeabilization solution kit (Thermo Fisher Scientific, USA; catalog no. 00-5523-00). The cells were incubated with primary anti-mouse TMEM173/STING rabbit antibody (Proteintech; catalog no. 19851-1-AP) overnight at 4 °C. After washing, the CD11c+ cells were stained for 30 h at 4 °C with anti-mouse Siglec F (clone E50-2440) labeled with APC/Cyanine7 (BioLegend; catalog no. 155532), and secondary anti-rabbit labeled with Alexa Fluor-647 (Abcam; catalog no. ab150079). All the flow antibodies used in these experiments are listed in **Table 4**. Flow cytometry experiment were analyzed using the Cytek Aurora flow cytometer (Cytek Biosciences), and the results was analyzed by FlowJo software.

Table 4. List of mouse (M) antibodies used in flow cytometry.

Antibodies	Fluorophore	Reactivity	Clone	Host/ Isotype	Source	Dilution
CD16/CD32 (FcγRIII/FcγRII)	-	M	-	Rat IgG2b, κ	BD bioscience	1:100
TMEM173/STING	-	M	-	Rabbit	Proteintech (#19851-1-AP)	1:500
Rabbit IgG	Alexa Fluor® 647	R	-	Goat	Abcam (#ab150079)	1:1000
CD170 (Siglec-F)	APC/Cyanine 7	M	E50-2440	Rat IgG2a, κ	BD bioscience	1:400

2.14. Materials used in nanoparticle experiments.

Poly (Lactic-co-Glycolic Acid) 50:50 (PLGA), Mw 38–54 kDa, Kolliphor®, 3-(4,5-dimethyldiazol-2-yl)-2, 5-diphenyltetrazolium bromide (MTT), phosphate buffer saline (PBS), dimethyl sulfoxide (DMSO), paraformaldehyde (PFA), curcumin, SpectraPor® Float-A-Lyzer ® dialysis device with a 3–5 kDa molecular weight cut-off were purchased from Sigma-Aldrich (St. Louis, Missouri, USA). Pierce protein concentrator MWCO 100 kDa was acquired from Thermo Scientific (Waltham, Massachusetts, USA). Mounting Medium with 4,6-diamidino-2-phenylindole (DAPI) were purchased from Abcam (Cambridge, UK).

2.15. H151 nanoparticles (NP-H151) synthesis

Triplicate batches of NP-H151 were synthesized by modified nanoprecipitation method (Attia et al., 2021) as illustrated in **figure 3.9.A**. Briefly, 35 mg of Poly (Lactic-co-Glycolic Acid) (PLGA) (38-54 kDa) were dissolved in 5 mL of dimethyl sulfoxide (DMSO). 5 µL of H151 (10 mg/mL) was added to the polymer solution. The solution was dropped in 20 mL of deionized water containing Kollifor (1% w/v) and stirred overnight at 700 rpm at room temperature (RT). The formed NP were collected by ultracentrifugation at 20,000 rpm for 20 minutes at 20°C and then washed three times with distilled water. Blank PLGA NP without H151 were synthesized using the same procedure.

2.16. Physicochemical characterization of synthesized NP-H151 characterization and morphology evaluation

2.16.1. Particle Size, Polydispersity Index, and Zeta Potential

Dynamic light scattering (DLS) was used to determine NP size distribution (in nm), polydispersity index (PDI), and zeta potential (in mv) of NP-H151 and blank PLGA NP which performed using the Malvern Zeta sizer (Malvern Panalytical Ltd, Malvern, United Kingdom). We reported both the intensity-weighted mean value and surface charge value as the mean ± SD of three measurements.

2.16.2. H151 entrapment efficiency in PLGA NP

Entrapment efficiency (EE) of H151 in PLGA NP was determined using a fluorescence spectrophotometer at RT. The fluorescent intensity was measured at an excitation of 300 nm and an emission of 520 nm using a SynergyHTX microplate reader (Biotek, Winooski, Vermont, USA). Samples were quantified using a standard curve prepared by serial dilution over 0.046–6 µg/mL range (R^2 = 0.999). The EE% (mean ± SD) of H151 in PLGA NP was calculated from three different NP batches using the following equation:

$$\text{Entrapment efficiency \%} = \frac{\text{Measured drug load}}{\text{Theoretical drug load}} \text{X } 100$$

2.16.3. Scanning Electron Microscopy

A scanning electron microscope (SEM) was used to examine NP-H151 and PLGA NP formulations for their morphology, size, surface structure, and topography. Briefly, on a clean slide cover, a drop of the redispersed sample was applied and allowed to dry under vacuum. Drying was then followed by mounting the sample on carbon tape, then sputter-coating under a high vacuum with gold. Using Thermo Scientific Apreo SEM, photomicrographs of gold-coated samples were taken at an acceleration voltage of 5 kV (FEI Company, Hillsboro, Oregon, USA).

2.16.4. In vitro release of H151 from PLGA NP

A dialysis technique was performed in triplicates to evaluate drug release from PLGA NP (Errico et al., 2009).The freshly synthesized PLGA-H151 nanosuspension was

concentrated by centrifugation at 5000 rpm for 30 min using Pierce protein concentrator MWCO 100 kDa (Thermo Scientific,Waltham, Massachusetts, USA). Three milliliters of the concentrated H151 nanosuspension (n = 3) were filled into SpectraPor® Float-A-Lyzer ® dialysis device using a 3–5 kDa molecular weight as cut-off (Sigma-Aldrich, St. Louis, Missouri, USA). Then, the dialysis device was submerged in 10 mL of diffusion medium, DMSO: WATER (70:30), to ensure sink condition. The medium was maintained uniform by stirring in a heated water bath at 37°C. 100 µL from samples were withdrawn over the 48 h at 0, 5, 15, 30 min, and then at 1, 2, 4, 6, 8, 24 and 48 h. Withdrawn volumes were replenished with a fresh medium. The fluorescence of the released H151 in the withdrawn aliquots was measured at an excitation of 300 nm and an emission of 520 nm using a SynergyHTX microplate reader (Biotek, Winooski, Vermont, USA). The mean ± SD percentage of the cumulative amount of drug released was used to expressed the results as per the following equation:

$$\text{Cumulative drug released \%} = \frac{\text{Cumulative concentration of released drug}}{\text{The total amount of drug in nanoparticles}} \text{X } 100$$

2.17. Cell viability assay

For the determination of cell viability, 3-(4,5-dimethyldiazol-2-yl)-2, 5-diphenyltetrazolium bromide (MTT) assay was performed as previously described (Mdkhana et al., 2021b) with slight modification. Briefly, fibroblasts were seeded in 96-well plates at density of 4 X 10^4 cells per well and cultured overnight. Next, the cells were treated with 1 µM of NP-H151, H151 as free drug and blank NP followed by incubation of the culture plates for 24 h at 37 °C at 5 % CO_2. Following the treatment incubation, fibroblasts were washed and 10 µL of MTT solution was added to incubate at 37 °C for 3 h. Then, the formed formazan crystals were dissolved with 100 µL dimethyl sulfoxide (DMSO). Finally, the absorbance was measured using a SynergyTM HTX microplate reader at 570 nm (BioTek, Winooski, VT, USA).

2.18. Determination of cellular uptake using confocal microscopy

2.18.1. Synthesis of Curcumin PLGA NP (CUR-PLGA NP)

CUR-PLGA NP were synthesized by modified nanoprecipitation method (Attia et al., 2021). Briefly, 35 mg of PLGA was dissolved in 5 mL of DMSO. Then, 1 mL of CUR (6.25

mg/ml) was added to the polymer solution. The solution was dropped in 20 mL of water containing Kollifor (1% w/v) and stirred overnight at 700 rpm at room temperature. The formed NP were collected by ultracentrifugation at 20,000 rpm for 20 min at 17°C and then washed three times with distilled water.

2.18.2. Curcumin entrapment efficiency in NP

Entrapment efficiency (EE) of curcumin in PLGA NP was determined using a fluorescence spectrophotometer at room temperature. The curcumin absorbance was measured at a wavelength of 480 nm using a SynergyHTX microplate reader (Biotek, Winooski, Vermont, USA). Samples were quantified using a standard curve prepared by serial dilution over 7.81-500 µg/mL range (R^2 = 0.998). The EE% (mean ± SD) of cucrcumin in PLGA NP was calculated using the following equation:

$$\text{Entrapment efficiency \%} = \frac{\text{Measured drug load}}{\text{Theoretical drug load}} \text{X } 100$$

2.18.3. Confocal microscopy

In vitro cellular uptake of NP-H151 was investigated in fibroblasts using a confocal laser scanning microscope (Haider et al., 2020). Coverslip were placed in 6-well plate where the fibroblasts were seeded on (1 X 10^5 cells/well). 1µM of CUR-PLGA NP were used to treat fibroblasts for 24 h at 37 °C. Next, the fibroblasts were fixed by 5 % paraformaldehyde solution for 30 min after washing the cells with PBS for three times. The nuclei of fibroblasts were then stained for 20 min at RT using a mounting media containing 4,6-diamidino-2-phenylindole (DAPI) after washing the cells twice with PBS. Using a confocal microscope (Nikon eclipse Ti Melville,NY 11747–3064, USA), the fluorescent images of CUR-PLGA NP were captured with a violet laser (405 nm) and blue laser (488 nm) using a magnification of 60x.

2.19. Statistical analysis

The results are presented as mean ± standard error of the mean (SEM) *via* GraphPad Prism software, version 8.00 (GraphPad Software, Inc. La Jolla, CA, USA). Statistical comparisons were performed using unpaired independent student's t-test for baseline expression comparison, one-way ANOVA followed by the post hoc Bonferroni test for multiple comparisons, and two-way ANOVA followed by post hoc Bonferroni test for multiple

comparisons among different groups. Statistical significance was accepted at a level of $p < 0.05$.

Chapter III.

Results

Recently, STING pathway has emerged as an interesting and effective target to control chronic lung inflammation, such as asthma. Therefore, we first determined the activation level of STING pathway during chronic lung inflammation.

3.1. STING level is increased in the lungs of various inflammatory mouse models based on in-silico data.

The expression of the STING was evaluated using transcriptomic datasets of alveolar macrophages (GSE148590) and lungs (GSE137324 and GSE132377) obtained from HDM sensitized mice. Following HDM sensitization, STING level was increased in both alveolar macrophages and whole lung tissue. GSE148590 data showed that STING level was significantly increased ($p<0.001$) in alveolar macrophages after three weeks of HDM sensitization (**Fig. 3.1.A**). In a second study (GSE137324), STING was elevated after four weeks ($p<0.0001$) and 15 weeks ($p<0.0001$) of HDM exposure (**Fig. 3.1.B**). Interestingly, STING upregulation was more pronounced ($p<0.05$) after 15 weeks compared to four weeks. The STING gene was also increased ($p<0.0001$) in whole lung tissue samples when mice were sensitized with HDM plus cyclic-di-GMP in a third study by Gerthoffer et al (GSE132377) (**Fig. 3.1.C**).

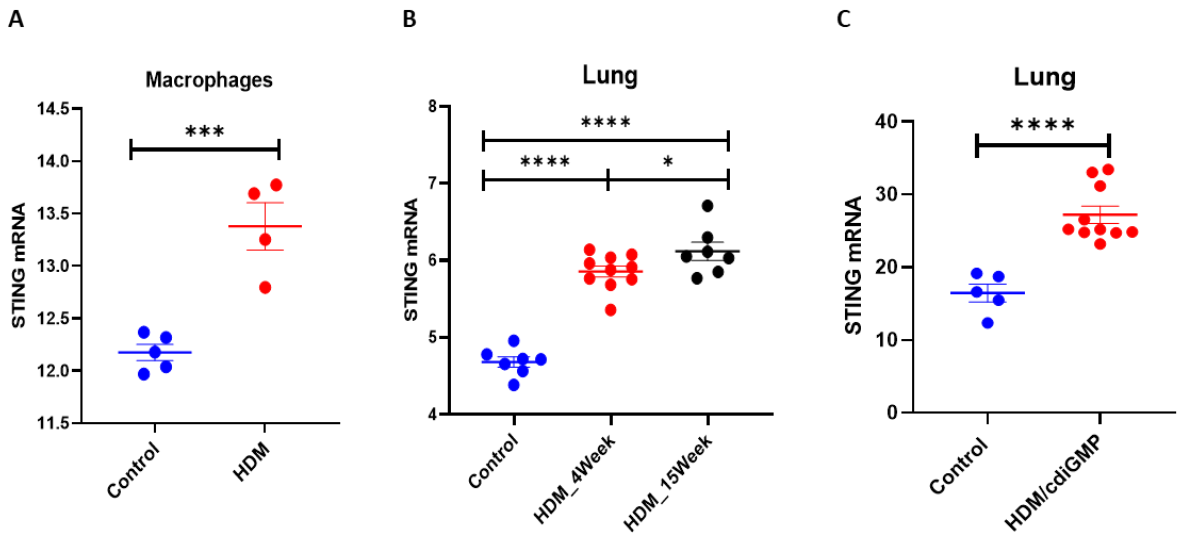

Figure 3.1. STING level is increased in the lungs of various inflammatory mouse models based on in-silico data.

(A) The gene expression of STING was elevated in macrophages from HDM sensitized mice compared to unsensitized group. The values were compared across the different groups using unpaired student's t-test between the groups. **(B)** STING mRNA level was higher in lung tissues upon HDM sensitization for 4 weeks and to higher extend after 15 weeks of HDM sensitization, compared to control group. The values were compared across the different groups using one-way ANOVA followed by post hoc Bonferroni test for multiple comparisons. **(C)** STING expression was increased in lung tissues from HDM plus cyclic-di-GMP sensitized mice compared to unsensitized group. The values were compared across the different groups using unpaired student's t-test between the groups. Results are presented as mean (± SEM) and relative to control group. The following datasets were used; GSE148590 (n=4 HDM, vs n=5 controls), GSE137324 (n=10 HDM_4weeks, n=7 HDM_15weeks, vs n=7 controls), and GSE132377 (n=10 HDM/cdiGMP, vs n=5 controls). For all analyses, $p < 0.05$ was considered significant. $*p < 0.05$, $***p < 0.001$, $****p < 0.0001$.

3.2. Elevated baseline STING expression in severe asthma fibroblasts.

We then examined the baseline profile of the STING pathway in severe asthma human bronchial fibroblasts to understand its role in the pathogenesis of this diseases. The mRNA and protein expression levels of intermediates in the STING pathway, such as STING, TBK1, IRF3 and interferon type I (IFN-β), were examined in fibroblasts from healthy, and severe asthmatic patients. At baseline, in comparison to healthy fibroblasts, STING gene expression was higher in severe asthma with a 3.4 fold increase ($p<0.001$) as shown in **figure 3.2.A**. The baseline expression of TBK1 gene was elevated in severe asthma by 2.3 fold ($p<0.05$) (**Fig. 3.2.B**). Similarly, IFN-β gene expression was increased in severe asthma by 3.5 fold ($p<0.0001$) (**Fig. 3.2.C**).

We next investigated the protein expression of STING, TBK1, and IRF3 in these fibroblasts. STING protein level was elevated in severe asthma by 2.5 fold ($p<0.05$) when compared to healthy fibroblasts (**Fig. 3.2.D**). Further, TBK1 protein level was higher in severe asthma by 2.0 fold ($p<0.05$) (**Fig. 3.2.E**). In severe asthma, the protein level of IRF3 was increased by 5.0 fold ($p<0.05$) in comparison to healthy (**Fig. 3.2.F**).

These results suggest that STING pathway is elevated in severe asthma fibroblasts.

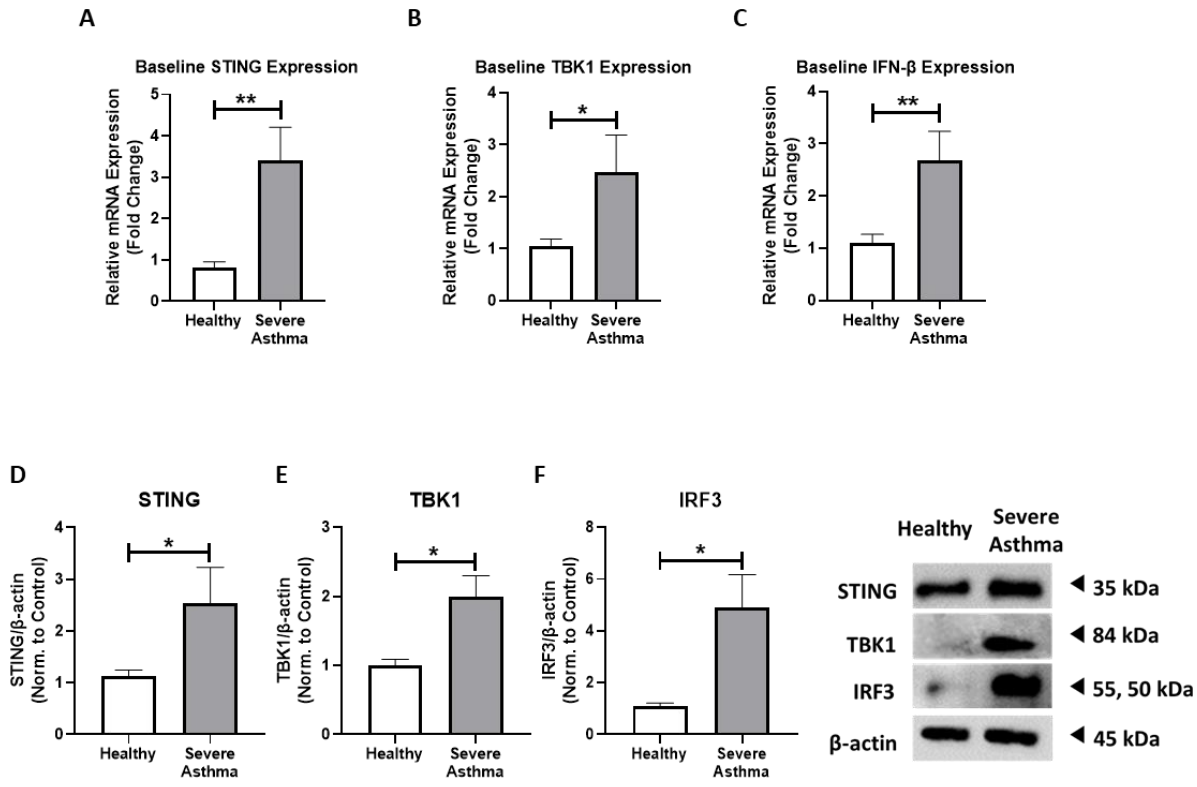

Figure 3.2. Elevated baseline STING expression in severe asthma fibroblasts.

The baseline gene expression of STING **(A)**, TBK1 **(B)**, and IFN-β **(C)** in healthy, and severe asthmatic fibroblasts. Data representative of 3-6 independent experiments from 3-5 unique donors in each group. Representative western blots of STING pathway in healthy, and severe asthmatic fibroblasts. Densitometric analysis of immunoblots depicting expression of STING **(D)**, TBK1 **(E)**, and IRF3 **(F)**. β-actin was used as a loading control. Data representative of 2-3 independent experiments from 2-3 unique donors in each group. Results are presented as mean (± SEM) and relative to healthy fibroblasts. The values were compared across the different groups using independent student's t-test between the groups. $*p < 0.05$, $**p < 0.01$.

3.3. House dust mite plus cyclic-di-GMP induce severe asthma in a mouse model with steroid hyporesponsiveness.

Our next goal was to establish a steroid resistant mouse model in order to investigate STING activity *in-vivo*; thus, the combination of HDM antigen with cyclic-di-GMP (cdiGMP) as an adjuvant was used to develop lung inflammation with Th1/Th17 bias with corticosteroid-resistance as previously established (**Fig. 3.3.A**). We first studied the gene expression of IFN-

γ and IL-17 and both showed to be upregulated in HDM/cdiGMP-immunized mice by 10.3 fold ($p<0.05$), and 7.1 fold ($p<0.01$), respectively, relative to control mice (**Fig. 3.3.B and C**).

Moreover, lung inflammation was also confirmed by histological examination of lung tissue sections. Control mice showed clear bronchiolar lumens with no inflammatory cell infiltration (**Fig. 3.3.D and E**). While HDM/cdiGMP-immunized mice had intense mucus staining ($p<0.01$) and narrowed bronchiolar lumen with peribronchial, perivascular, and parenchymal infiltration of inflammatory cells ($p<0.0001$) (**Fig. 3.3.D and E**).

The major mechanism underlining the steroid resistance in severe asthma is the dysregulation of GRα/GRβ ratio. Hence, we investigated this next in our mouse model of severe asthma with steroid resistance. Interestingly, HDM/cdiGMP-immunized mice showed a significant increase in GRβ by 6.9 fold ($p<0.001$), while the GRα expression did not significantly change, in comparison to control mice (**Fig. 3.3.F and G**). Further, the GRα/GRβ ratio was significantly lowered ($p<0.0001$) in HDM/cdiGMP-immunized mice relative to control mice group (**Fig. 3.3.H**).

AHR of HDM/cdiGMP-immunized mice increased with escalating doses of methacholine (MCh) and was higher than non-immunized mice (PBS) as represented by total resistance ($p<0.05$) (**Fig. 3.3.I**), and small airways resistance ($p<0.001$) (**Fig. 3.3.J**). Interestingly, AHR of treated HDM/cdiGMP mice with dexamethasone was not significantly reduced in comparison to untreated HDM/cdiGMP mice (**Fig. 3.3.I and J**).

This data confirmed the establishment of sustained lung tissue inflammation with steroid hyporesponsiveness, a characteristic feature of severe asthma, in our mouse model.

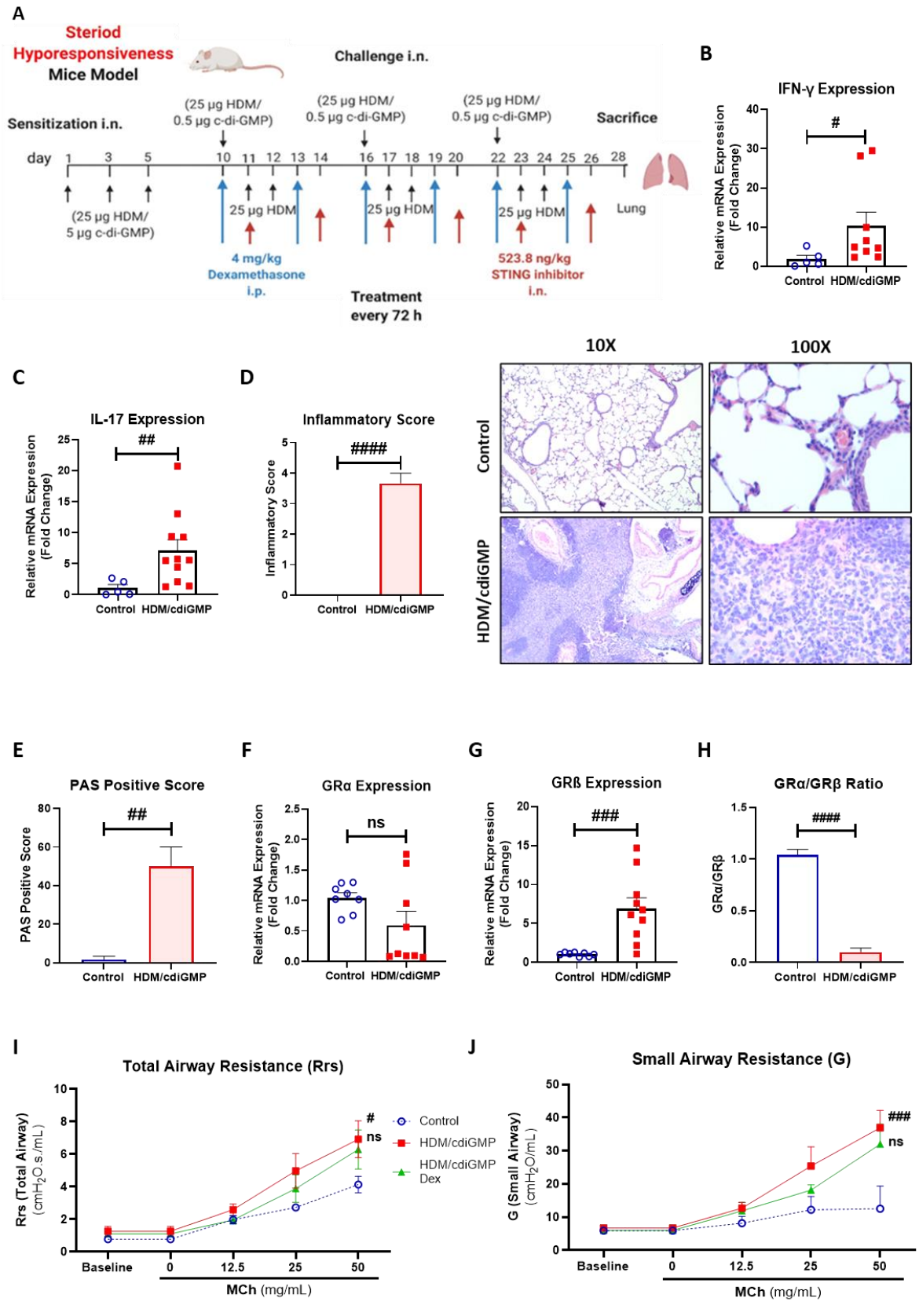
A
Steriod
Hyporesponsiveness
Mice Model
Challenge i.n.
Sensitization i.n.
(25 µg HDM/
0.5 µg c-di-GMP)
(25 µg HDM/
0.5 µg c-di-GMP)
(25 µg HDM/
0.5 µg c-di-GMP)
Sacrifice
day 1 3 5 10 11 12 13 14 16 17 18 19 20 22 23 24 25 26 28
(25 µg HDM/
5 µg c-di-GMP)
25 µg HDM
25 µg HDM
25 µg HDM
Lung
4 mg/kg
Dexamethasone
i.p.
523.8 ng/kg
STING inhibitor
i.n.
Treatment
every 72 h
B
IFN-γ Expression
Relative mRNA Expression
(Fold Change)
#
Control HDM/cdiGMP
C
IL-17 Expression
Relative mRNA Expression
(Fold Change)
##
Control HDM/cdiGMP
D
Inflammatory Score
Inflammatory Score
####
Control HDM/cdiGMP
10X
100X
Control
HDM/cdiGMP
E
PAS Positive Score
PAS Positive Score
##
Control HDM/cdiGMP
F
GRα Expression
Relative mRNA Expression
(Fold Change)
ns
Control HDM/cdiGMP
G
GRß Expression
Relative mRNA Expression
(Fold Change)
###
Control HDM/cdiGMP
H
GRα/GRβ Ratio
GRα/GRβ
####
Control HDM/cdiGMP
I
Total Airway Resistance (Rrs)
Rrs (Total Airway)
(cmH2O.s./mL)
#
ns
Control
HDM/cdiGMP
HDM/cdiGMP
Dex
Baseline 0 12.5 25 50
MCh (mg/mL)
J
Small Airway Resistance (G)
G (Small Airway)
(cmH2O/mL)
###
ns
Baseline 0 12.5 25 50
MCh (mg/mL)

Figure 3.3. House dust mite plus cyclic-di-GMP induce severe asthma mouse model with steroid hyporesponsiveness.

(**A**) Schematics of the asthma model used in the study. Mice were sensitized and challenged with or without treatments. The gene expression of IFN-γ (**B**), IL-17 (**C**) were compared severer asthma vs control mice. Data representative of n = 5-11 mice in each group. (**G**) Inflammation score in H&E-stained lung tissues H&E. (**H**) PAS positive score of PAS stained lung sections. Data presented as mean (± SEM) and representative of n = 3-4 mice in each group. The gene expression of GRα (**D**), GRβ (**E**) and GRα/GRβ ratio (**F**) were compared severer asthma vs control mice. Data representative of n = 5-11 mice in each group. The values were compared across the different groups using independent student's t-test between the groups. ns P > 0.05, #P < 0.05, ##P < 0.01, ###P < 0.001, ####P < 0.0001 vs control mice. Data showed airway function measurements by forced oscillatory technique using different doses of MCh. (**I**) Assessment of total airway resistance (Rrs) to MCh. (**J**) Assessment of small airway resistance to MCh. Data representative of n = 6-9 mice in each group. The values were compared across the different groups using two-way ANOVA followed by post hoc Bonferroni test for multiple comparisons. Results are presented as mean (± SEM) and relative to control mice. ns p > 0.05 vs severe asthma mice. #P < 0.05, ##P < 0.01, ###P < 0.001, ####P < 0.0001 vs control mice.

3.4. The elevated baseline level of STING pathway in lung tissue of steroid resistant asthmatic mouse model.

To confirm the in silico results of the increased level of STING in severe asthmatic mice model (**Fig.1**), the mRNA and protein expression levels of STING pathway intermediates, cGAS, STING, TBK1, and IRF3, were examined in HDM/cdiGMP-immunized mice relative to control mice. The gene expression of cGAS, STING, TBK1, and IRF3, in lung tissue were upregulated in HDM/cdiGMP-immunized mice by 2.4 fold ($p<0.05$), 5.6 fold ($p<0.01$), 4.3 fold ($p<0.001$), and 2.8 fold ($p<0.01$), respectively, when compared to control mice (**Fig. 3.4.A-D**). Further, the mRNA levels of type I interferons, IFN-α, and IFN-β, were also upregulated by 12.0 fold ($p<0.01$), and 5.2 fold ($p<0.01$), respectively, in HDM/cdiGMP-immunized mice in comparison to control mice (**Fig. 3.4.E and F**).

In parallel, the expression and activation of protein level were detected using western blot analysis. The lung cells from all the groups were stimulated or not with 10 μg/ml HDM overnight to investigate the level of phosphorylation. Interestingly, the activation of STING, TBK1, and IRF3 by phosphorylation was increased in the HDM/cdiGMP group by 3.5 fold ($p<0.001$), 6.1 fold ($p<0.001$), and 3.4 fold ($p<0.001$), respectively, when compared to control

group (**Fig. 3.4.G-L**). Interestingly, increased IFN-β was secreted upon HDM/cdiGMP sensitization and challenge when compared with vehicle control group by 74% ($p<0.05$) (**Fig. 3.4.M**).

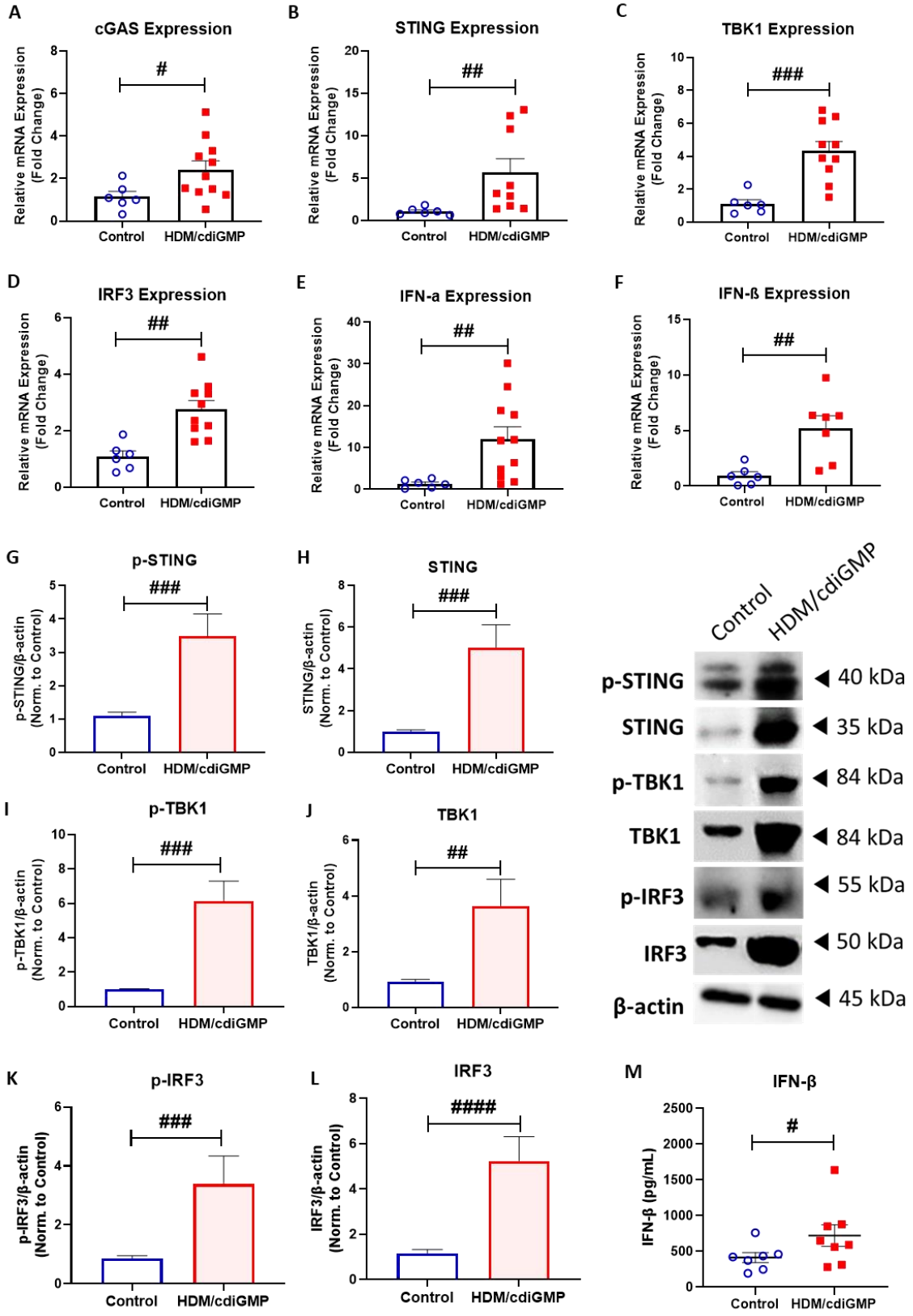

Figure 3.4. The elevated baseline level of STING pathway in lung tissue of steroid resistant asthmatic mouse model.

The gene expression of cGAS (**A**), STING (**B**), TBK1 (**C**), IRF3 (**D**), IFN-α (**E**) and IFN-β (**F**) was compared in treated and untreated severer asthma mice. Data representative of n = 5-11 mice in each group. Representative western blots and densitometric analysis of STING pathway members in mice model, the lung cells from all the groups were stimulated or not with 10 μg/ml HDM overnight (**G-L**). β-actin was used as a loading control. Data representative from of n = 4-13 mice in each group. Concentration of IFN-β from lung homogenate was analyzed by ELISA (**M**). Data representative from n = 7-8 mice in each group. Results are presented as mean (± SEM) and relative to control mice. The values were compared across the different groups using independent student's t-test between the groups. ∗p < 0.05, ∗∗p < 0.01, ∗∗∗p < 0.001, ∗∗∗∗p < 0.0001 vs. severe asthma mice. #p < 0.05, ##p < 0.01, ###p < 0.001, ####p < 0.0001 vs. control mice.

3.5. Upregulation of STING in polynucleated alveolar macrophages in response to IL-33 challenge.

It is well appreciated that HDM exposure triggers IL-33 production, which is the initial danger signal in asthma. Therefore, we challenged the mice with IL-33 in order to investigate STING activation (**Fig. 3.5.A**). Upon sorting CD11c+ cells from lung tissue, we have identified a population of SiglecF+ representing resident tissue-associated AMs. We observed a strong infiltration of CD11c+ SiglecF+ AMs in lung tissue of IL-33 challenged mice compared to control group (**Fig. 3.5.B**). As previously described, IL-33 induced DNA damage in resident tissue-associated AMs resulted in signs of polynucleation and polyploidy. Therefore, we used Hoechst 33342 staining to stain DNA and to characterize the polynucleation. We have characterized DNA content into high DNA representing polynucleated AMs and low DNA representing mononucleated AMs. Interestingly, the high DNA content were expressed only in IL-33 challenged mice (**Fig.3.5.C**). Since, STING was associated with cytosolic self-dsDNA in response to DNA damage, we then thought to investigate the STING expression by flow cytometry. The expression of STING showed an increase in AMs sorted from IL-33 challenged mice relative to control group (**Fig.3.5.D**), which was to higher extent in high DNA content AMs from IL-33 challenged mice in comparison to low DNA content AMs (**Fig.3.5.E**).

Upon combining the human and mouse data, the STING pathway appears to be upregulated in chronic lung inflammation which may underline the poor disease management observed in this subset.

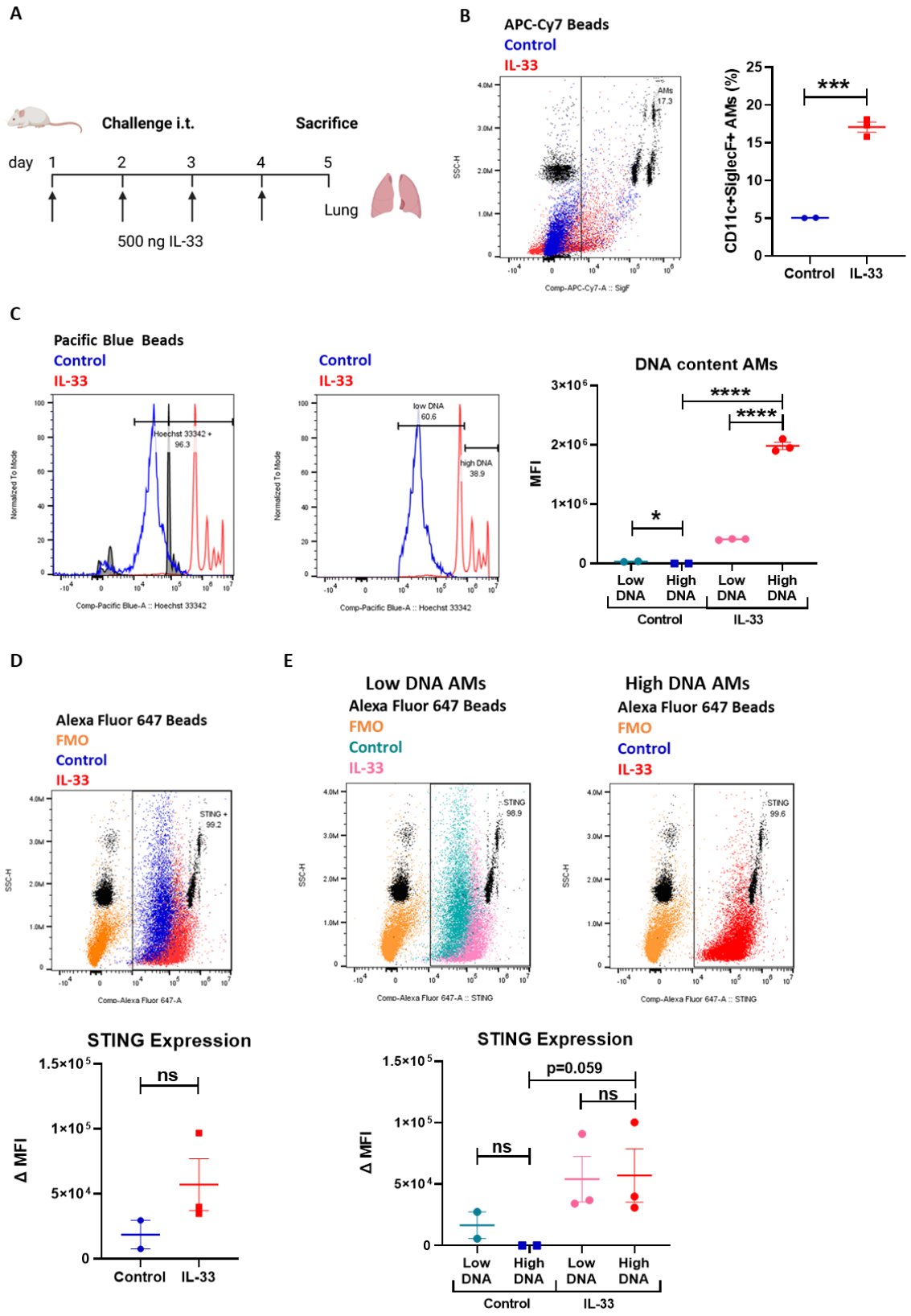
A
Challenge i.t.
Sacrifice
day 1 2 3 4 5
Lung
500 ng IL-33
B
APC-Cy7 Beads
Control
IL-33
AMs
17.3
SSC-H
Comp-APC-Cy7-A :: SigF
CD11c+SiglecF+ AMs (%)
***
Control
IL-33
C
Pacific Blue Beads
Control
IL-33
Hoechst 33342 +
96.3
Normalized To Mode
Comp-Pacific Blue-A :: Hoechst 33342
low DNA
60.6
high DNA
38.9
DNA content AMs
MFI
****
****
*
Low DNA
High DNA
Low DNA
High DNA
Control
IL-33
D
Alexa Fluor 647 Beads
FMO
Control
IL-33
STING +
99.2
SSC-H
Comp-Alexa Fluor 647-A
STING Expression
Δ MFI
ns
Control
IL-33
E
Low DNA AMs
Alexa Fluor 647 Beads
FMO
Control
IL-33
STING
98.9
Comp-Alexa Fluor 647-A :: STING
High DNA AMs
Alexa Fluor 647 Beads
FMO
Control
IL-33
STING
99.6
Comp-Alexa Fluor 647-A :: STING
STING Expression
Δ MFI
p=0.059
ns
ns
Low DNA
High DNA
Low DNA
High DNA
Control
IL-33

Figure 3.5. Upregulation of STING in polynucleated alveolar macrophages in response to IL-33 challenge.

(**A**) Schematics of pulmonary IL-33 challenge used in this study. Mice were challenged intratracheally with IL-33 for four days. (**B**) Dot plots of CD11c+ sorted cells from control (Blue) or IL-33 (red)-immunized mice. SiglecF were used to discriminate AMs from other CD11c+ sorted lung cells. AMs were identified by expression of SiglecF+ and CD11c+, while dendritic cells are SiglecF- CD11c+, and eosinophils are SglecF+ CD11c intermediate. Results are presented as percentage of SiglecF+ cells in CD11c sorted lung cells (± SEM). (**C**) Quantification of DNA content by Hoechst 33342 staining whereas the high DNA content represented the polynucleated AMs and low DNA content represented the mononucleated AMs upon 4× PBS (Blue) or IL-33(red) exposure. Results are presented as MFI (± SEM). Data representative from n = 2-3 mice in each group. The values were compared across the different groups using one-way ANOVA followed by post hoc Bonferroni test for multiple comparisons. $*p < 0.05$, $****p < 0.0001$. (**E**) Dot plots of STING+ AMs from control (Blue) or IL-33 (red)-immunized mice. Results are presented as MFI of the signal normalized to the FMO control (ΔMFI) (± SEM). (**F**) Dot plots of STING+ in low DNA or high DNA content AMs. Results are presented as ΔMFI (± SEM). Data representative from n = 2-3 mice in each group. The values were compared across the different groups using one-way ANOVA followed by post hoc Bonferroni test for multiple comparisons.

We next investigated the responsiveness of STING pathway to steroid treatment versus a combination of steroid and STING inhibitor.

3.6. In-silico transcriptomic analysis of severe asthma mouse models revealed that elevation of STING expression correlates with steroid hyporesponsiveness

Analysis of the GSE132377 dataset revealed that STING gene levels differed significantly between groups ($p<0.001$), with HDM/cyclic-di-GMP exposure triggering a significant increase in STING expression. However, such increase was not significantly changed upon dexamethasone treatment (**Fig. 3.6**). This suggested that STING elevation is resistant to steroid treatment.

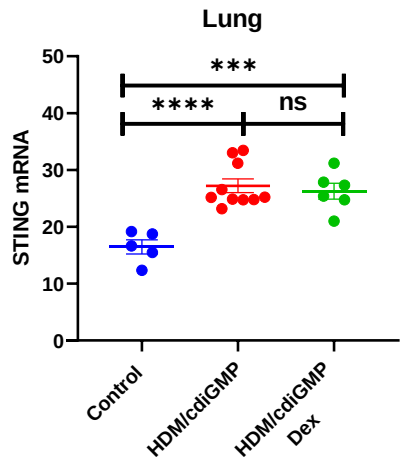

Figure 3.6. In-silico transcriptomic analysis of severe asthma mouse models revealed elevation of STING activity with steroid hyporesponsiveness.

STING expression was increased in lung tissues from HDM sensitized mice compared to unsensitized group. Results are presented as mean (± SEM) and relative to control group. The following dataset was used; GSE132377 (n=10 HDM/cdiGMP, n=10 HDM/cdiGMP + dexamethasone, vs n=5 controls). The values were compared across the different groups using one-way ANOVA followed by post hoc Bonferroni test for multiple comparisons. For all analyses, $p < 0.05$ was considered significant. ***$p < 0.001$, ****$p < 0.0001$.

3.7. STING expression and activity is resistant to dexamethasone therapy in severe asthmatic fibroblasts but sensitive to combination of STING inhibitor and dexamethasone.

Healthy non-smoker fibroblasts were first stimulated with *dermatophagoides pteronyssinus* HDM which is known to activate cGAS-STING pathway. STING, TBK1, IFN-β, and IL-6 gene expression levels were detected in healthy fibroblasts upon HDM stimulation for 4 h and showed upregulation by 2.0 fold ($p<0.01$), 2.1 fold ($p<0.05$), 5.1 fold ($p<0.0001$), and 3.0 fold ($p<0.0001$), respectively in comparison to unstimulated control, as shown in **figure 3.7.A-D.** Upon treatment with dexamethasone, the upregulated STING, TBK1, IFN-β and IL-6 were significantly decreased by 1.1 fold ($p<0.05$), 1.3 fold ($p<0.05$), 2.9 fold ($p<0.05$), and 0.3 fold ($p<0.0001$), respectively when compared to HDM stimulation (**Fig. 3.7.A-D**). We next used the proposed combination of dexamethasone and STING inhibitor (H151), which significantly downregulated the mRNA levels of STING, TBK1 and IFN-β by 0.5 fold

($p<0.05$), 0.4 fold ($p<0.01$), and 0.8 fold ($p<0.05$), respectively, upon the combination treatment in comparison to dexamethasone single treatment (**Fig. 3.7.A-C**).

In parallel, both the protein expression and activity were affected upon HDM stimulation in healthy fibroblasts. The phosphorylated STING, TBK1, and IRF3 was induced by 1.9 fold ($p<0.001$), 1.9 fold ($p<0.01$), and 2.5 fold ($p<0.01$), respectively, upon 8h stimulation by HDM relative to unstimulated control. Then, the treatment with dexamethasone significantly inhibited the activation by phosphorylation of STING, TBK1, and IRF3 by 0.6 fold ($p<0.01$), 0.8 fold ($p<0.05$), 0.8 fold ($p<0.05$), respectively when compared to HDM stimulation. The phosphorylation of STING, TBK1, and IRF3 was further inhibited when treated with the proposed dexamethasone and H151 combination by 0.8 fold ($p<0.01$), 0.4 fold ($p<0.05$), and 0.5 fold ($p<0.05$), respectively in comparison to dexamethasone treatment (**Fig. 3.7.E-J**). Further, the IFN-β secretion was suppressed by 22% ($p<0.05$) upon treatment with the proposed combination for 24 h stimulation when compared to dexamethasone treatment alone (**Fig. 3.7.K**).

Since STING pathway was also activated in severe asthmatic fibroblasts (**Fig. 3.2**), we then thought to investigate the inhibition of STING pathway by commonly used steroid treatment, dexamethasone, upon HDM stimulation. First, severe asthmatic fibroblasts were stimulated with *dermatophagoides pteronyssinus* HDM for 4 h, the gene expression of STING, TBK1, and IFN-β were upregulated by 2.8 fold ($p<0.001$), 2.5 fold ($p<0.01$), and 3.7 fold ($p<0.001$), respectively in comparison to unstimulated control, as shown in **figure 3.8.A-C.** However, the upregulated STING, TBK1, and IFN-β were significantly decreased upon treatment with dexamethasone, by 0.9 fold ($p<0.001$), 1.2 fold ($p<0.05$), and 1.1 fold ($p<0.001$), respectively in comparison to HDM stimulation (**Fig. 3.8.A-C**). Then, the combination of dexamethasone and STING inhibitor (H151) significantly downregulated the mRNA levels of STING, TBK1 and IFN-β by 0.3 fold ($p<0.05$), 0.4 fold ($p<0.05$), and 0.5 fold ($p<0.05$), respectively, when compared to dexamethasone single treatment (**Fig. 3.8.A-C**).

In parallel, the effect of the proposed treatment was also confirmed on the protein level using western blot analysis. The activation of STING, TBK1, and IRF3 by phosphorylation was induced by HDM stimulation for 8h by 3.1 fold ($p<0.01$), 2.6 fold ($p<0.01$), and 2.0 fold ($p<0.05$), respectively, relative to unstimulated control. Upon dexamethasone treatment, the phosphorylated STING, TBK1, and IRF3 were not significantly inhibited when compared to HDM stimulation. Then, the proposed dexamethasone and H151 combination further inhibited the phosphorylation of STING, TBK1, and IRF3 by 1.2 fold ($p<0.05$), 1.9 fold ($p<0.001$), and

1.7 fold ($p<0.01$), respectively in comparison to dexamethasone treatment (**Fig. 3.8.D-I**). Importantly, dexamethasone did not significantly suppress IFN-β secretion while H151 as well as the combination significantly suppressed the release of this proinflammatory cytokine (**Fig. 3.8.J**).

Collectively, STING inhibitor has an additive anti-inflammatory effect when combined with commonly used steroid treatment in severe asthma.

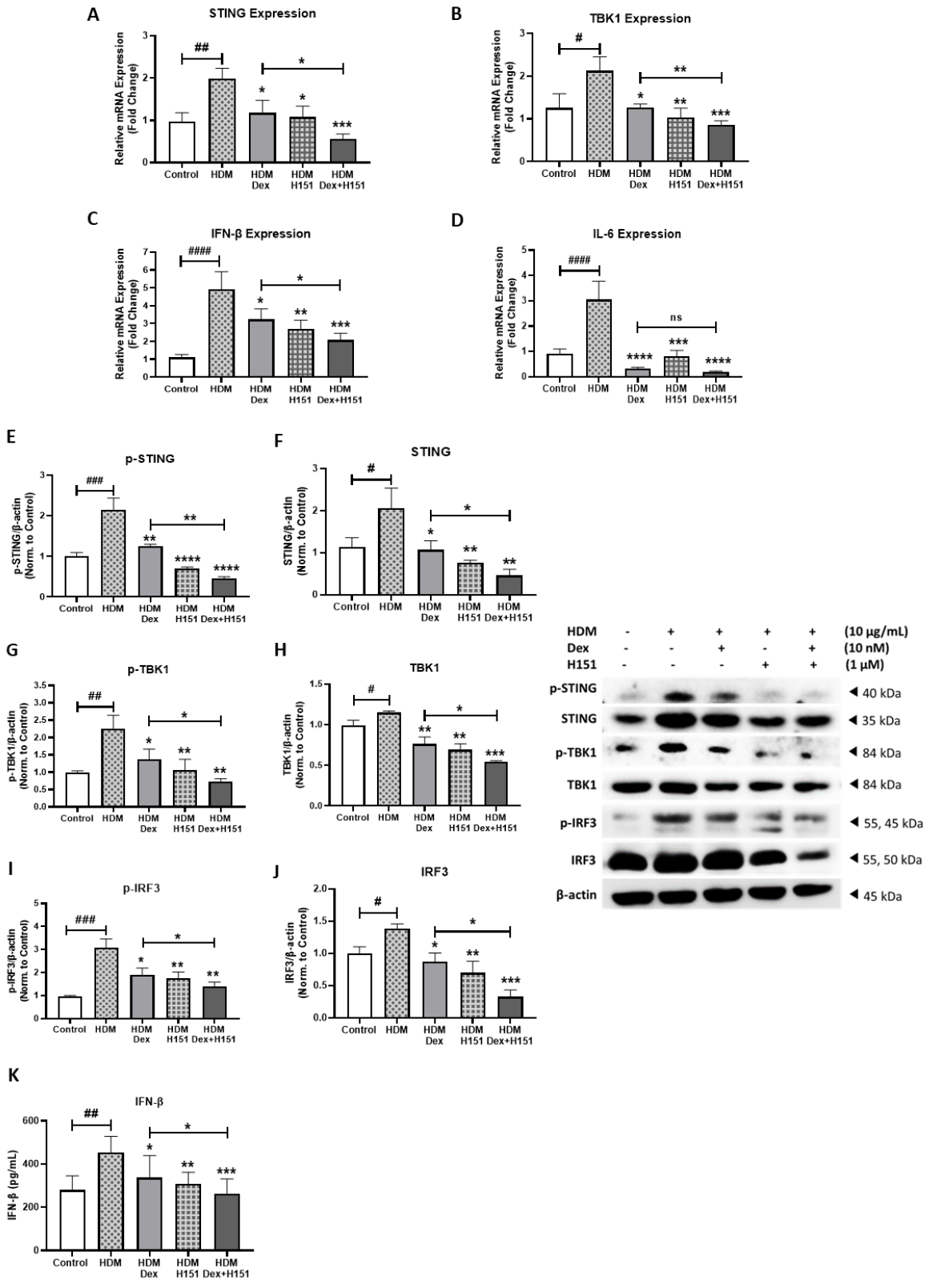

Figure 3.7. STING pathway is suppressed by dexamethasone in healthy non-smoker fibroblasts and STING inhibitor induced an additive effect.

The gene expression of STING **(A)**, TBK1 **(B)**, IFN-β **(C),** and IL-6 (**D**) was compared upon stimulation with HDM for 4 h, then treatment with dexamethasone (Dex), and STING inhibitor (H151) either alone or in combination in healthy fibroblasts. Data representative of 2 independent experiments from 2 unique donors. At indicated concentration of the stimulant and treatment for 8 h, representative western blots and densitometric analysis of immunoblots depicting the expression of STING pathway members **(E-J)**. Data representative from two unique donors. β-actin was used as a loading control. Concentration of type I IFN (IFN-β) in the culture media upon 24 h stimulation was analyzed by ELISA **(K)**. Data representative from two unique donors. Results are presented as mean (± SEM) and relative to unstimulated control. The values were compared across the different groups using one-way ANOVA followed by post hoc Bonferroni test for multiple comparisons. $*p < 0.05$, $**p < 0.01$, $***p < 0.001$, $****p < 0.0001$ vs. HDM stimulation. $\#p < 0.05$, $\#\#p < 0.01$, $\#\#\#p < 0.001$, $\#\#\#\#p < 0.0001$ vs. unstimulated control.

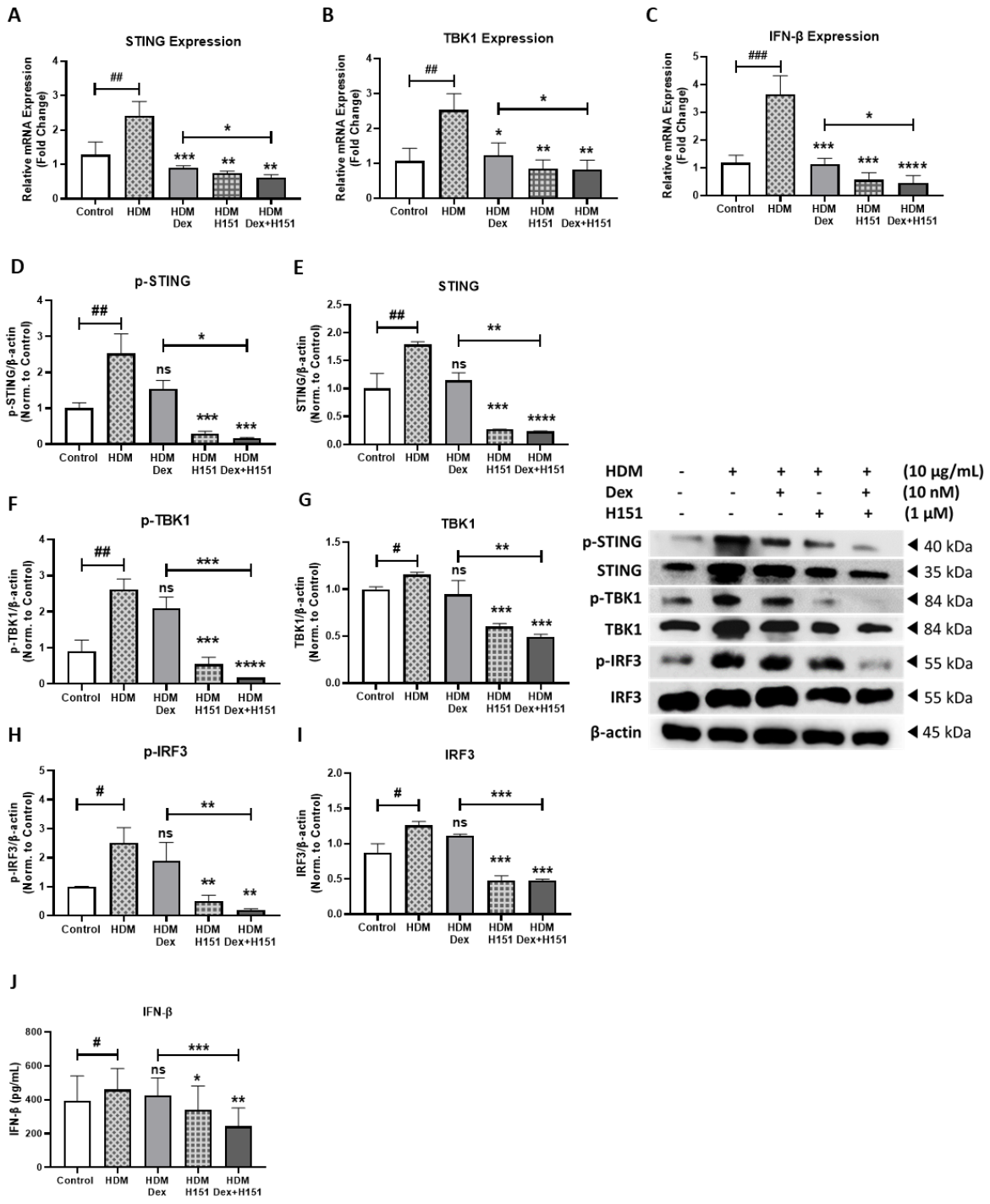

Figure 3.8. STING activity is resistant to dexamethasone therapy in severe asthmatic fibroblasts but sensitive to combination of STING inhibitor and dexamethasone.

The gene expression of STING **(A)**, TBK1 **(B)**, and IFN-β **(C)** was compared upon stimulation for 4 h with HDM, then treatment with Dex, H151 and combination in severe asthmatic fibroblasts. Data representative of 2-4 independent experiments from 4 unique donors. Representative western blots and densitometric analysis of STING pathway members in severe asthmatic fibroblasts at indicated

concentration of the stimulant and treatment for 8 h **(D-I)**. β-actin was used as a loading control. Data representative from two independent experiments. Concentration of IFN-β in the culture media after 24 h of stimulation was analyzed by ELISA **(J)**. Data representative from two independent experiments. Results are presented as mean (± SEM) and relative to unstimulated control. The values were compared across the different groups using one-way ANOVA followed by post hoc Bonferroni test for multiple comparisons. ∗p < 0.05, ∗∗p < 0.01, ∗∗∗p < 0.001, ∗∗∗∗p < 0.0001 vs. HDM stimulation. #p < 0.05, ##p < 0.01, ###p < 0.001, ####p < 0.0001 vs. unstimulated control.

3.8. STING pathway in severe asthma mouse model is resistant to dexamethasone treatment, but responsive to combination treatment of STING inhibitor and dexamethasone.

In the severe asthma mice model, STING pathway was activated (**Fig. 3.4**), and in agreement to the in-vitro work on severe asthmatic fibroblasts, we first investigated whether the commonly used steroid treatment, dexamethasone, inhibits STING pathway in our in-vivo model of steroid resistant severe asthma. Upon dexamethasone treatment, the upregulated gene expression of STING pathway intermediates, cGAS, STING, TBK1, IRF3, IFN-α, and IFN-β were not significantly reduced when compared to HDM/cdiGMP-immunized mice (**Fig. 3.9.A-F**). We next proposed the use of dexamethasone in combination with STING inhibitor (H151). Then, the effect of combination treatment on both the gene and protein expression of STING pathway intermediates were examined. The mRNA levels of cGAS, STING, and IRF3 were not significant reduced when treated with combination therapy when compared to dexamethasone single treatment, except for TBK1 ($p<0.05$) (**Fig. 3.9.A-D**). Interestingly, the gene expression of IFN-α, and IFN-β were significantly reduced upon combination treatment relative to dexamethasone treated group by 6.2 fold ($p<0.05$), and 3.1 fold ($p<0.05$), respectively (**Fig. 3.9.E and F**).

Similarly, the protein level was examined using western blot. The lung cells from all the groups were stimulated or not with 10 μg/ml HDM overnight to investigate the level of phosphorylation. The increase in the phosphorylated STING intermediates and the secreted IFN-β were not significantly lowered by dexamethasone treated group relative to HDM/cdiGMP untreated group (**Fig. 3.9.G-M**). The phosphorylation of STING, TBK1, and IRF3 upon dexamethasone and H151 treatment was significantly lowered by 1.1 fold ($p<0.05$), 1.7 fold ($p<0.05$), and 1.4 fold ($p<0.05$), respectively, when compared to dexamethasone alone treatment group (**Fig. 3.9.G-L**). However, the protein level of STING, TBK1, and IRF3 upon

dexamethasone and H151 treatment was not significantly changed when compared to dexamethasone alone treatment group (**Fig. 3.9.G-L**). Interestingly, the combination treatment group suppressed IFN-β secretion by 41% ($p<0.05$) when compared to dexamethasone treatment alone group (**Fig. 3.9.M**).

Taken together, STING pathway appears to be refractory to corticosteroid in severe asthmatics which may underline the poor disease management. STING inhibitor augmented the inhibition of the activated STING in-vivo model with corticosteroid-resistant features.

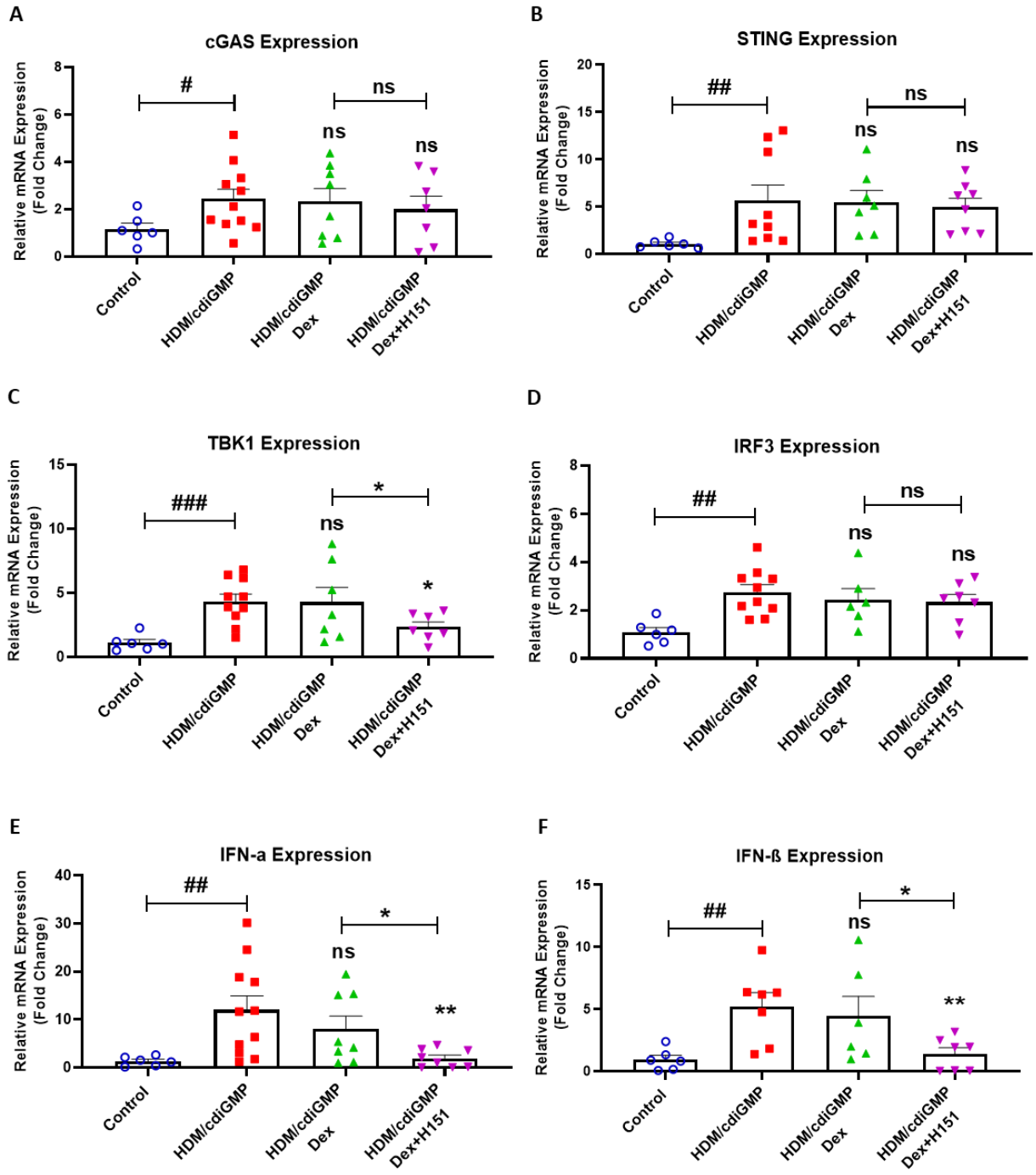

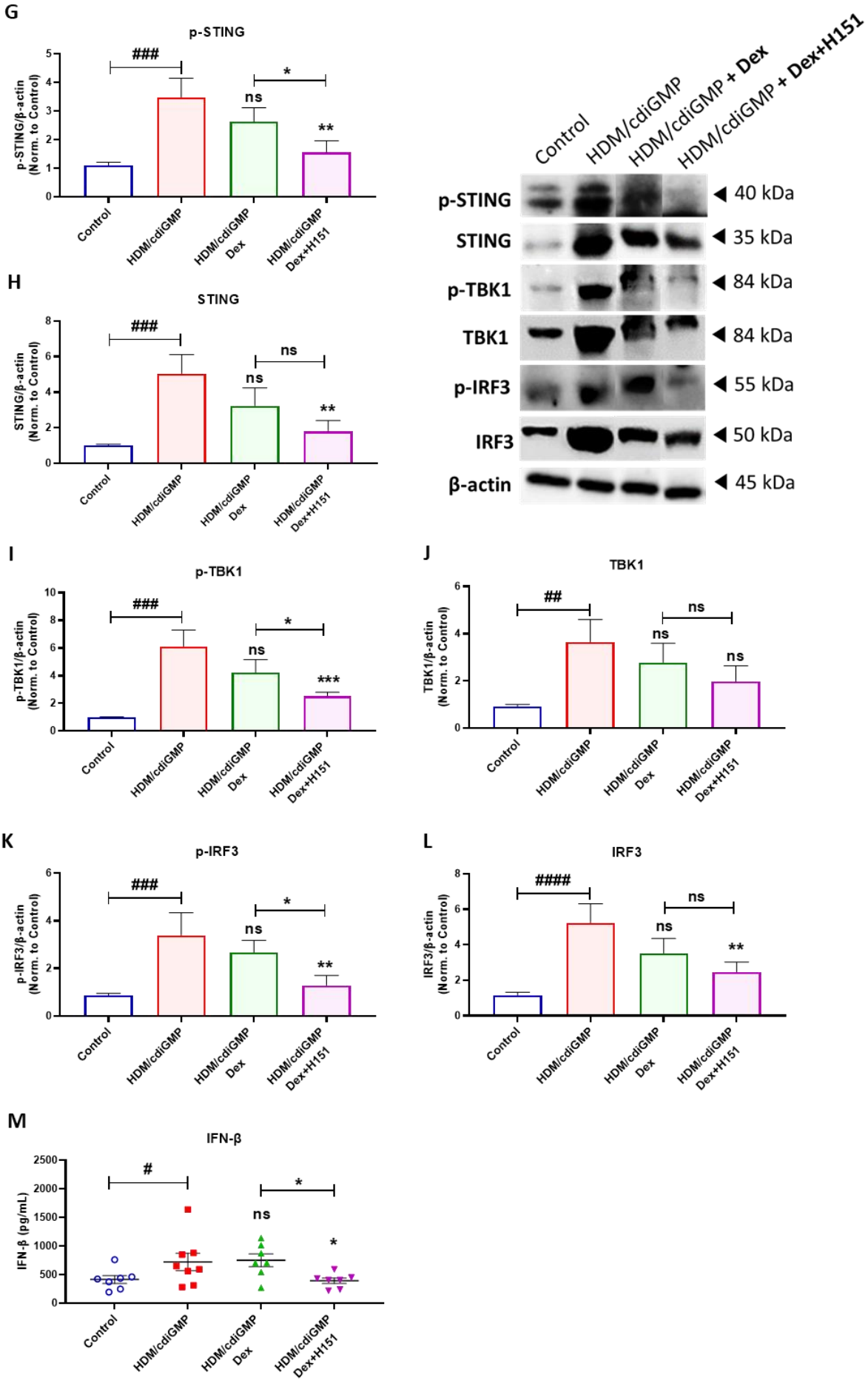
G
p-STING
p-STING/β-actin (Norm. to Control)
###
*
ns
**
Control
HDM/cdiGMP
HDM/cdiGMP Dex
HDM/cdiGMP Dex+H151
H
STING
STING/β-actin (Norm. to Control)
###
ns
ns
**
Control
HDM/cdiGMP
HDM/cdiGMP Dex
HDM/cdiGMP Dex+H151
Control
HDM/cdiGMP
HDM/cdiGMP + Dex
HDM/cdiGMP + Dex+H151
p-STING
40 kDa
STING
35 kDa
p-TBK1
84 kDa
TBK1
84 kDa
p-IRF3
55 kDa
IRF3
50 kDa
β-actin
45 kDa
I
p-TBK1
p-TBK1/β-actin (Norm. to Control)
###
*
ns
***
Control
HDM/cdiGMP
HDM/cdiGMP Dex
HDM/cdiGMP Dex+H151
J
TBK1
TBK1/β-actin (Norm. to Control)
##
ns
ns
ns
Control
HDM/cdiGMP
HDM/cdiGMP Dex
HDM/cdiGMP Dex+H151
K
p-IRF3
p-IRF3/β-actin (Norm. to Control)
###
*
ns
**
Control
HDM/cdiGMP
HDM/cdiGMP Dex
HDM/cdiGMP Dex+H151
L
IRF3
IRF3/β-actin (Norm. to Control)
####
ns
ns
**
Control
HDM/cdiGMP
HDM/cdiGMP Dex
HDM/cdiGMP Dex+H151
M
IFN-β
IFN-β (pg/mL)
#
*
ns
*
Control
HDM/cdiGMP
HDM/cdiGMP Dex
HDM/cdiGMP Dex+H151

Figure 3.9. STING pathway in severe asthma mouse model is resistant to dexamethasone treatment, but responsive to combination treatment of STING inhibitor and dexamethasone.
The gene expression of cGAS (**A**), STING (**B**), TBK1 (**C**), IRF3 (**D**), IFN-α (**E**) and IFN-β (**F**) was compared in treated and untreated severer asthma mice. Data representative of n = 5-11 mice in each group. Representative western blots and densitometric analysis of STING pathway members in mice model, the whole lung cells from all the groups were stimulated or not with 10 μg/ml HDM for overnight to investigate the level of phosphorylation (**G-L**). β-actin was used as a loading control. Data representative from of n = 4-13 mice in each group. Concentration of IFN-β from lung homogenate was analyzed by ELISA (**M**). Data representative from n = 7-8 mice in each group. Results are presented as mean (± SEM) and relative to control mice. The values were compared across the different groups using one-way ANOVA followed by post hoc Bonferroni test for multiple comparisons. ∗p < 0.05, ∗∗p < 0.01, ∗∗∗p < 0.001, ∗∗∗∗p < 0.0001 vs. severe asthma mice. #p < 0.05, ##p < 0.01, ###p < 0.001, ####p < 0.0001 vs. control mice.

We then studied the ability of NP loaded with STING inhibitor to better controlled lung inflammation and steroid hyporesponsiveness more effectively than free drug in vivo in a murine model of chronic airway inflammation.

3.9. Synthesis and physiochemical characterization of nanoparticle encapsulating H151 (NP-H151).

Since the STING inhibitor, H151, potentiated the anti-inflammatory effect of dexamethasone and improved the response of severe asthmatic in-vivo murine model to steroids, we proposed the use of a nanoparticle system encapsulating H151 to improve drug delivery to the lungs, decrease toxicity, and enhance drug efficacy.

One of the polymeric nanoparticles that is food and drug administration (FDA) approved is poly lactic-co-glycolic acid (PLGA), which is extensively used for the pulmonary delivery of small molecules and drugs. NP-H151 and blank NP were successfully synthesized via nanoprecipitation method as illustrated in **figure 3.10.A**. The mean (±SD) particles size distribution, polydispersity index (PDI), and surface charge of formed NP-H151 were 89.8 ± 0.43 nm with a PDI of 0.084 ± 0.008, and -14.03 ± 4.4 mV, respectively. For the blank PLGA NP, the mean (±SD) particle size distribution, PDI, and surface charge were 109 ± 0.1 nm with a PDI of 0.10 ± 0.01, and -15.9 ± 3.3 Mv, respectively (**Fig. 3.10.B**). Interestingly, majority of

H151 was successfully entrapped in the synthesized PLGA NP with 96.2% ± 2.6 as entrapment efficiency (EE)%.

We next analyzed the developed NP using SEM microscope. The morphology, surface structure, and topography of NP-H151 was shown in **figure 3.10.C**. The SEM micrographs of PLGA-H151 NP showed quite spherical, smooth-shaped particles, which aligned well with the reported particles size distribution obtained through the dynamic light scattering (DLS) measurements. To confirm the ability of NP to efficiently release the drug, a drug release assay was performed. The release of H151 from PLGA NP revealed a biphasic release pattern. A burst release of H151 was observed in the first 8 h up to 61.7%. Followed by a sustained release during 48 h, where complete release of H151 from the PLGA NP was observed (**Fig. 3.10.D**).

A

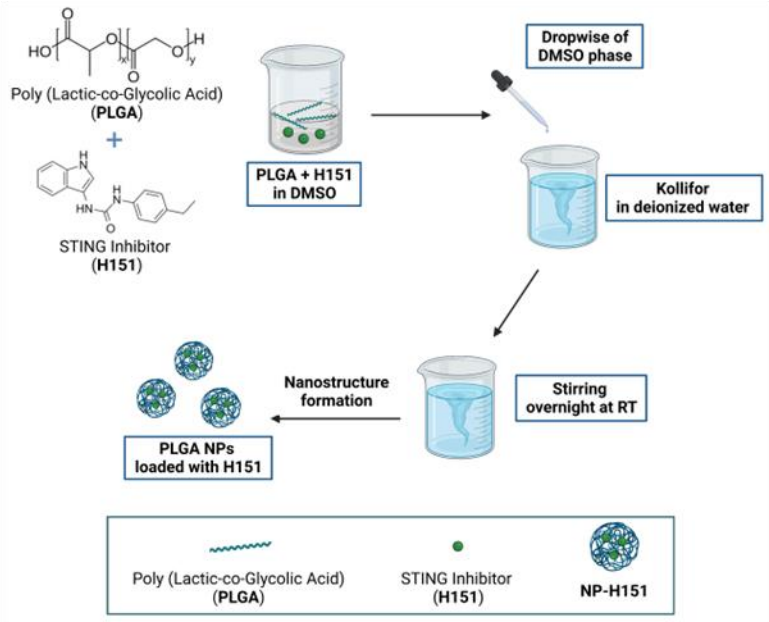

B

Parameters	Blank PLGA NP	NP-H151
Size (nm)	109 ± 0.1	89.78 ± 0.43
PDI	0.10 ± 0.01	0.084 ± 0.008
Zeta Potential (mV)	– 15.86 ± 3.27	– 14.03 ± 4.41
Entrapment Efficiency (%)	-	96.2 ± 2.6

C

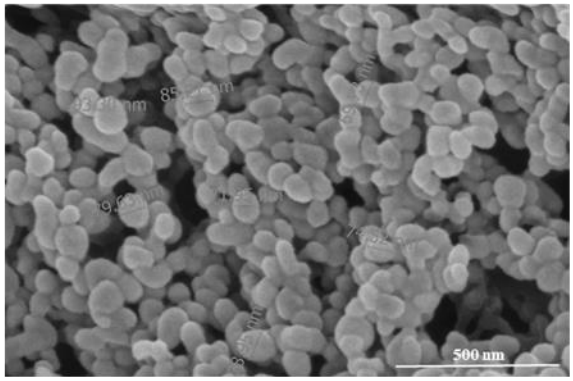

D

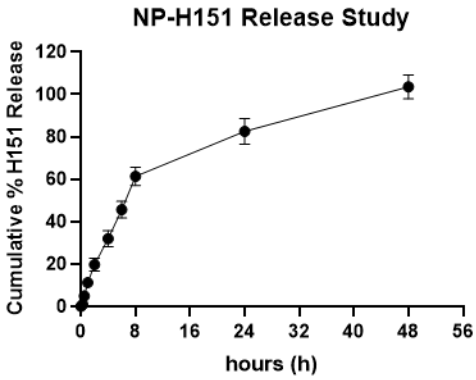

Figure 3.10. Synthesis and physiochemical characterization of nanoparticle encapsulating H151 (NP-H151).

(**A**) Schematic representation of the steps involved in H151 encapsulated in PLGA NP synthesis by modified single step nanoprecipitation method. (**B**) Size, surface charge, and entrapment efficiency of synthesized PLGA NP and NP-H151 (n = 3, mean ± SD). (**C**) SEM images of NP-H151 synthesized by nanoprecipitation method. Scale Bar: 500 nm. (**D**) Cumulative in vitro release profile of H151 from PLGA NP at 37 ◦C for up to 48 h. The percentage of cumulative drug released were calculated using the following equation: Cumulative % drug released = cumulative concentration of released drug / the total amount of drug in nanoparticles X 100 (n = 3, mean ± SEM).

3.10. PLGA loaded with H151 is less toxic than free H151 on severe asthma fibroblasts.

MTT cell viability assay was used to evaluate the cytotoxic effect of blank NP, NP-H151 and free H151 in severe asthmatic fibroblasts for 24 h. Severe asthmatic fibroblasts treated with blank NP, free H151, and NP-H151 showed a cell viability of 86.2%, 78.5% ($p<0.05$), and 81.7%, respectively (**Fig. 3.11.A**). The encapsulation of H151 in PLGA NP appeared to improve the cell viability in comparison to H151 alone, possibly due to its controlled release at 24h.

Cellular uptake or internalization of the NP is one of the most important physio-chemical parameters that should be considered prior to in vivo application. NP internalization in the severe asthmatic fibroblasts was tracked using confocal microscopy. To do that we used curcumin (CUR) which exploit its fluorescence property; thus, serving as a drug model instead of H151. The synthesized CUR-PLGA NP showed an EE% of 93.8%. The fluorescent micrographs revealed high accumulation of CUR-PLGA NP in severe asthma fibroblasts after 24 h of treatment compered to untreated fibroblasts (**Fig. 3.11.B and C**).

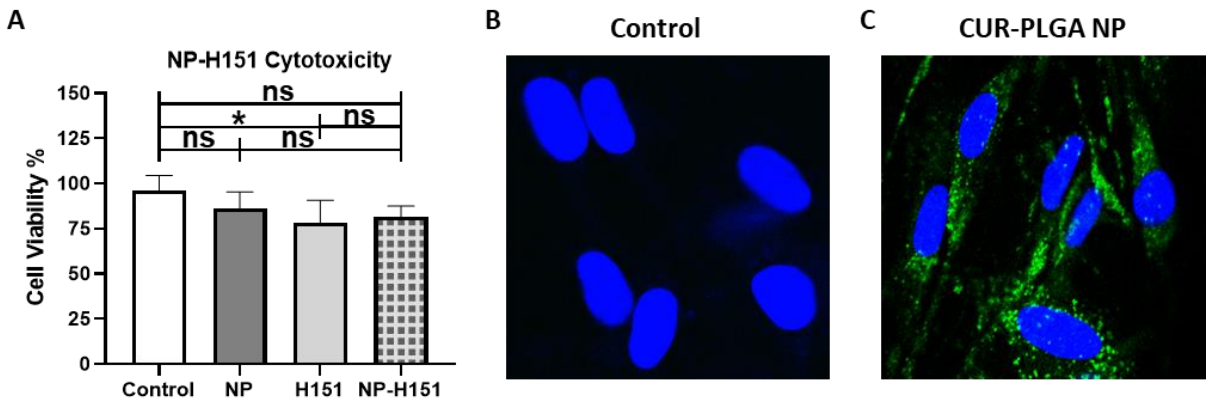

Figure. 3.11. PLGA loaded with H151 is less toxic than free H151 on severe asthma fibroblasts.

(**A**) Severe asthmatic fibroblasts were treated with a concentration of 1µM of H151, NP-H151 and blank NP. Data representative of 2 independent experiments. Results are presented as mean (± SEM) and relative to untreated control. The values were compared across the different groups using one-way ANOVA followed by post hoc Bonferroni test for multiple comparisons. ns $p > 0.05$, $*p < 0.05$ vs. untreated control. Cellular uptake study in fibroblasts showing qualitative analysis of CUR-PLGA NP cellular localization using 60x confocal microscopy images; (**B**) control (no treatment), (**C**) optimized CUR-PLGA-NPs.

3.11. NP-H151 inhibits STING in-vitro through controlled release.

To study the effect of NP-H151 compared to free H151 in inhibiting STING at the mRNA level, severe asthmatic fibroblasts were treated for different time points, 4 h, 8 h, and 24 h with blank NP, H151, and NP-H151. As has been demonstrated earlier (**Fig. 3.8.A**), HDM stimulated STING expression in severe asthmatic fibroblasts in comparison to unstimulated control, as shown in **figure 3.12.A-C**. However, the upregulated STING was not significantly decreased upon treatment with NP-H151 at 4 h in comparison to HDM stimulation (**Fig. 3.12.A**). Interestingly, with time the sustained release of H151 from NPs significantly inhibited the upregulated STING expression at 8 h and 24 h by 1.2 fold ($p<0.0001$), and 1.5 fold ($p<0.001$), respectively, compared to HDM stimulation (**Fig. 3.12.B and C**). We observed no significant difference in the inhibition of the STING expression by NP-H151 at 8 h and 24 h in comparison to free H151 (**Fig. 3.12.B and C**). This comes along with the earlier in-vitro release study where H151 showed a burst release from NPs in the first 8 h, followed by a sustained release during 48 h (**Fig. 3.10.D**).

Altogether, NP-H151 showed enhanced inhibitory effect when compared to free H151 in severe asthma fibroblasts.

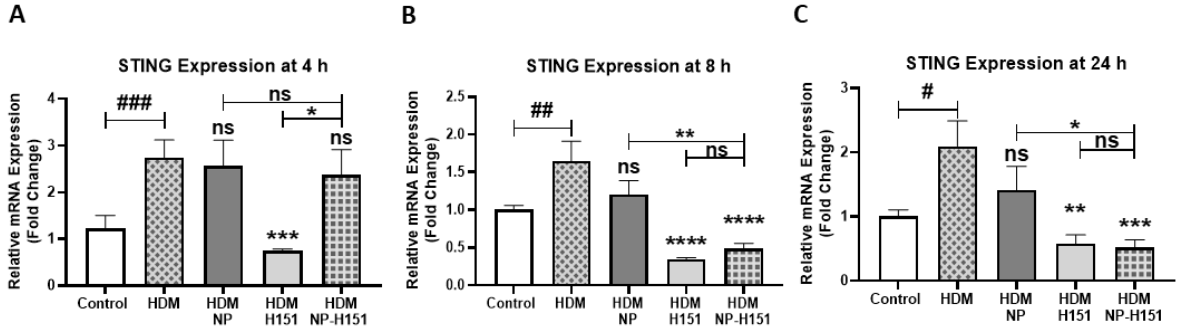

Figure 3.12. NP-H151 inhibits STING in-vitro through controlled release.

Severe asthmatic fibroblasts were stimulated with HDM then treated with a concentration of 1μM of H151, NP -H151 and blank NP to study the gene expression of STING at 4 h (**A**), 8 h (**B**), and 24 h (**C**). Data representative of 4 independent experiments Results are presented as mean (± SEM) and relative to untreated control. The values were compared across the different groups using one-way ANOVA followed by post hoc Bonferroni test for multiple comparisons. ∗p < 0.05, ∗∗p < 0.01, ∗∗∗p < 0.001, ∗∗∗∗p < 0.0001 vs. HDM stimulation. #p < 0.05, ##p < 0.01, ###p < 0.001, vs. unstimulated control.

3.12. NP-H151 inhibit STING pathway more effectively than free H-151 in severe asthmatic mice model.

Then in order to enhance the H151 delivery further toward the small airways and increase bioavailability, decrease muco-ciliary clearance, and improve passage through mucus filled; we proposed loading of H151 in a nanoparticle system. The effects of NP-H151 treatment on STING activation in lung tissue of our mouse model were investigated on both the gene and protein expression. The mRNA levels of cGAS, STING, TBK1, and IRF3 were significantly reduced when treated with dexamethasone and NP-H151 by 2.0 fold ($p<0.05$), 5.0 fold ($p<0.05$), 2.3 fold ($p<0.05$), and 2.3 fold ($p<0.05$), respectively, when compared to dexamethasone and free H151 treated group (**Fig. 3.13.A-D**). The gene expression of IFN-α, and IFN-β were significantly downregulated by 2.0 fold ($p<0.01$), and 1.4 fold ($p<0.05$), respectively upon dexamethasone and NP-H151 treatment relative to dexamethasone and free H151 (**Fig. 3.13.E and F**).

Further, to examine the effect of NP-H151 treatment on the protein level, western blot was used. The lung cells from all the groups were stimulated or not with 10 μg/ml HDM overnight to investigate the level of phosphorylation. The activation by phosphorylation of STING, TBK1, and IRF3 upon dexamethasone and NP-H151 treatment were significantly lowered by 0.7 fold ($p<0.05$), 0.9 fold ($p<0.05$), and 0.7 fold ($p<0.05$), respectively, when compared to dexamethasone and free H151 treatment group (**Fig. 3.13.G-L**). Interestingly, NP-H151 treated group decreased IFN-β secretion by 30% ($p<0.05$) when compared to dexamethasone single treatment group (**Fig. 3.13.M**). The PLGA NP itself did not exert any effect on STING pathway, when used in combination with dexamethasone treatment (**Fig. 3.13.A-M**).

Collectively, STING inhibitor H151 encapsulated in NP significantly augmented the inhibition of STING pathway by dexamethasone compared to free H151 in severe asthma mouse model.

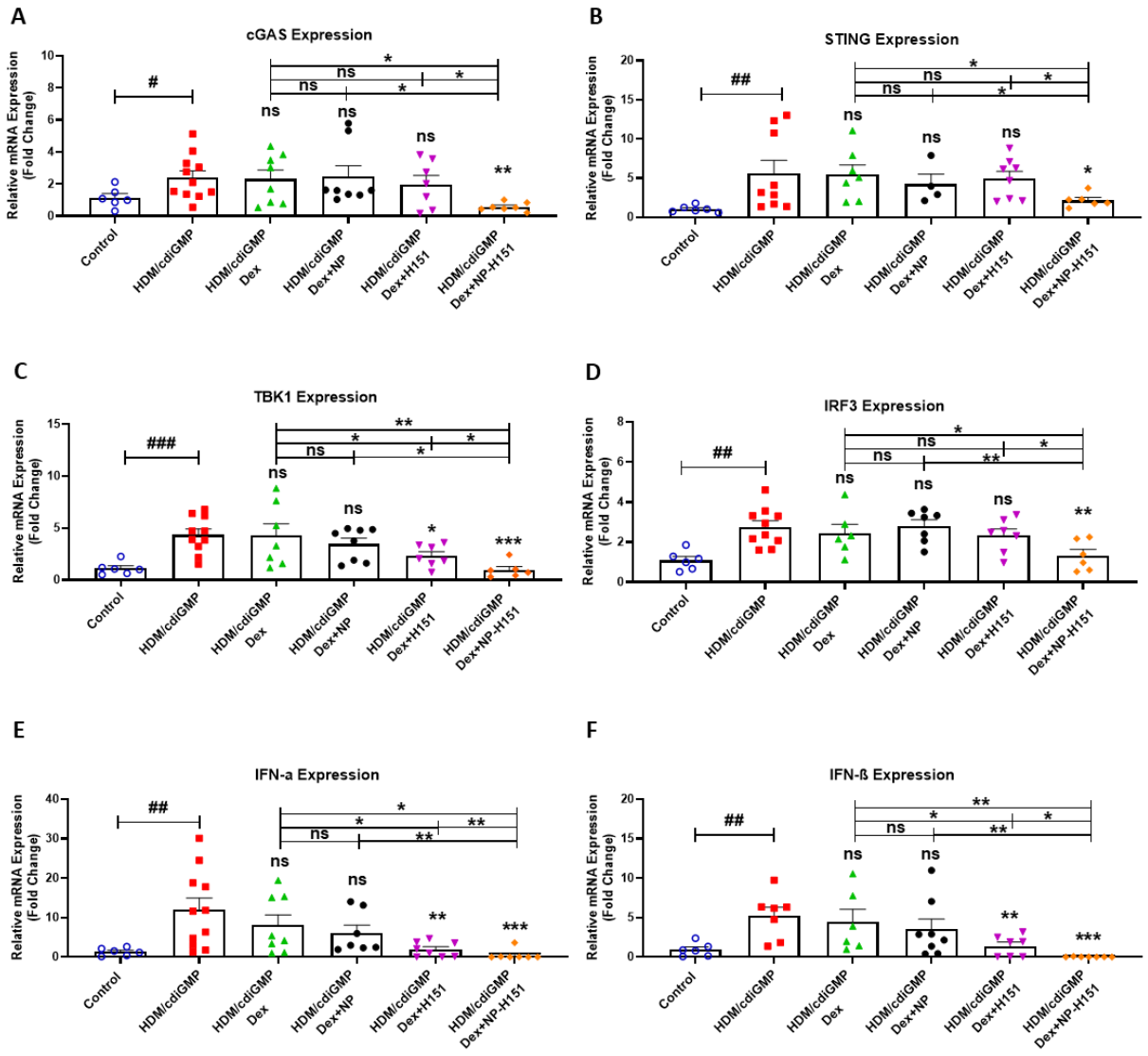

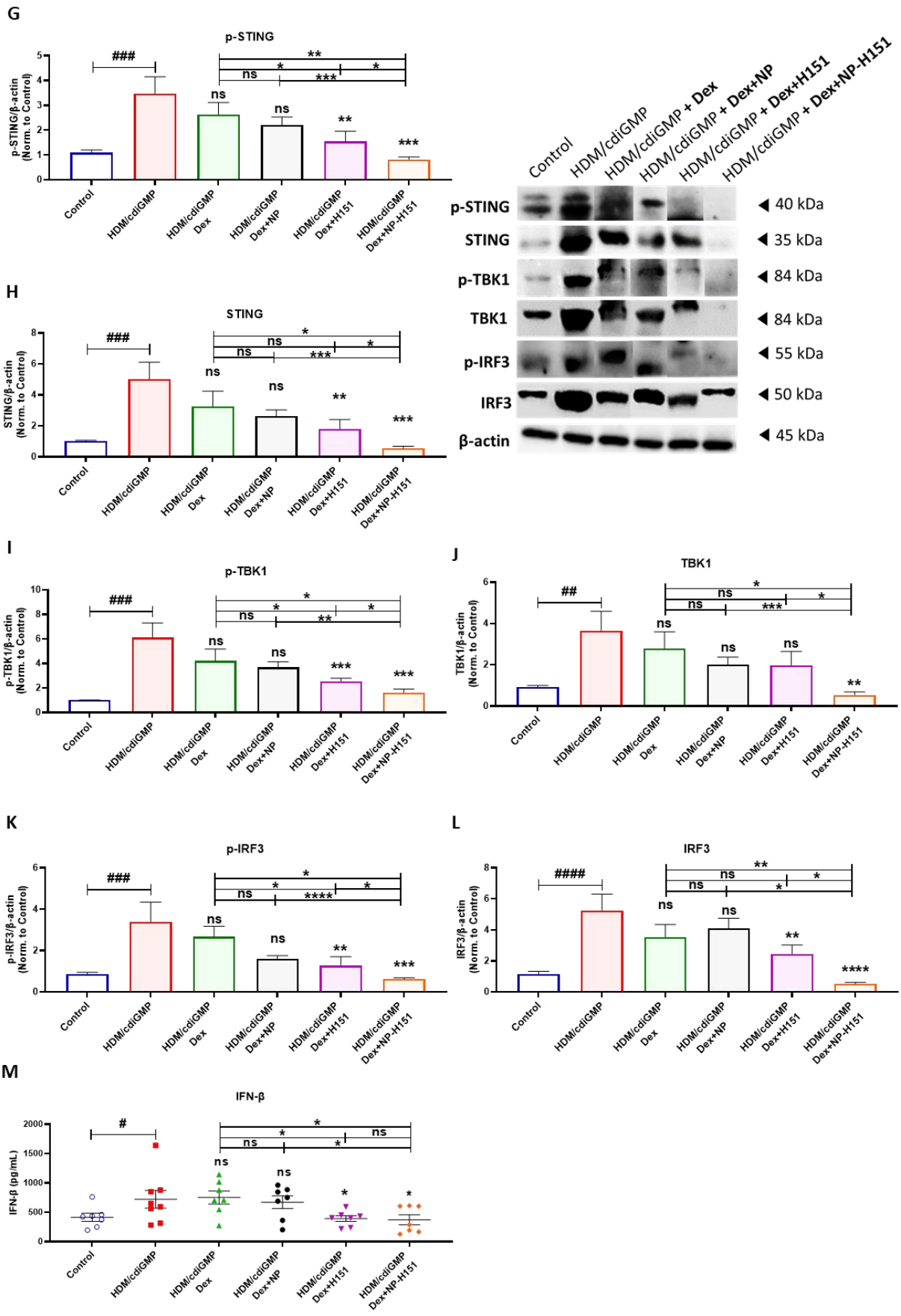
G
p-STING
p-STING/β-actin (Norm. to Control)
H
STING
STING/β-actin (Norm. to Control)
I
p-TBK1
p-TBK1/β-actin (Norm. to Control)
J
TBK1
TBK1/β-actin (Norm. to Control)
K
p-IRF3
p-IRF3/β-actin (Norm. to Control)
L
IRF3
IRF3/β-actin (Norm. to Control)
M
IFN-β
IFN-β (pg/mL)
Control
HDM/cdiGMP
HDM/cdiGMP + Dex
HDM/cdiGMP + Dex+NP
HDM/cdiGMP + Dex+H151
HDM/cdiGMP + Dex+NP-H151
p-STING
STING
p-TBK1
TBK1
p-IRF3
IRF3
β-actin
40 kDa
35 kDa
84 kDa
84 kDa
55 kDa
50 kDa
45 kDa

Figure 3.13. NP-H151 inhibit STING pathway more effectively than free H-151 in severe asthmatic mice model.

The gene expression of cGAS (**A**), STING (**B**), TBK1 (**C**), IRF3 (**D**), IFN-α (**E**) and IFN-β (**F**) was compared in treated and untreated severer asthma mice. Data representative of n = 5-11 mice in each group. Representative western blots and densitometric analysis of STING pathway members in mice model, the lung cells from all the groups were stimulated or not with 10 μg/ml HDM overnight to investigate the level of phosphorylation (**G-L**). β-actin was used as a loading control. Data representative from of n = 4-13 mice in each group. Concentration of IFN-β from lung homogenate was analyzed by ELISA (**M**). Data representative from n = 7-8 mice in each group. Results are presented as mean (± SEM) and relative to control mice. The values were compared across the different groups using one-way ANOVA followed by post hoc Bonferroni test for multiple comparisons. ∗p < 0.05, ∗∗p < 0.01, ∗∗∗p < 0.001, ∗∗∗∗p < 0.0001 vs. severe asthma mice. #p < 0.05, ##p < 0.01, ###p < 0.001, ####p < 0.0001 vs. control mice.

3.13. Nanoparticles loaded with H151 controls lung inflammation and increase airway responsiveness to steroid in severe asthma mouse model.

We next investigated whether the combination of dexamethasone and STING inhibitor, H151, improves steroid responsiveness, and alleviates lung inflammation and AHR. First, the HDM/cdiGMP-immunized mice treated with dexamethasone and NP-H151 demonstrated lower levels of lung inflammation with no evidence of inflammatory cells infiltration ($p<0.0001$), and less intense mucus staining ($p<0.01$) compared to untreated HDM/cdiGMP mice group (**Fig. 3.14.A and B**).

Importantly, the gene expression of GRβ showed a significant downregulation upon dexamethasone and NP-H151 treatment by 3.8 fold ($p<0.05$) relative to single treatment with dexamethasone, and by 2.7 fold ($p<0.05$) compared to dexamethasone and free H151 treatment (**Fig. 3.14.C**). Further, the GRα/GRβ ratio was significantly increased upon dexamethasone and NP-H151 treatment compared to treated immunized group with dexamethasone alone ($p<0.05$) (**Fig. 3.14.D**).

Interestingly, our proposed combination of dexamethasone and NP-H151 significantly lowered the airway resistance in HDM/cdiGMP mice at total airways (**Fig. 3.14.E**), and at small airways level when compared to untreated ($p<0.0001$) or treated with dexamethasone only ($p<0.001$) or treated with free H151 (**Fig. 3.14.F**); which indicated that the proposed NP-H151 could easily target the small airways and could enhance drug availability to the site of

injury. Blank NP had no effect on either lung inflammation (**Fig. 3.14.A and B**), or AHR (**Fig. 3.14.E and F**).

Taken together, administration of NP loaded with STING inhibitor H151 in severe asthma murine model augments steroid responsiveness by downregulating GRβ, increasing GRα/GRβ ratio, lowering the airway hyperresponsiveness and inflammation.

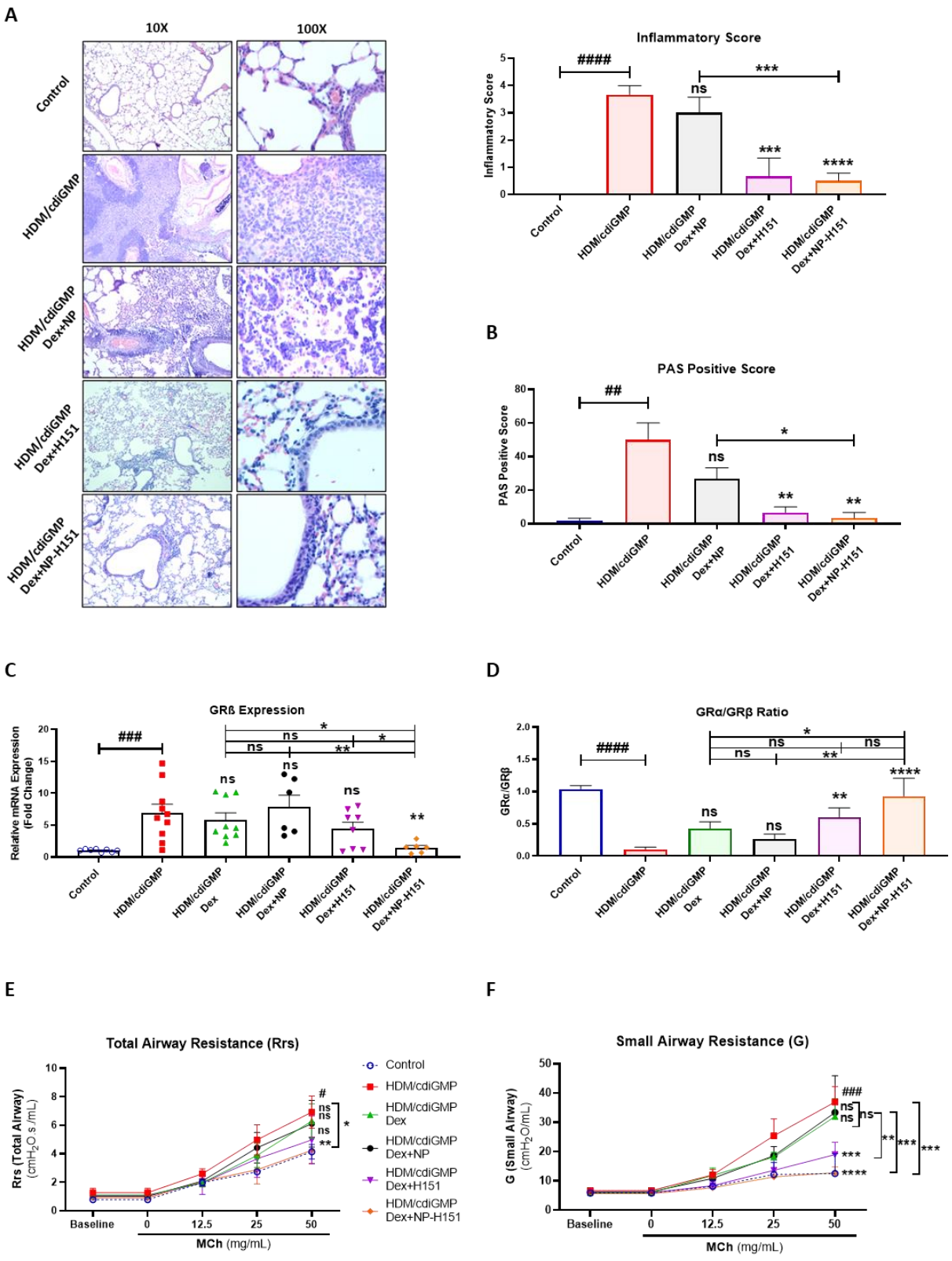

Figure 3.14. Nanoparticles loaded with H151 controls lung inflammation and increase airway responsiveness to steroid in severe asthma mouse model.

The gene expression of GRβ (**A**) and GRα/GRβ ratio (**B**) in treated and untreated severer asthma mice. Data representative of n = 5-11 mice in each group. (**C**) Inflammation score in H&E stained lung tissues. (**D**) PAS positive score of PAS stained lung sections. Scale bar: 200 μm. Data presented as mean (± SEM) and representative of n = 3-4 mice in each group. The values were compared across the different groups using one-way ANOVA followed by post hoc Bonferroni test for multiple comparisons. Data showed airway function measurements by forced oscillatory technique using different doses of MCh. (**E**) Assessment of total airway resistance (Rrs) to MCh. (**F**) Assessment of small airway resistance to MCh. Data representative of n = 6-9 mice in each group. The values were compared across the different groups using two-way ANOVA followed by post hoc Bonferroni test for multiple comparisons. Results are presented as mean (± SEM) and relative to control mice. $*p < 0.05$, $**p < 0.01$, $***p < 0.001$, $****p < 0.0001$ vs. severe asthma mice. #p < 0.05, ##p < 0.01, ###p < 0.001, ####p < 0.0001 vs. control mice.

Chapter IV.
Discussion

In this study, the STING pathway was found to be upregulated in lung tissue of steroid resistant asthma mouse model, and bronchial fibroblasts isolated from severe asthmatic patients. The activated STING pathway was not suppressed by steroid treatment, while a combination of steroid and STING inhibitor significantly reduced the expression of STING/IFN-β signaling. This is the first study to investigate in-depth the activation of the STING pathway in human bronchial fibroblasts. In addition, loading STING inhibitor in PLGA nanoparticles improved its delivery to deep severe asthmatic lungs and enhanced its efficacy in controlling lung inflammation and restoring steroid sensitivity. Overall, the activated STING pathway plays a key role in severe asthma through the induction of IFN-I response and steroid hyporesponsiveness. STING inhibitor, H151, could be used as a potential adjuvant to steroid medication.

4.1. STING activation in severe asthma fibroblasts as well as severe asthma mice model is resistant to dexamethasone monotherapy but responsive to combination therapy of STING inhibitor and dexamethasone.

STING is a part of innate immune signaling pathway that senses cytosolic dsDNA and leads to type I IFN response (Benmerzoug et al., 2018; Ma et al., 2020; Nascimento et al., 2019). This pathway is known to drive inflammation in different chronic diseases, such as systemic lupus erythematosus (An et al., 2017; Kato et al., 2018; Thim-Uam et al., 2020), rheumatoid arthritis (Wang et al., 2019), acute lung injury (He et al., 2021; Ning et al., 2020; Wu et al., 2021), silicosis (Benmerzoug et al., 2019; Benmerzoug et al., 2018), asthma (Doherty, 2020; Han et al., 2020; Nunokawa et al., 2021; Ozasa et al., 2019), and COPD (Lu et al., 2018; Nascimento et al., 2019).

HDM, the most common source of allergens in asthmatic patients, significantly increased oxidative DNA damage in lung tissue (Chan et al., 2016), which could be detected in the peripheral blood of asthmatic patients, and positively correlated to disease severity (Gaballah et al., 2018; Saini et al., 2019). Therefore, the release of self-dsDNA is significantly associated with the asthmatic exacerbation (Toussaint et al., 2017), potentially activates STING

pathway in asthmatic lung tissue. The upstream of SITNG pathway, cGAS, detected cytosolic dsDNA in IL-33 stimulated epithelial cells, and asthmatic mice models which promoted Th2 immunity (Han et al., 2020). Further, cGAMP, a selective STING stimulant, significantly increased serum IgE levels (Nunokawa et al., 2021; Ozasa et al., 2019), B cell proportion (Nunokawa et al., 2021), and eosinophil infiltration (Ozasa et al., 2019), in bronchoalveolar lavage fluid (BALF) of HDM-induced asthmatic mouse model. Interestingly, STING activation played an important role in severe asthma with fungal sensitization by promoting type 1 inflammation via inhibition of ILC2 and activation of ILC1 (Cavagnero et al., 2021; Doherty, 2020). Furthermore, the expression of transcriptional factor IRF5, downstream of STING pathway, is significantly increased in severe asthmatics when compared to mild asthmatics or healthy controls (Oriss et al., 2017). In addition, the ISGs level from sputum and peripheral blood of asthmatic patients is significantly higher when compared to healthy control (Bhakta et al., 2018), and positively associated with neutrophilic asthma (da Silva et al., 2017). Our data is in line with the previous findings, where severe asthmatic fibroblasts are enriched with STING at the baseline profile (**Fig. 3.2**), and further elevated upon HDM stimulation at both mRNA and protein levels (**Fig. 3.8**).

Glucocorticoids differentially target innate immune responses through the cytosolic DNA sensing pathway (Wang et al., 2017). Dexamethasone treatment suppressed TBK1 activation; inhibiting IRF3 phosphorylation (McCoy et al., 2008), disrupting IRF3-glucocorticoid receptor protein complex (Reily et al., 2006), and decreasing IFN-I secretion (Flammer et al., 2010; Wang et al., 2017). Supporting these findings, here we showed STING/IFN-β pathway was responsive to dexamethasone in healthy fibroblasts (**Fig. 3.7**). However, dexamethasone did not affect the activity of this pathway in fibroblasts from severe asthmatic patients (**Fig. 3.8**), while STING inhibitor had an additive anti-inflammatory effect when combined with commonly used steroid treatment, dexamethasone (**Fig. 3.7 and Fig. 3.8**). Steroid hyporesponsiveness in severe asthma is associated with decreased GR-alpha expression (Vazquez-Tello et al., 2013), increased GR-beta expression (Ramakrishnan et al., 2019; Vazquez-Tello et al., 2013). and lowered GRα/GRβ ratio (Al Heialy et al., 2020), which could explain the lack of steroid activity of steroid on STING pathway.

The asthma development is mainly associated with the sensitization to aeroallergens, HDM (Holgate, 2012; Kubo, 2017); resulting in the secretion of alarmins, such as IL-33, IL-25, and TSLP. IL-33 in turn induced the recruitment and activation of AMs thereby

contributing to the airway inflammation in mice (Chan et al., 2019). It has been reported that AMs in response to IL-33 stimulation exhibiting signs of polynucleation, polyploidy, and micronuclei formation (Quell et al., 2020). Our data is in line with the previous reports, where we observed a significant increase in the recruitment of AMs and its DNA content in lung of IL-33 challenged group relative to control (**Fig.3.5.B and C**). Interestingly, we have shown substantial enrichment of the STING profile in AMs of IL-33 challenged group compared to control (**Fig.3.5.E**), which was further elevated in the high DNA content AMs of IL-33 challenged group relative to low DNA content AMs (**Fig.3.5.F**). The formation of micronuclei was significantly associated with STING activation (de Oliveira Mann et al., 2017; Mackenzie et al., 2017); which could explain the increased expression of STING in polynucleated AMs.

Moreover, we established a mouse model with severe asthmatic features using two allergens, HDM and cyclic-di-GMP, to mimic the complex immune response observed in human severe asthma (Raundhal et al., 2015). Cyclic-di-GMP (cdiGMP) has potent adjuvant properties by inducing a Th1-Th17 response (Ebensen et al., 2007). Moreover, cyclic-di-GMP leads to the activation of TBK1 kinase which indeed activated multiple IRF family members including IRF3, IRF5, and IRF7. Additionally, IRF5 expression, one of STING downstream genes, was positively correlated with disease severity and steroid hyporesponsiveness (Oriss et al., 2017). Interestingly, here, we showed an upregulation of GRβ and decreased GRα/GRβ ratio upon sensitization in comparison to the control group (**Fig. 3.3.G and H**). Furthermore, HDM/cdiGMP sensitized mice had significantly higher AHR than control mice, while dexamethasone treatment did not significantly reduce AHR compared to untreated sensitized mice (**Fig. 3.3.I and J**). We confirmed that STING/IFN-I at both mRNA and protein levels were activated in severe asthmatic mice lung compared to the control group (**Fig. 3.4**). Despite dexamethasone treatment, a high level of STING pathway was maintained in the lungs of severe asthmatic mice (**Fig. 3.9**). Further, the combination of dexamethasone and free H151 significantly reduced the activation of the STING pathway at the protein level compared to dexamethasone alone (**Fig. 3.9**). Therefore, we proposed the use of nanoparticles as a way of increasing the delivery of H151 to the small airways and prolonging the effect of the drug.

Pulmonary drug delivery represents a challenge which results from airway anatomy, and lungs defense mechanisms, such as mucociliary clearance, and phagocytosis (Halwani et al., 2016). Pulmonary exposition of biodegradable and biocompatible drug nanocarriers offers a promising approach for the efficient delivery of therapeutic agents to the lung tissue (Ratemi

et al., 2016). This is mostly because of its biocompatibility, biodegradability, prolonged retention time in the lungs, enhanced intracellular drug uptake, sustained drug release, reduced mucociliary clearance and drug toxicity (Halwani et al., 2016; Ratemi et al., 2016).

Among the several nanoparticle (NPs) types, an attractive option for pulmonary drug administration is the polymeric system. The main advantages of polymeric NPs over other NPs are their stability, controlled synthesis, and sustained drug release pattern (Ratemi et al., 2016). One of the food and drug administration (FDA)-approved polymeric nanoparticles is poly lactic-co-glycolic acid (PLGA) (Abulateefeh, 2023), which in particular, used extensively for the development of controlled delivery of small molecules and drugs (Mir et al., 2017). PLGA NPs have been used for pulmonary delivery of a variety of drugs. Previously, PLGA was loaded with antibiotics, tobramycin and polymyxin B, for the treatment of pulmonary infections with *pseudomonas aeruginosa*; to reduce drug toxicity and increase bioavailability (Ungaro et al., 2012; Wu et al., 2022b). Further, PLGA was used as nanocarrier for allergen vaccination to increase vaccine efficacy, prolong potency, and decrease side effects (Luo et al., 2020). PLGA NP was also loaded with medicinal plant extract (glycyrrhizic acid) to decrease the extract toxicity as treatment for asthma (Chen et al., 2022). To effectively protect the peptides from enzymatic degradation, PLGA NP was loaded with anti-asthmatic candidates, alpha 1-antitrypsin (α1AT) (Pirooznia et al., 2012), and vasoactive intestinal peptide (VIP) (Athari et al., 2016). Therefore, PLGA was identified as an optimal system of pulmonary delivery for the purpose of this study.

The particle size of NP-H151 prepared in this study ranged from 89 to 110 nm (**Fig. 3.10.B**), which is the optimal size range for rapid cellular uptake (Mangal et al., 2017). The low polydispersity values showed that the formed NP were not aggregated and can be efficiently resuspended in a water medium following their lyophilization. The Z-potential values of blank NP and NP-H151 were comparable demonstrating that the drug is encapsulated inside the NP and not absorbed on the surface. Further, the spherical morphology of PLGA NP prepared in this study (**Fig. 3.10.C**), as FDA-approved NPs is suitable for pulmonary drug administration to treat asthma (Abulateefeh, 2023).

PLGA has been approved as a safe biodegradable and biocompatible polymer; because it hydrolyzed to produce lactic and glycolic acids (Makadia et al., 2011; Semete et al., 2010). Through the citric acid cycle, lactic acid is converted to carbon dioxide and water, while glycolic acid is either excreted in the urine or oxidized to glyoxylic acid. Here, we have showed

that the viability of treated cells with blank and loaded nanoparticles was unchanged and remained more than 80% (**Fig. 3.11.A**).

One of the main advantages of PLGA NPs is sustained drug release. In line with previous studies, the release of drug from PLGA NP revealed a biphasic release pattern (**Fig. 3.10.D**); which a significant factor in the design of anti-asthmatic drugs (Chen et al., 2022). PLGA exhibits a pH-sensitive where the acidic pH in inflamed lung tissue (pH = 6.4 - 6.8) plays an effective role in releasing drugs from PLGA via hydrolysis of ester bonds in the polymer backbone (Athari et al., 2016). As shown in **figure 3.10.D**, more than half of H151 is released from PLGA NP at the first 8 hours, then gradual release during 48 h till a complete release of H151. Consistent with the drug release assay, the NP-H151 did not significantly inhibit STING in-vitro after 4 h, but considerably inhibited it after 8 h and 24 h, compared with the stimulated severe asthmatic fibroblasts (**Fig. 3.12**).

4.2. NP-H151 controls lung inflammation in severe asthma mice model more effectively than free H-151

In this study, severe asthmatic mice with steroid hyporesponsiveness were treated intranasally with free H151, PLGA-encapsulated H151, and blank PLGA NP groups in combination with dexamethasone. Interestingly, H151-loaded PLGA nanoparticles effectively inhibited the STING/TBK1/IRF3 at both mRNA and protein levels compared to the free H151 treated group (**Fig. 3.13**). Further, lung tissue from the NP-H151 treated group showed lower lung inflammation with no evidence of inflammatory cells infiltration, and less intense mucus staining. Lung tissue from the free H151 treated group showed mild infiltration by inflammatory cells, whereas the blank PLGA nanoparticles had no therapeutic benefit (**Fig. 3.14.A and B**). Both H151-loaded PLGA nanoparticles and free H151 reduced AHR, however, NP-H151 treatment more effectively inhibited AHR which is similar to the normal group at total and small airways level (**Fig. 3.14.E and F**). Collectively, this indicates that PLGA NP enhances the bioavailability of H151 at the site of action compared to free H151. Therefore, PLGA can be considered as a useful delivery system to the deep lungs in form of nasal drops for STING inhibitor in the treatment and control of asthma.

Here we showed that treatment of HDM/cdiGMP-immunized mice with dexamethasone and NP-H151 showed significant downregulation of GRβ relative to treatment with dexamethasone and free H151 (**Fig. 3.14.C**). Further, the GRα/GRβ ratio was significantly increased upon dexamethasone and NP-H151 treatment compared to HDM/cdiGMP-

immunized mice group (**Fig. 3.14.D**). These effects come along with restoring glucocorticoid responsiveness. Previously, IRF5-deficient mice, one of STING downstream gene, resulted in lower Th1/Th17 response and higher in Th2 response compared to wild type mice upon sensitization with HDM/cdiGMP; which induced a steroid-sparing effect (Oriss et al., 2017). STAT1, a well-studied molecule involved in IFN signaling, promotes both IRF5 transcription as well as activation in severe asthmatic mice (Oriss et al., 2017). Further, the stimulation of IRF5 is associated with NF-κB activation (Saliba et al., 2014), which could result in glucocorticoid resistance. To the best of our knowledge, this is the first study to associate GRβ attenuation with STING inhibition. The link between STING signaling and GRβ expression is not well investigated and requires further evaluation.

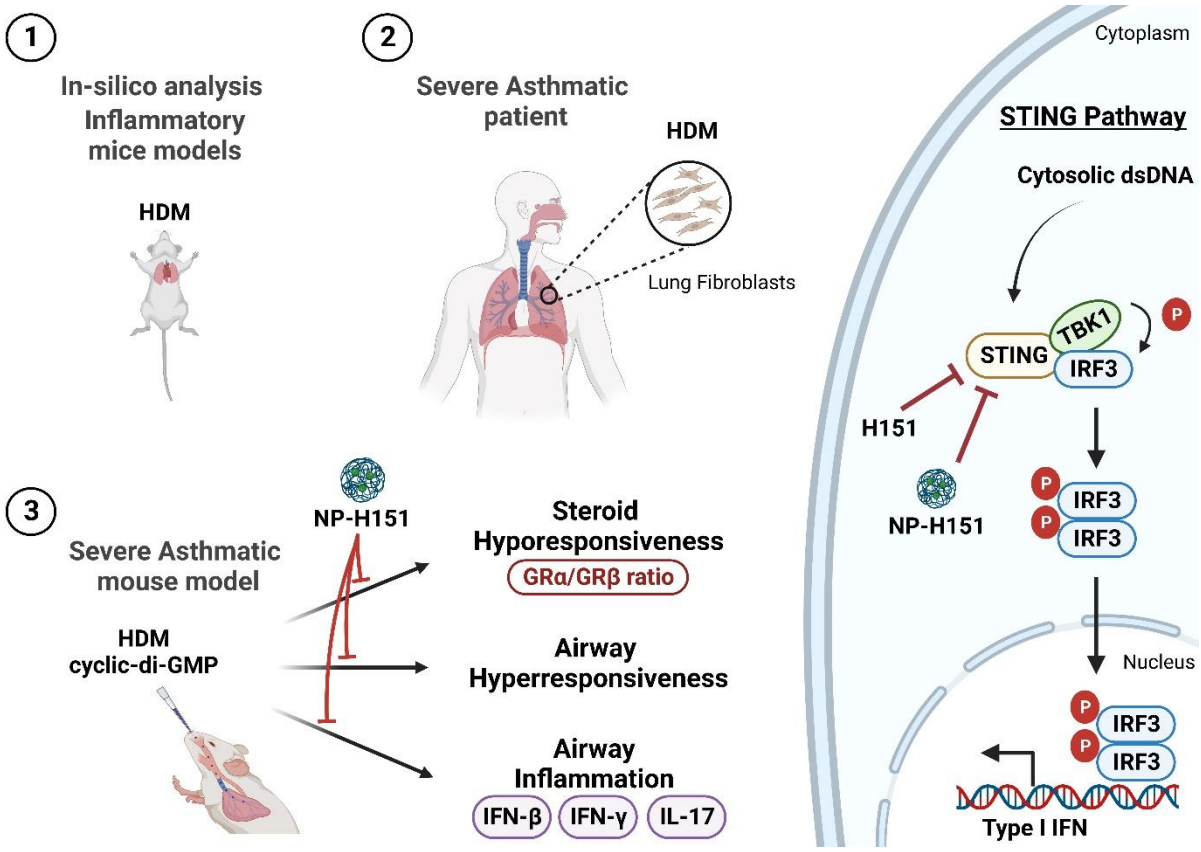

Figure 4.1. Schematic representation of STING activation in severe asthma.

(1) In-silico analysis of three datasets, **(2)** the fibroblasts isolated from severe asthmatic patients, and **(3)** the developed severe asthmatic mouse model revealed an elevation in the baseline expression of STING pathway. Further, upon stimulation with HDM, STING pathway was activated via phosphorylation of STING, TBK1, and IRF3, which in turn resulted in type I interferon response.

Interestingly, STING activity is resistant to dexamethasone therapy but responsive to combination of STING inhibitor and dexamethasone in severe asthmatic fibroblasts and mouse model. Nanoparticles loaded with STING inhibitor, therefore, was synthesized to enhanced drug delivery to small severe asthmatic airways and increase the efficacy. Intranasal administration of nanoparticles loaded with STING inhibitor controlled lung inflammation and restored steroid sensitivity more effectively than free STING inhibitor in severe asthmatic mouse model.

Chapter V.
Conclusion

Conclusions and recommendations

The current work underscores the importance of STING pathway in severe asthma pathogenesis via inducing IFN-I secretion, pulmonary inflammation, and steroid hyporesponsiveness. Therefore, the STING inhibitor may be used in combination with routine steroid treatment to increase steroid sensitivity and control lung inflammation, thus preventing asthma progression. In conclusion, a critical evaluation of the expression of immune response regulators such as STING pathway in the diseased airways would represent a more personalized approach to treating chronic respiratory diseases, particularly asthma.

Furthermore, our work suggests that the use of nanoparticles loaded with STING inhibitor alleviates disease symptoms and restores steroid sensitivity in severe asthmatics more efficiently than free STING inhibitor. Therefore, the application of biocompatible nanoparticles for drug delivery offers a promising approach to inhibit inflammatory pathways characteristic of chronic lung inflammation.

Limitations of the study

There are a number of limitations to this study. We were restricted in the number of donors; therefore, we used three biological replicates from each donor to confirm our results. In addition, the limited number of mice included in the pulmonary IL-33 challenge; could explain the statistical non-significance. Furthermore, the prolonged effect of NP-H151 to control lung tissue inflammation was not determined.

Future work

The STING pathway in epithelial cells has been studied previously, where stimulation of human bronchial epithelial (HBE) cells by IL-33 induced cytosolic dsDNA accumulation which was sensed by cGAS and promoted Th2 immunity via the production of granulocyte-macrophage colony-stimulating factor (GM-CSF) (Han et al., 2020). In our study, the activation of STING pathway was studied in fibroblasts from severe asthmatics patients and the role of STING inhibitor to augment the anti-inflammatory effects of commonly used

steroid, dexamethasone was examined. In fact, examining the STING pathway in other structural cells, including airway smooth muscles from severe asthmatics, would be of interest.

It would be of interest to study the activation of STING in IL-33 challenged murine model through detection of p-STING and IFN-I (IFN-α and IFN-β) using flow cytometry and ELISA, respectively. Further, the sign of polynucleation in AMs should be confirmed using immunofluorescence as previously described (Quell et al., 2020).

STING signaling has recently been linked to fibrosis via the upregulation of fibrotic hallmarks, specifically TGF-β, and collagen I (COL1A1), in cardiac (Zhang et al., 2020), hepatic (Luo et al., 2018), renal (Chung et al., 2019), and pulmonary inflammation (Sun et al., 2020). It will therefore be interesting to investigate the alleviated fibrotic markers in severe asthma murine models and the effect of STING inhibitors in combination with steroids to inhibit fibrosis. In fact, we have studied that in the context COPD and found that STING inhibitor in combination with dexamethasone alleviates fibrosis in fibroblasts isolated from COPD patients. Kindly, see the **appendix 6.4.5**.

Here, we assessed the cytotoxicity of nanoparticles to primary fibroblasts, where viability of cells treated with nanoparticles remained more than 80%. However, the in-vivo toxicity has yet to be determined, which could be performed via histopathological evaluation. Further, the ability of NP-H151 to maintain sustained control of lung tissue inflammation would also be of interest to be investigated.

Abstract

Inhibiting DNA Sensing Pathway to Control Steroid Resistant Lung Inflammation

Bushra Ahmed Mdkhana

Background: Asthma is a complex pulmonary disease that involves chronic inflammation of the airways and affects millions of individuals worldwide. Current anti-inflammatory drugs have a variety of limitations, including side effects that accompany with long-term usage or the development of resistance. House dust mites (HDM), the most common asthmatic allergen, result in the release of double-stranded DNA (dsDNA), which could activate DNA-sensing pathways such as STING. The purpose of this study was to investigate the role of the STING pathway in inducing pulmonary inflammation and contributing to steroid resistance in severe asthma. **Methods:** STING pathway level was investigated in human bronchial fibroblasts and lung tissue from steroids hyporesponsive severe asthmatic mice model at baseline, following stimulation, and upon treatment with dexamethasone and/or STING inhibitor, at both mRNA and protein levels. STING inhibitor was encapsulated in PLGA nanoparticles, and its physiochemical characteristics were evaluated. In the asthma mouse model, steroid response, airway hyperresponsiveness (AHR), and inflammation markers were assessed. **Results:** Asthma presented with higher baseline levels of the STING/IFN-I pathway, which was further elevated upon stimulation with HDM. In the airways steroids resistant mouse model, STING activation was resistant to dexamethasone monotherapy but responsive to STING inhibitor and dexamethasone combination treatment. Therefore, nanoparticles encapsulating STING inhibitor were synthesized to enhance drug delivery and efficacy in severe asthmatic airways. Intranasal administration of nanoparticles loaded with STING inhibitor controlled lung inflammation and restored steroid sensitivity more effectively than free STING inhibitor in the severe asthmatic mouse model. **Conclusion:** These findings support the concept that the STING pathway plays an important role in severe asthma pathogenesis, via the induction of pulmonary inflammation and enhancement of steroid resistance. Further, nanoparticles loaded with STING inhibitor were suggested as a way of increasing the delivery, decreasing the toxicity and enhancing the effectiveness of STING inhibitor.

Zusammenfassung

Hintergrund: Asthma ist eine komplexe Lungenerkrankung, die mit einer chronischen Entzündung der Atemwege einhergeht und Millionen von Menschen weltweit betrifft. Gegenwärtige entzündungshemmende Medikamente haben eine Vielzahl von Einschränkungen, einschließlich Nebenwirkungen, die mit einer langfristigen Anwendung oder der Entwicklung von Resistenzen einhergehen. Hausstaubmilben (HDM), das häufigste Asthmaallergen, führen zur Freisetzung von doppelsträngiger DNA (dsDNA), die DNA-Sensorwege wie STING aktivieren können. Der Zweck dieser Studie war es, die Rolle des STING-Signalwegs bei der Induktion einer Lungenentzündung und seinen Beitrag zur Steroidresistenz bei schwerem Asthma zu untersuchen. **Methoden:** Der STING-Signalweg wurde in humanen Bronchialfibroblasten und Lungengewebe in Steroiden hyporesponsiven Mäusemodellen mit schwerem Asthma untersucht. Dies wurde zu Studienbeginn, nach Stimulation und nach Behandlung mit Dexamethason und/oder STING-Inhibitor sowohl auf mRNA- als auch auf Proteinebene untersucht. Der STING-Inhibitor wurde in PLGA-Nanopartikel eingekapselt und seine physikalisch-chemischen Eigenschaften wurden bewertet. Im Asthma-Mausmodell wurden die Steroidreaktion, die Hyperreaktivität der Atemwege (AHR) und Entzündungsmarker bewertet. **Ergebnisse:** Asthmatische Mäuse wiesen höhere Ausgangsspiegel des STING/IFN-I-Signalwegs auf, die nach Stimulation mit HDM weiter erhöht wurden. Im Mausmodell mit Resistenz gegen Atemwegssteroide war die STING-Aktivierung resistent gegen eine Dexamethason-Monotherapie, sprach aber auf eine Kombinationsbehandlung mit STING-Inhibitor und Dexamethason an. Daher wurden Nanopartikel synthetisiert, die STING-Hemmer verkapselt, um die Arzneimittelabgabe und -wirksamkeit in Atemwegen mit schwerem Asthma zu verbessern. Die intranasale Verabreichung von STING-Inhibitor beladenen Nanopartikeln kontrollierte die Lungenentzündung und stellte die Steroidempfindlichkeit wirksamer wieder her als freier STING-Inhibitor im Mausmodell mit schwerem Asthma. **Schlussfolgerung:** Diese Ergebnisse unterstützen das Konzept, dass der STING-Signalweg eine wichtige Rolle bei der Pathogenese von schwerem Asthma spielt, über die Induktion einer Lungenentzündung und die Verstärkung der Steroidresistenz. Darüber hinaus wurden mit STING-Inhibitor beladene Nanopartikel vorgeschlagen, um die Abgabe zu erhöhen, die Toxizität zu verringern und die Wirksamkeit des STING-Inhibitors zu verbessern.

Bibliography

Aboumatar, H., Garcia Morales, E. E., Jager, L. R., Naqibuddin, M., Kim, S., Saunders, J., . . . Wise, R. (2022). Comparing Self-Management Programs with and without Peer Support among Patients with Chronic Obstructive Pulmonary Disease: A Clinical Trial. *Ann Am Thorac Soc, 19*(10), 1687-1696. doi:10.1513/AnnalsATS.202108-932OC

Aboumatar, H., Naqibuddin, M., Chung, S., Adebowale, H., Bone, L., Brown, T., . . . Group, B. S. P. F. P. (2017). Better Respiratory Education and Treatment Help Empower (BREATHE) study: Methodology and baseline characteristics of a randomized controlled trial testing a transitional care program to improve patient-centered care delivery among chronic obstructive pulmonary disease patients. *Contemp Clin Trials, 62*, 159-167. doi:10.1016/j.cct.2017.08.018

Aboumatar, H., Naqibuddin, M., Neiman, J., Saunders, J., Kim, S., Chaudhry, H., . . . Wise, R. (2020). Methodology and baseline characteristics of a randomized controlled trial testing a health care professional and peer-support program for patients with chronic obstructive pulmonary disease: The BREATHE2 study. *Contemp Clin Trials, 94*, 106023. doi:10.1016/j.cct.2020.106023

Abulateefeh, S. R. (2023). Long-acting injectable PLGA/PLA depots for leuprolide acetate: successful translation from bench to clinic. *Drug Deliv Transl Res, 13*(2), 520-530. doi:10.1007/s13346-022-01228-0

Ait-Khaled, N., Enarson, D., & Bousquet, J. (2001). Chronic respiratory diseases in developing countries: the burden and strategies for prevention and management. *Bull World Health Organ, 79*(10), 971-979.

Akira, S., Uematsu, S., & Takeuchi, O. (2006). Pathogen recognition and innate immunity. *Cell, 124*(4), 783-801. doi:10.1016/j.cell.2006.02.015

Al-Hammadi, S., & Al-Zaabi, O. (2013). Asthma diagnosis and treatment - 1027. Body mass index of asthmatic children in United Arab Emirates. *World Allergy Organization Journal, 6*(1), P26-P26. doi:10.1186/1939-4551-6-S1-P26

Al-Maskari, F., Bener, A., Al-Kaabi, A., Al-Suwaidi, N. A., Norman, N., & Brebner, J. J. A. e. i. (2000). Asthma and respiratory symptoms among school children in United Arab Emirates. *32 4*, 159-163.

Al-Muhsen, S., Johnson, J. R., & Hamid, Q. (2011). Remodeling in asthma. *J Allergy Clin Immunol, 128*(3), 451-462; quiz 463-454. doi:10.1016/j.jaci.2011.04.047

Al Heialy, S., Gaudet, M., Ramakrishnan, R. K., Mogas, A., Salameh, L., Mahboub, B., & Hamid, Q. (2020). Contribution of IL-17 in Steroid Hyporesponsiveness in Obese Asthmatics Through Dysregulation of Glucocorticoid Receptors alpha and beta. *Front Immunol, 11*, 1724. doi:10.3389/fimmu.2020.01724

Al Zaabi, A., Asad, F., Abdou, J., Al Musaabi, H., Al Saiari, M. B., Buhussien, A. S., . . . Soriano, J. B. (2011). Prevalence of COPD in Abu Dhabi, United Arab Emirates. *Respir Med, 105*(4), 566-570. doi:10.1016/j.rmed.2010.12.008

Allinne, J., Scott, G., Lim, W. K., Birchard, D., Erjefalt, J. S., Sanden, C., . . . Orengo, J. M. (2019). IL-33 blockade affects mediators of persistence and exacerbation in a model of chronic airway inflammation. *J Allergy Clin Immunol, 144*(6), 1624-1637 e1610. doi:10.1016/j.jaci.2019.08.039

Alsowaidi, S., Abdulle, A., & Bernsen, R. (2010a). Prevalence and risk factors of asthma among adolescents and their parents in Al-Ain (United Arab Emirates). *Respiration, 79*(2), 105-111. doi:10.1159/000219248

Alsowaidi, S., Abdulle, A., Bernsen, R., & Zuberbier, T. (2010b). Allergic rhinitis and asthma: a large cross-sectional study in the United Arab Emirates. *Int Arch Allergy Immunol, 153*(3), 274-279. doi:10.1159/000314368

Alzaabi, A., Alseiari, M., & Mahboub, B. (2014). Economic burden of asthma in Abu Dhabi: a retrospective study. *Clinicoecon Outcomes Res, 6*, 445-450. doi:10.2147/CEOR.S68920

An, J., Durcan, L., Karr, R. M., Briggs, T. A., Rice, G. I., Teal, T. H., . . . Elkon, K. B. (2017). Expression of Cyclic GMP-AMP Synthase in Patients With Systemic Lupus Erythematosus. *Arthritis Rheumatol, 69*(4), 800-807. doi:10.1002/art.40002

An, X., Zhu, Y., Zheng, T., Wang, G., Zhang, M., Li, J., . . . Li, X. (2019). An Analysis of the Expression and Association with Immune Cell Infiltration of the cGAS/STING Pathway in Pan-Cancer. *Mol Ther Nucleic Acids, 14*, 80-89. doi:10.1016/j.omtn.2018.11.003

Andzinski, L., Spanier, J., Kasnitz, N., Kroger, A., Jin, L., Brinkmann, M. M., . . . Lienenklaus, S. (2016). Growing tumors induce a local STING dependent Type I IFN response in dendritic cells. *Int J Cancer, 139*(6), 1350-1357. doi:10.1002/ijc.30159

Athari, S. S., Mortaz, E., Pourpak, Z., Moin, M., & Moazzeni, S. M. (2016). VIP-loaded PLGA as an anti-asthma nanodrug candidate. *Comparative Clinical Pathology, 25*(4), 791-796. doi:10.1007/s00580-016-2265-6

Attia, A. M., Enan, E. T., Hashish, A. A., El-Kannishy, M. H. S., Gardouh, A. R., Tawfik, K. M., . . . Zaitone, S. A. (2021). Chemopreventive Effect of 5-Flurouracil Polymeric

Hybrid PLGA-Lecithin Nanoparticles against Colon Dysplasia Model in Mice and Impact on p53 Apoptosis. *Biomolecules, 11*(1). doi:10.3390/biom11010109

Avriel, A., Rozenberg, D., Raviv, Y., Heimer, D., Bar-Shai, A., Gavish, R., . . . Douvdevani, A. (2016). Prognostic utility of admission cell-free DNA levels in patients with chronic obstructive pulmonary disease exacerbations. *International journal of chronic obstructive pulmonary disease, 11*, 3153-3161. doi:10.2147/COPD.S113256

Barber, G. N. (2011). Cytoplasmic DNA innate immune pathways. *Immunol Rev, 243*(1), 99-108. doi:10.1111/j.1600-065X.2011.01051.x

Barber, G. N. (2015). STING: infection, inflammation and cancer. *Nat Rev Immunol, 15*(12), 760-770. doi:10.1038/nri3921

Barnes, P. J. (2009). Role of HDAC2 in the pathophysiology of COPD. *Annu Rev Physiol, 71*, 451-464. doi:10.1146/annurev.physiol.010908.163257

Barnes, P. J. (2013). Corticosteroid resistance in patients with asthma and chronic obstructive pulmonary disease. *J Allergy Clin Immunol, 131*(3), 636-645. doi:10.1016/j.jaci.2012.12.1564

Barnes, P. J. (2019). Inflammatory endotypes in COPD. *Allergy, 74*(7), 1249-1256. doi:10.1111/all.13760

Behandy, A., Faisal, A., & Sawaf, E. (2015). *Epidemiological Profile and Clinical Characteristics of the Childhood Asthma Among School Students in Dubai , UAE*.

Bener, A., Abdulrazzaq, Y. M., Debuse, P., & al-Mutawwa, J. (1994). Prevalence of asthma among Emirates school children. *Eur J Epidemiol, 10*(3), 271-278. doi:10.1007/BF01719349

Benmerzoug, S., Bounab, B., Rose, S., Gosset, D., Biet, F., Cochard, T., . . . Quesniaux, V. F. J. (2019). Sterile Lung Inflammation Induced by Silica Exacerbates Mycobacterium tuberculosis Infection via STING-Dependent Type 2 Immunity. *Cell Rep, 27*(9), 2649-2664 e2645. doi:10.1016/j.celrep.2019.04.110

Benmerzoug, S., Rose, S., Bounab, B., Gosset, D., Duneau, L., Chenuet, P., . . . Quesniaux, V. F. J. (2018). STING-dependent sensing of self-DNA drives silica-induced lung inflammation. *Nat Commun, 9*(1), 5226. doi:10.1038/s41467-018-07425-1

Bergeron, C., Al-Ramli, W., & Hamid, Q. (2009). Remodeling in asthma. *Proc Am Thorac Soc, 6*(3), 301-305. doi:10.1513/pats.200808-089RM

Bhakta, N. R., Christenson, S. A., Nerella, S., Solberg, O. D., Nguyen, C. P., Choy, D. F., . . . Woodruff, P. G. (2018). IFN-stimulated Gene Expression, Type 2 Inflammation, and Endoplasmic Reticulum Stress in Asthma. *Am J Respir Crit Care Med, 197*(3), 313-324. doi:10.1164/rccm.201706-1070OC

Branchett, W. J., O'Garra, A., & Lloyd, C. M. (2020). Transcriptomic analysis reveals diverse gene expression changes in airway macrophages during experimental allergic airway disease. *Wellcome Open Res, 5*, 101. doi:10.12688/wellcomeopenres.15875.2

Caminati, M., Pham, D. L., Bagnasco, D., & Canonica, G. W. (2018). Type 2 immunity in asthma. *World Allergy Organ J, 11*(1), 13. doi:10.1186/s40413-018-0192-5

Cavagnero, K. J., Badrani, J. H., Naji, L. H., Amadeo, M. B., Leng, A. S., Lacasa, L. D., . . . Doherty, T. A. (2021). Cyclic-di-GMP Induces STING-Dependent ILC2 to ILC1 Shift During Innate Type 2 Lung Inflammation. *Front Immunol, 12*, 618807. doi:10.3389/fimmu.2021.618807

Celebioglu, E. (2020). COPD Phenotypes Defined by Atopy and Asthma. *Chest, 158*(6), 2239-2240. doi:10.1016/j.chest.2020.08.2077

Ceylan, E., Kocyigit, A., Gencer, M., Aksoy, N., & Selek, S. (2006). Increased DNA damage in patients with chronic obstructive pulmonary disease who had once smoked or been exposed to biomass. *Respir Med, 100*(7), 1270-1276. doi:10.1016/j.rmed.2005.10.011

Chan, B. C. L., Lam, C. W. K., Tam, L. S., & Wong, C. K. (2019). IL33: Roles in Allergic Inflammation and Therapeutic Perspectives. *Front Immunol, 10*, 364. doi:10.3389/fimmu.2019.00364

Chan, T. K., Loh, X. Y., Peh, H. Y., Tan, W. N. F., Tan, W. S. D., Li, N., . . . Engelward, B. P. (2016). House dust mite-induced asthma causes oxidative damage and DNA double-strand breaks in the lungs. *J Allergy Clin Immunol, 138*(1), 84-96 e81. doi:10.1016/j.jaci.2016.02.017

Chang, Y., Al-Alwan, L., Risse, P. A., Halayko, A. J., Martin, J. G., Baglole, C. J., . . . Hamid, Q. (2012). Th17-associated cytokines promote human airway smooth muscle cell proliferation. *FASEB J, 26*(12), 5152-5160. doi:10.1096/fj.12-208033

Chen, L., Ge, Q., Tjin, G., Alkhouri, H., Deng, L., Brandsma, C. A., . . . Oliver, B. G. (2014). Effects of cigarette smoke extract on human airway smooth muscle cells in COPD. *Eur Respir J, 44*(3), 634-646. doi:10.1183/09031936.00171313

Chen, L., Mehrabi Nasab, E., & Athari, S. S. (2022). Effect of Loaded Glycyrrhizic Acid on PLGA Nano-particle on Treatment of Allergic Asthma. *Iran J Allergy Asthma Immunol, 21*(1), 65-72. doi:10.18502/ijaai.v21i1.8617

Chung, K. F., Wenzel, S. E., Brozek, J. L., Bush, A., Castro, M., Sterk, P. J., . . . Teague, W. G. (2014). International ERS/ATS guidelines on definition, evaluation and treatment of severe asthma. *Eur Respir J, 43*(2), 343-373. doi:10.1183/09031936.00202013

Chung, K. W., Dhillon, P., Huang, S., Sheng, X., Shrestha, R., Qiu, C., . . . Susztak, K. (2019). Mitochondrial Damage and Activation of the STING Pathway Lead to Renal Inflammation and Fibrosis. *Cell Metab, 30*(4), 784-799 e785. doi:10.1016/j.cmet.2019.08.003

Cottini, M., Lombardi, C., & Micheletto, C. (2015). Small airway dysfunction and bronchial asthma control : the state of the art. *Asthma Res Pract, 1*, 13. doi:10.1186/s40733-015-0013-3

da Silva, J., Hilzendeger, C., Moermans, C., Schleich, F., Henket, M., Kebadze, T., . . . Louis, R. (2017). Raised interferon-beta, type 3 interferon and interferon-stimulated genes - evidence of innate immune activation in neutrophilic asthma. *Clin Exp Allergy, 47*(3), 313-323. doi:10.1111/cea.12809

Dankers, W., Northcott, M., Bennett, T., D'Cruz, A., Sherlock, R., Gearing, L. J., . . . Jones, S. A. (2022). Type 1 interferon suppresses expression and glucocorticoid induction of glucocorticoid-induced leucine zipper (GILZ). *Front Immunol, 13*, 1034880. doi:10.3389/fimmu.2022.1034880

de Groot, J. C., Ten Brinke, A., & Bel, E. H. (2015). Management of the patient with eosinophilic asthma: a new era begins. *ERJ Open Res, 1*(1). doi:10.1183/23120541.00024-2015

de Oliveira Mann, C. C., & Kranzusch, P. J. (2017). cGAS Conducts Micronuclei DNA Surveillance. *Trends Cell Biol, 27*(10), 697-698. doi:10.1016/j.tcb.2017.08.007

Deng, L., Liang, H., Xu, M., Yang, X., Burnette, B., Arina, A., . . . Weichselbaum, R. R. (2014). STING-Dependent Cytosolic DNA Sensing Promotes Radiation-Induced Type I Interferon-Dependent Antitumor Immunity in Immunogenic Tumors. *Immunity, 41*(5), 843-852. doi:10.1016/j.immuni.2014.10.019

Dhanwani, R., Takahashi, M., & Sharma, S. (2018). Cytosolic sensing of immuno-stimulatory DNA, the enemy within. *Curr Opin Immunol, 50*, 82-87. doi:10.1016/j.coi.2017.11.004

Dharmage, S. C., Perret, J. L., & Custovic, A. (2019). Epidemiology of Asthma in Children and Adults. *Front Pediatr, 7*, 246. doi:10.3389/fped.2019.00246

Doherty, T. A. (2020). Roles of STING and innate lymphoid cell plasticity in severe asthma. In: National Institute of Health (NIH).

Ebensen, T., Schulze, K., Riese, P., Link, C., Morr, M., & Guzman, C. A. (2007). The bacterial second messenger cyclic diGMP exhibits potent adjuvant properties. *Vaccine, 25*(8), 1464-1469. doi:10.1016/j.vaccine.2006.10.033

El Hasnaoui, A., Rashid, N., Lahlou, A., Salhi, H., Doble, A., Nejjari, C., & Group, B. S. (2012). Chronic obstructive pulmonary disease in the adult population within the Middle East and North Africa region: rationale and design of the BREATHE study. *Respir Med, 106 Suppl 2*, S3-15. doi:10.1016/S0954-6111(12)70010-0

Enweasor, C., Flayer, C. H., & Haczku, A. (2021). Ozone-Induced Oxidative Stress, Neutrophilic Airway Inflammation, and Glucocorticoid Resistance in Asthma. *Front Immunol, 12*, 631092. doi:10.3389/fimmu.2021.631092

Errico, C., Bartoli, C., Chiellini, F., & Chiellini, E. (2009). Poly(hydroxyalkanoates)-based polymeric nanoparticles for drug delivery. *J Biomed Biotechnol, 2009*, 571702. doi:10.1155/2009/571702

Evasovic, J. M., & Singer, C. A. (2019). Regulation of IL-17A and implications for TGF-beta1 comodulation of airway smooth muscle remodeling in severe asthma. *Am J Physiol Lung Cell Mol Physiol, 316*(5), L843-L868. doi:10.1152/ajplung.00416.2018

Fallahzadeh, A., Sharifnejad Tehrani, Y., Sheikhy, A., Ghamari, S. H., Mohammadi, E., Saeedi Moghaddam, S., . . . Farzadfar, F. (2022). The burden of chronic respiratory disease and attributable risk factors in North Africa and Middle East: findings from global burden of disease study (GBD) 2019. *Respir Res, 23*(1), 268. doi:10.1186/s12931-022-02187-3

Fehrenbach, H., Wagner, C., & Wegmann, M. (2017). Airway remodeling in asthma: what really matters. *Cell Tissue Res, 367*(3), 551-569. doi:10.1007/s00441-016-2566-8

Fenech, M., Knasmueller, S., Bolognesi, C., Holland, N., Bonassi, S., & Kirsch-Volders, M. (2020). Micronuclei as biomarkers of DNA damage, aneuploidy, inducers of chromosomal hypermutation and as sources of pro-inflammatory DNA in humans. *Mutat Res Rev Mutat Res, 786*, 108342. doi:10.1016/j.mrrev.2020.108342

Finkelstein, E. A., Malkin, J. D., Baid, D., Alqunaibet, A., Mahdi, K., Al-Thani, M. B. H., . . . Herbst, C. H. (2021). The impact of seven major noncommunicable diseases on direct medical costs, absenteeism, and presenteeism in Gulf Cooperation Council countries. *J Med Econ, 24*(1), 828-834. doi:10.1080/13696998.2021.1945242

Fitzgerald, K. A., & Kagan, J. C. (2020). Toll-like Receptors and the Control of Immunity. *Cell, 180*(6), 1044-1066. doi:10.1016/j.cell.2020.02.041

Flammer, J. R., Dobrovolna, J., Kennedy, M. A., Chinenov, Y., Glass, C. K., Ivashkiv, L. B., & Rogatsky, I. (2010). The type I interferon signaling pathway is a target for glucocorticoid inhibition. *Mol Cell Biol, 30*(19), 4564-4574. doi:10.1128/MCB.00146-10

Gaballah, H. H., Gaber, R. A., Sharshar, R. S., & Elshweikh, S. A. (2018). NOD2 expression, DNA damage and oxido-inflammatory status in atopic bronchial asthma: Exploring their nexus to disease severity. *Gene, 660*, 128-135. doi:10.1016/j.gene.2018.03.061

Gauthier, M., Chakraborty, K., Oriss, T. B., Raundhal, M., Das, S., Chen, J., . . . Ray, A. (2017). Severe asthma in humans and mouse model suggests a CXCL10 signature underlies corticosteroid-resistant Th1 bias. *JCI Insight, 2*(13). doi:10.1172/jci.insight.94580

GBD. (2020). Global burden of 369 diseases and injuries in 204 countries and territories, 1990-2019: a systematic analysis for the Global Burden of Disease Study 2019. *Lancet, 396*(10258), 1204-1222. doi:10.1016/S0140-6736(20)30925-9

GINA. (2022). Global Strategy for Asthma Management and Prevention. Retrieved from www.ginasthma.org

GOLD. (2022). *Global Strategy for the Diagnosis, Management, and Prevention of Chronic Obstructive Lung Disease*. In. Retrieved from www.goldcopd.org

Gregory, L. G., & Lloyd, C. M. (2011). Orchestrating house dust mite-associated allergy in the lung. *Trends Immunol, 32*(9), 402-411. doi:10.1016/j.it.2011.06.006

Guo, Y. K., Ming, S. L., Zeng, L., Chang, W. R., Pan, J. J., Zhang, C., . . . Chu, B. B. (2021). Inhibition of histone deacetylase 1 suppresses pseudorabies virus infection through cGAS-STING antiviral innate immunity. *Mol Immunol, 136*, 55-64. doi:10.1016/j.molimm.2021.05.012

Haag, S. M., Gulen, M. F., Reymond, L., Gibelin, A., Abrami, L., Decout, A., . . . Ablasser, A. (2018). Targeting STING with covalent small-molecule inhibitors. *Nature, 559*(7713), 269-273. doi:10.1038/s41586-018-0287-8

Haider, M., Elsherbeny, A., Jagal, J., Hubatova-Vackova, A., & Saad Ahmed, I. (2020). Optimization and Evaluation of Poly(lactide-co-glycolide) Nanoparticles for Enhanced Cellular Uptake and Efficacy of Paclitaxel in the Treatment of Head and Neck Cancer. *Pharmaceutics, 12*(9). doi:10.3390/pharmaceutics12090828

Halwani, R., Al-Kufaidy, R., Vazquez-Tello, A., Pureza, M. A., BaHammam, A. S., Al-Jahdali, H., . . . Al-Muhsen, S. (2014). IL-17 Enhances Chemotaxis of Primary Human B Cells during Asthma. *PLoS One, 9*(12), e114604. doi:10.1371/journal.pone.0114604

Halwani, R., Al-Muhsen, S., Al-Jahdali, H., & Hamid, Q. (2011). Role of transforming growth factor-beta in airway remodeling in asthma. *Am J Respir Cell Mol Biol, 44*(2), 127-133. doi:10.1165/rcmb.2010-0027TR

Halwani, R., Al-Muhsen, S., & Hamid, Q. (2010). Airway remodeling in asthma. *Curr Opin Pharmacol, 10*(3), 236-245. doi:10.1016/j.coph.2010.06.004

Halwani, R., Al-Muhsen, S., & Hamid, Q. (2013). T helper 17 cells in airway diseases: from laboratory bench to bedside. *Chest, 143*(2), 494-501. doi:10.1378/chest.12-0598

Halwani, R., Sultana Shaik, A., Ratemi, E., Afzal, S., Kenana, R., Al-Muhsen, S., & Al Faraj, A. (2016). A novel anti-IL4Ralpha nanoparticle efficiently controls lung inflammation during asthma. *Exp Mol Med, 48*(10), e262. doi:10.1038/emm.2016.89

Hamid, Q., & Tulic, M. (2009). Immunobiology of asthma. *Annu Rev Physiol, 71*, 489-507. doi:10.1146/annurev.physiol.010908.163200

Hamzaoui, A., Chaouch, N., Grairi, H., Ammar, J., & Hamzaoui, K. (2005). Inflammatory process of CD8+ CD28- T cells in induced sputum from asthmatic patients. *Mediators Inflamm, 2005*(3), 160-166. doi:10.1155/MI.2005.160

Han, Y., Chen, L., Liu, H., Jin, Z., Wu, Y., Wu, Y., . . . Yan, F. (2020). Airway Epithelial cGAS Is Critical for Induction of Experimental Allergic Airway Inflammation. *J Immunol, 204*(6), 1437-1447. doi:10.4049/jimmunol.1900869

Hastie, A. T., Steele, C., Dunaway, C. W., Moore, W. C., Rector, B. M., Ampleford, E., . . . Program, N. S. A. R. (2018). Complex association patterns for inflammatory mediators in induced sputum from subjects with asthma. *Clin Exp Allergy, 48*(7), 787-797. doi:10.1111/cea.13129

He, Y. Q., Zhou, C. C., Deng, J. L., Wang, L., & Chen, W. S. (2021). Tanreqing Inhibits LPS-Induced Acute Lung Injury In Vivo and In Vitro Through Downregulating STING Signaling Pathway. *Front Pharmacol, 12*, 746964. doi:10.3389/fphar.2021.746964

Hilzendeger, C., da Silva, J., Henket, M., Schleich, F., Corhay, J. L., Kebadze, T., . . . Louis, R. (2016). Reduced sputum expression of interferon-stimulated genes in severe COPD. *Int J Chron Obstruct Pulmon Dis, 11*, 1485-1494. doi:10.2147/COPD.S105948

Hinds, T. D., Jr., Ramakrishnan, S., Cash, H. A., Stechschulte, L. A., Heinrich, G., Najjar, S. M., & Sanchez, E. R. (2010). Discovery of glucocorticoid receptor-beta in mice with a role in metabolism. *Mol Endocrinol, 24*(9), 1715-1727. doi:10.1210/me.2009-0411

Holgate, S. T. (2012). Innate and adaptive immune responses in asthma. *Nat Med, 18*(5), 673-683. doi:10.1038/nm.2731

Hu, B., Jin, C., Li, H. B., Tong, J., Ouyang, X., Cetinbas, N. M., . . . Flavell, R. A. (2016). The DNA-sensing AIM2 inflammasome controls radiation-induced cell death and tissue injury. *Science, 354*(6313), 765-768. doi:10.1126/science.aaf7532

Hussein, H., Al Behandy, N. S., Al Faisal, W., El Sawaf, E., Wasfy, A., Alshareef, N., & Altheeb, A. S. (2018). *Prevalence of bronchial asthma and its association with obesity and overweight among adolescents in Dubai, UAE*. Paper presented at the 12th International Conference on Allergy, Asthma and Clinical Immunology, Russia.

Ibrahim, N. M., Almarzouqi, F. I., Al Melaih, F. A., Farouk, H., Alsayed, M., & AlJassim, F. M. (2021). Prevalence of asthma and allergies among children in the United Arab Emirates: A cross-sectional study. *World Allergy Organ J, 14*(10), 100588. doi:10.1016/j.waojou.2021.100588

Icardi, L., Lievens, S., Mori, R., Piessevaux, J., De Cauwer, L., De Bosscher, K., & Tavernier, J. (2012). Opposed regulation of type I IFN-induced STAT3 and ISGF3 transcriptional activities by histone deacetylases (HDACS) 1 and 2. *FASEB J, 26*(1), 240-249. doi:10.1096/fj.11-191122

Iwasaki, A., Foxman, E. F., & Molony, R. D. (2017). Early local immune defences in the respiratory tract. *Nat Rev Immunol, 17*(1), 7-20. doi:10.1038/nri.2016.117

Jensen, S., & Thomsen, A. R. (2012). Sensing of RNA viruses: a review of innate immune receptors involved in recognizing RNA virus invasion. *J Virol, 86*(6), 2900-2910. doi:10.1128/JVI.05738-11

Kato, Y., Park, J., Takamatsu, H., Konaka, H., Aoki, W., Aburaya, S., . . . Kumanogoh, A. (2018). Apoptosis-derived membrane vesicles drive the cGAS-STING pathway and enhance type I IFN production in systemic lupus erythematosus. *Ann Rheum Dis, 77*(10), 1507-1515. doi:10.1136/annrheumdis-2018-212988

Kawai, T., & Akira, S. (2010). The role of pattern-recognition receptors in innate immunity: update on Toll-like receptors. *Nat Immunol, 11*(5), 373-384. doi:10.1038/ni.1863

Kis, K., Liu, X., & Hagood, J. S. (2011). Myofibroblast differentiation and survival in fibrotic disease. *Expert Rev Mol Med, 13*, e27. doi:10.1017/S1462399411001967

Krupina, K., Goginashvili, A., & Cleveland, D. W. (2021). Causes and consequences of micronuclei. *Curr Opin Cell Biol, 70*, 91-99. doi:10.1016/j.ceb.2021.01.004

Kubo, M. (2017). Innate and adaptive type 2 immunity in lung allergic inflammation. *Immunol Rev, 278*(1), 162-172. doi:10.1111/imr.12557

Kumar, V. (2019). A STING to inflammation and autoimmunity. *J Leukoc Biol, 106*(1), 171-185. doi:10.1002/JLB.4MIR1018-397RR

Kuruvilla, M. E., Lee, F. E., & Lee, G. B. (2019). Understanding Asthma Phenotypes, Endotypes, and Mechanisms of Disease. *Clin Rev Allergy Immunol, 56*(2), 219-233. doi:10.1007/s12016-018-8712-1

Kwon, J., & Bakhoum, S. F. (2020). The Cytosolic DNA-Sensing cGAS-STING Pathway in Cancer. *Cancer Discov, 10*(1), 26-39. doi:10.1158/2159-8290.CD-19-0761

Lambrecht, B. N., Hammad, H., & Fahy, J. V. (2019). The Cytokines of Asthma. *Immunity, 50*(4), 975-991. doi:10.1016/j.immuni.2019.03.018

Li, L. B., Leung, D. Y., Martin, R. J., & Goleva, E. (2010). Inhibition of histone deacetylase 2 expression by elevated glucocorticoid receptor beta in steroid-resistant asthma. *Am J Respir Crit Care Med, 182*(7), 877-883. doi:10.1164/rccm.201001-0015OC

Li, Y., Wilson, H. L., & Kiss-Toth, E. (2017). Regulating STING in health and disease. *J Inflamm (Lond), 14*, 11. doi:10.1186/s12950-017-0159-2

Lian, Q., Xu, J., Yan, S., Huang, M., Ding, H., Sun, X., . . . Geng, M. (2017). Chemotherapy-induced intestinal inflammatory responses are mediated by exosome secretion of double-strand DNA via AIM2 inflammasome activation. *Cell Res, 27*(6), 784-800. doi:10.1038/cr.2017.54

Lintsov, A., Pleskach, N., Spivak, I., Slizhov, P., Shevelev, S., Uslontsev, B., . . . Mikhelson, V. (2019). Analysis of micronuclei in buccal epithelial cells from asthmatic patients. *European Respiratory Journal, 54*(suppl 63), PA5212. doi:10.1183/13993003.congress-2019.PA5212

Liu, Y., Crowe, W. N., Wang, L., Lu, Y., Petty, W. J., Habib, A. A., & Zhao, D. (2019). An inhalable nanoparticulate STING agonist synergizes with radiotherapy to confer long-term control of lung metastases. *Nat Commun, 10*(1), 5108. doi:10.1038/s41467-019-13094-5

Liu, Y., Jesus, A. A., Marrero, B., Yang, D., Ramsey, S. E., Sanchez, G. A. M., . . . Goldbach-Mansky, R. (2014). Activated STING in a vascular and pulmonary syndrome. *N Engl J Med, 371*(6), 507-518. doi:10.1056/NEJMoa1312625

Lommatzsch, M., & Virchow, J. C. (2014). Severe asthma: definition, diagnosis and treatment. *Dtsch Arztebl Int, 111*(50), 847-855. doi:10.3238/arztebl.2014.0847

Lu, C., Zhang, X., Ma, C., Xu, W., Gan, L., Cui, J., . . . Wang, H. (2018). Nontypeable Haemophilus influenzae DNA stimulates type I interferon expression via STING signaling pathway. *Biochimica et Biophysica Acta (BBA) - Molecular Cell Research, 1865*(4), 665-673. doi:10.1016/j.bbamcr.2018.01.011

Luo, X., Li, H., Ma, L., Zhou, J., Guo, X., Woo, S. L., . . . Wu, C. (2018). Expression of STING Is Increased in Liver Tissues From Patients With NAFLD and Promotes Macrophage-Mediated Hepatic Inflammation and Fibrosis in Mice. *Gastroenterology, 155*(6), 1971-1984 e1974. doi:10.1053/j.gastro.2018.09.010

Luo, X. Q., Zhong, J. W., Qiu, S. Y., Zhi, M., Yang, L. Q., Zhou, Y. L., . . . Mo, L. H. (2020). A20-OVA Nanoparticles Inhibit Allergic Asthma in a Murine Model. *Inflammation, 43*(3), 953-961. doi:10.1007/s10753-020-01181-5

Ma, R., Ortiz Serrano, T. P., Davis, J., Prigge, A. D., & Ridge, K. M. (2020). The cGAS-STING pathway: The role of self-DNA sensing in inflammatory lung disease. *FASEB J, 34*(10), 13156-13170. doi:10.1096/fj.202001607R

Mackenzie, K. J., Carroll, P., Martin, C. A., Murina, O., Fluteau, A., Simpson, D. J., . . . Jackson, A. P. (2017). cGAS surveillance of micronuclei links genome instability to innate immunity. *Nature, 548*(7668), 461-465. doi:10.1038/nature23449

Mahboub, B., Al-Hammadi, S., Rafique, M., Sulaiman, N., Pawankar, R., Al Redha, A. I., & Mehta, A. C. (2012). Population prevalence of asthma and its determinants based on European Community Respiratory Health Survey in the United Arab Emirates. *BMC Pulm Med, 12*, 4. doi:10.1186/1471-2466-12-4

Mahboub, B., Al Heialy, S., Hachim, M. Y., Ramakrishnan, R. K., Alzaabi, A., Seliem, R. M., . . . Hamid, Q. (2021). Vitamin D Regulates the Expression of Glucocorticoid Receptors in Blood of Severe Asthmatic Patients. *J Immunol Res, 2021*, 9947370. doi:10.1155/2021/9947370

Mahboub, B., Alzaabi, A., Soriano, J. B., Salameh, L., Mutairi, Y. A., Yusufali, A. A., . . . Haughney, J. (2014). Case-finding of chronic obstructive pulmonary disease with questionnaire, peak flow measurements and spirometry: a cross-sectional study. *BMC Res Notes, 7*, 241. doi:10.1186/1756-0500-7-241

Makadia, H. K., & Siegel, S. J. (2011). Poly Lactic-co-Glycolic Acid (PLGA) as Biodegradable Controlled Drug Delivery Carrier. *Polymers (Basel), 3*(3), 1377-1397. doi:10.3390/polym3031377

Mallol, J., Crane, J., von Mutius, E., Odhiambo, J., Keil, U., Stewart, A., & Group, I. P. T. S. (2013). The International Study of Asthma and Allergies in Childhood

(ISAAC) Phase Three: a global synthesis. *Allergol Immunopathol (Madr), 41*(2), 73-85. doi:10.1016/j.aller.2012.03.001

Maluf, S. W., Mergener, M., Dalcanale, L., Costa, C. C., Pollo, T., Kayser, M., . . . Teixeira, P. J. (2007). DNA damage in peripheral blood of patients with chronic obstructive pulmonary disease (COPD). *Mutat Res, 626*(1-2), 180-184. doi:10.1016/j.mrgentox.2006.10.002

Mangal, S., Gao, W., Li, T., & Zhou, Q. T. (2017). Pulmonary delivery of nanoparticle chemotherapy for the treatment of lung cancers: challenges and opportunities. *Acta Pharmacol Sin, 38*(6), 782-797. doi:10.1038/aps.2017.34

Marie, I. J., Chang, H. M., & Levy, D. E. (2018). HDAC stimulates gene expression through BRD4 availability in response to IFN and in interferonopathies. *J Exp Med, 215*(12), 3194-3212. doi:10.1084/jem.20180520

Matthews, J. G., Ito, K., Barnes, P. J., & Adcock, I. M. (2004). Defective glucocorticoid receptor nuclear translocation and altered histone acetylation patterns in glucocorticoid-resistant patients. *J Allergy Clin Immunol, 113*(6), 1100-1108. doi:10.1016/j.jaci.2004.03.018

McBrien, C. N., & Menzies-Gow, A. (2017). The Biology of Eosinophils and Their Role in Asthma. *Front Med (Lausanne), 4*, 93. doi:10.3389/fmed.2017.00093

McCoy, C. E., Carpenter, S., Palsson-McDermott, E. M., Gearing, L. J., & O'Neill, L. A. (2008). Glucocorticoids inhibit IRF3 phosphorylation in response to Toll-like receptor-3 and -4 by targeting TBK1 activation. *J Biol Chem, 283*(21), 14277-14285. doi:10.1074/jbc.M709731200

Mdkhana, B., Saheb Sharif-Askari, N., Ramakrishnan, R. K., Goel, S., Hamid, Q., & Halwani, R. (2021a). Nucleic Acid-Sensing Pathways During SARS-CoV-2 Infection: Expectations versus Reality. *J Inflamm Res, 14*, 199-216. doi:10.2147/JIR.S277716

Mdkhana, B., Zaher, D. M., Abdin, S. M., & Omar, H. A. (2021b). Tangeretin boosts the anticancer activity of metformin in breast cancer cells via curbing the energy production. *Phytomedicine, 83*, 153470. doi:10.1016/j.phymed.2021.153470

Mir, M., Ahmed, N., & Rehman, A. U. (2017). Recent applications of PLGA based nanostructures in drug delivery. *Colloids Surf B Biointerfaces, 159*, 217-231. doi:10.1016/j.colsurfb.2017.07.038

Mirza, S., & Benzo, R. (2017). Chronic Obstructive Pulmonary Disease Phenotypes: Implications for Care. *Mayo Clin Proc, 92*(7), 1104-1112. doi:10.1016/j.mayocp.2017.03.020

Miyake, K., Shibata, T., Ohto, U., Shimizu, T., Saitoh, S. I., Fukui, R., & Murakami, Y. (2018). Mechanisms controlling nucleic acid-sensing Toll-like receptors. *Int Immunol, 30*(2), 43-51. doi:10.1093/intimm/dxy016

Nabe, T. (2020). Steroid-Resistant Asthma and Neutrophils. *Biol Pharm Bull, 43*(1), 31-35. doi:10.1248/bpb.b19-00095

Nachmias, N., Langier, S., Brzezinski, R. Y., Siterman, M., Stark, M., Etkin, S., . . . Bar-Shai, A. (2019). NLRP3 inflammasome activity is upregulated in an in-vitro model of COPD exacerbation. *PLoS One, 14*(5), e0214622. doi:10.1371/journal.pone.0214622

Nascimento, M., Gombault, A., Lacerda-Queiroz, N., Panek, C., Savigny, F., Sbeity, M., . . . Couillin, I. (2019). Self-DNA release and STING-dependent sensing drives inflammation to cigarette smoke in mice. *Scientific Reports, 9*(1), 14848. doi:10.1038/s41598-019-51427-y

National Asthma, E., & Prevention, P. (2002). National Asthma Education and Prevention Program. Expert Panel Report: Guidelines for the Diagnosis and Management of Asthma Update on Selected Topics--2002. *J Allergy Clin Immunol, 110*(5 Suppl), S141-219.

Ning, L., Wei, W., Wenyang, J., Rui, X., & Qing, G. (2020). Cytosolic DNA-STING-NLRP3 axis is involved in murine acute lung injury induced by lipopolysaccharide. *Clin Transl Med, 10*(7), e228. doi:10.1002/ctm2.228

Nunokawa, H., Murakami, Y., Ishii, T., Narita, T., Ishii, H., Takizawa, H., & Yamashita, N. (2021). Crucial role of stimulator of interferon genes-dependent signaling in house dust mite extract-induced IgE production. *Sci Rep, 11*(1), 13157. doi:10.1038/s41598-021-92561-w

Ohta, K., Nagase, H., Suzukawa, M., & Ohta, S. (2017). Antibody therapy for the management of severe asthma with eosinophilic inflammation. *Int Immunol, 29*(7), 337-343. doi:10.1093/intimm/dxx045

Oriss, T. B., Raundhal, M., Morse, C., Huff, R. E., Das, S., Hannum, R., . . . Ray, A. (2017). IRF5 distinguishes severe asthma in humans and drives Th1 phenotype and airway hyperreactivity in mice. *JCI Insight, 2*(10). doi:10.1172/jci.insight.91019

Ozasa, K., Temizoz, B., Kusakabe, T., Kobari, S., Momota, M., Coban, C., . . . Ishii, K. J. (2019). Cyclic GMP-AMP Triggers Asthma in an IL-33-Dependent Manner That Is Blocked by Amlexanox, a TBK1 Inhibitor. *Front Immunol, 10*, 2212. doi:10.3389/fimmu.2019.02212

Panariti, A., Baglole, C. J., Sanchez, V., Eidelman, D. H., Hussain, S., Olivenstein, R., . . . Hamid, Q. (2018). Interleukin-17A and vascular remodelling in severe asthma;

lack of evidence for a direct role. *Clin Exp Allergy, 48*(4), 365-378. doi:10.1111/cea.13093

Paschalaki, K. E., Starke, R. D., Hu, Y., Mercado, N., Margariti, A., Gorgoulis, V. G., . . . Barnes, P. J. (2013). Dysfunction of endothelial progenitor cells from smokers and chronic obstructive pulmonary disease patients due to increased DNA damage and senescence. *Stem Cells, 31*(12), 2813-2826. doi:10.1002/stem.1488

Pauwels, R. A., & Rabe, K. F. (2004). Burden and clinical features of chronic obstructive pulmonary disease (COPD). *Lancet, 364*(9434), 613-620. doi:10.1016/S0140-6736(04)16855-4

Pfuntner, A., Wier, L. M., & Stocks, C. (2006). Most Frequent Conditions in U.S. Hospitals, 2011. In *Healthcare Cost and Utilization Project (HCUP) Statistical Briefs*. Rockville (MD).

Pirooznia, N., Hasannia, S., Lotfi, A. S., & Ghanei, M. (2012). Encapsulation of alpha-1 antitrypsin in PLGA nanoparticles: in vitro characterization as an effective aerosol formulation in pulmonary diseases. *J Nanobiotechnology, 10*, 20. doi:10.1186/1477-3155-10-20

Poon, A. H., & Hamid, Q. (2016). Severe Asthma: Have We Made Progress? *Ann Am Thorac Soc, 13 Suppl 1*, S68-77. doi:10.1513/AnnalsATS.201508-514MG

Pouwels, S. D., Faiz, A., den Boef, L. E., Gras, R., van den Berge, M., Boezen, H. M., . . . Nawijn, M. C. (2017). Genetic variance is associated with susceptibility for cigarette smoke-induced DAMP release in mice. *Am J Physiol Lung Cell Mol Physiol, 313*(3), L559-L580. doi:10.1152/ajplung.00466.2016

Quell, K. M., Dutta, K., Korkmaz, U. R., Nogueira de Almeida, L., Vollbrandt, T., Konig, P., . . . Laumonnier, Y. (2020). GM-CSF and IL-33 Orchestrate Polynucleation and Polyploidy of Resident Murine Alveolar Macrophages in a Murine Model of Allergic Asthma. *Int J Mol Sci, 21*(20). doi:10.3390/ijms21207487

Ramakrishnan, R. K., Al Heialy, S., & Hamid, Q. (2019). Role of IL-17 in asthma pathogenesis and its implications for the clinic. *Expert Rev Respir Med, 13*(11), 1057-1068. doi:10.1080/17476348.2019.1666002

Ramakrishnan, R. K., Bajbouj, K., Al Heialy, S., Mahboub, B., Ansari, A. W., Hachim, I. Y., . . . Hamid, Q. (2020a). IL-17 Induced Autophagy Regulates Mitochondrial Dysfunction and Fibrosis in Severe Asthmatic Bronchial Fibroblasts. *Front Immunol, 11*, 1002. doi:10.3389/fimmu.2020.01002

Ramakrishnan, R. K., Bajbouj, K., Guimei, M., Rawat, S. S., Kalaji, Z., Hachim, M. Y., . . . Hamid, Q. (2022). Bcl10 Regulates Lipopolysaccharide-Induced Pro-Fibrotic

Signaling in Bronchial Fibroblasts from Severe Asthma Patients. *Biomedicines, 10*(7). doi:10.3390/biomedicines10071716

Ramakrishnan, R. K., Bajbouj, K., Hachim, M. Y., Mogas, A. K., Mahboub, B., Olivenstein, R., . . . Hamid, Q. (2020b). Enhanced mitophagy in bronchial fibroblasts from severe asthmatic patients. *PLoS One, 15*(11), e0242695. doi:10.1371/journal.pone.0242695

Ramamoorthy, S., & Cidlowski, J. A. (2016). Corticosteroids: Mechanisms of Action in Health and Disease. *Rheum Dis Clin North Am, 42*(1), 15-31, vii. doi:10.1016/j.rdc.2015.08.002

Ramirez-Velazquez, C., Castillo, E. C., Guido-Bayardo, L., & Ortiz-Navarrete, V. (2013). IL-17-producing peripheral blood CD177+ neutrophils increase in allergic asthmatic subjects. *Allergy Asthma Clin Immunol, 9*(1), 23. doi:10.1186/1710-1492-9-23

Ratemi, E., Sultana Shaik, A., Al Faraj, A., & Halwani, R. (2016). Alternative approaches for the treatment of airway diseases: focus on nanoparticle medicine. *Clin Exp Allergy, 46*(8), 1033-1042. doi:10.1111/cea.12771

Raundhal, M., Morse, C., Khare, A., Oriss, T. B., Milosevic, J., Trudeau, J., . . . Ray, A. (2015). High IFN-gamma and low SLPI mark severe asthma in mice and humans. *J Clin Invest, 125*(8), 3037-3050. doi:10.1172/JCI80911

Reily, M. M., Pantoja, C., Hu, X., Chinenov, Y., & Rogatsky, I. (2006). The GRIP1:IRF3 interaction as a target for glucocorticoid receptor-mediated immunosuppression. *EMBO J, 25*(1), 108-117. doi:10.1038/sj.emboj.7600919

Ritchie, M. E., Phipson, B., Wu, D., Hu, Y., Law, C. W., Shi, W., & Smyth, G. K. (2015). limma powers differential expression analyses for RNA-sequencing and microarray studies. *Nucleic Acids Res, 43*(7), e47. doi:10.1093/nar/gkv007

Robins, S., Roussel, L., Schachter, A., Risse, P. A., Mogas, A. K., Olivenstein, R., . . . Rousseau, S. (2011). Steroid-insensitive ERK1/2 activity drives CXCL8 synthesis and neutrophilia by airway smooth muscle. *Am J Respir Cell Mol Biol, 45*(5), 984-990. doi:10.1165/rcmb.2010-0450OC

Rossnerova, A., Spatova, M., Rossner, P., Jr., Novakova, Z., Solansky, I., & Sram, R. J. (2011). Factors affecting the frequency of micronuclei in asthmatic and healthy children from Ostrava. *Mutat Res, 708*(1-2), 44-49. doi:10.1016/j.mrfmmm.2011.01.004

Saheb Sharif-Askari, F., Saheb Sharif-Askari, N., Goel, S., Hafezi, S., Assiri, R., Al-Muhsen, S., . . . Halwani, R. (2021). SARS-CoV-2 attenuates corticosteroid sensitivity by suppressing DUSP1 expression and activating p38 MAPK

pathway. *European journal of pharmacology, 908*, 174374-174374. doi:10.1016/j.ejphar.2021.174374

Saini, M., & Yadav, A. (2014). *Frequency of micronuclei in asthma patients*. Paper presented at the Future prospects on advancement in biological sciences, health issues and environmental protection, Lucknow, India.

Saini, M., & Yadav, A. S. (2019). DNA damage in the peripheral blood lymphocytes of asthmatic patients in relation to disease progression. *The Nucleus, 62*(1), 57-62. doi:10.1007/s13237-018-0250-y

Salameh, L., Mahboub, B., Almutairi, Y., Abu Shaban, A., & Almazrouie, S. (2013). *COPD case finding in UAE*. Paper presented at the European Respiratory Journal Annual Congress 2013. http://erj.ersjournals.com/content/42/Suppl_57/P1390.abstract

Saliba, D. G., Heger, A., Eames, H. L., Oikonomopoulos, S., Teixeira, A., Blazek, K., . . . Udalova, I. A. (2014). IRF5:RelA interaction targets inflammatory genes in macrophages. *Cell Rep, 8*(5), 1308-1317. doi:10.1016/j.celrep.2014.07.034

Samarasinghe, R. A., Witchell, S. F., & DeFranco, D. B. (2012). Cooperativity and complementarity: synergies in non-classical and classical glucocorticoid signaling. *Cell Cycle, 11*(15), 2819-2827. doi:10.4161/cc.21018

Schneider, W. M., Chevillotte, M. D., & Rice, C. M. (2014). Interferon-stimulated genes: a complex web of host defenses. *Annu Rev Immunol, 32*, 513-545. doi:10.1146/annurev-immunol-032713-120231

Semete, B., Booysen, L., Lemmer, Y., Kalombo, L., Katata, L., Verschoor, J., & Swai, H. S. (2010). In vivo evaluation of the biodistribution and safety of PLGA nanoparticles as drug delivery systems. *Nanomedicine, 6*(5), 662-671. doi:10.1016/j.nano.2010.02.002

She, L., Barrera, G. D., Yan, L., Alanazi, H. H., Brooks, E. G., Dube, P. H., . . . Li, X. D. (2021). STING activation in alveolar macrophages and group 2 innate lymphoid cells suppresses IL-33-driven type 2 immunopathology. *JCI Insight, 6*(3). doi:10.1172/jci.insight.143509

Sun, S. C., Han, R., Hou, S. S., Yi, H. Q., Chi, S. J., & Zhang, A. H. (2020). Juglanin alleviates bleomycin-induced lung injury by suppressing inflammation and fibrosis via targeting sting signaling. *Biomed Pharmacother, 127*, 110119. doi:10.1016/j.biopha.2020.110119

Swanson, K. V., Deng, M., & Ting, J. P. (2019). The NLRP3 inflammasome: molecular activation and regulation to therapeutics. *Nat Rev Immunol, 19*(8), 477-489. doi:10.1038/s41577-019-0165-0

Tageldin, M. A., Nafti, S., Khan, J. A., Nejjari, C., Beji, M., Mahboub, B., . . . Group, B. S. (2012). Distribution of COPD-related symptoms in the Middle East and North Africa: results of the BREATHE study. *Respir Med, 106 Suppl 2*, S25-32. doi:10.1016/S0954-6111(12)70012-4

Tan, X., Sun, L., Chen, J., & Chen, Z. J. (2018). Detection of Microbial Infections Through Innate Immune Sensing of Nucleic Acids. *Annu Rev Microbiol, 72*, 447-478. doi:10.1146/annurev-micro-102215-095605

Tarraf, H., Aydin, O., Mungan, D., Albader, M., Mahboub, B., Doble, A., . . . El Hasnaoui, A. (2018). Prevalence of asthma among the adult general population of five Middle Eastern countries: results of the SNAPSHOT program. *BMC Pulm Med, 18*(1), 68. doi:10.1186/s12890-018-0621-9

Thim-Uam, A., Prabakaran, T., Tansakul, M., Makjaroen, J., Wongkongkathep, P., Chantaravisoot, N., . . . Pisitkun, P. (2020). STING Mediates Lupus via the Activation of Conventional Dendritic Cell Maturation and Plasmacytoid Dendritic Cell Differentiation. *iScience, 23*(9), 101530. doi:10.1016/j.isci.2020.101530

Toussaint, M., Jackson, D. J., Swieboda, D., Guedán, A., Tsourouktsoglou, T. D., Ching, Y. M., . . . Johnston, S. L. (2017). Host DNA released by NETosis promotes rhinovirus-induced type-2 allergic asthma exacerbation. *Nat Med, 23*(6), 681-691. doi:10.1038/nm.4332

Trejo Bittar, H. E., Yousem, S. A., & Wenzel, S. E. (2015). Pathobiology of severe asthma. *Annu Rev Pathol, 10*, 511-545. doi:10.1146/annurev-pathol-012414-040343

Truyen, E., Coteur, L., Dilissen, E., Overbergh, L., Dupont, L. J., Ceuppens, J. L., & Bullens, D. M. (2006). Evaluation of airway inflammation by quantitative Th1/Th2 cytokine mRNA measurement in sputum of asthma patients. *Thorax, 61*(3), 202-208. doi:10.1136/thx.2005.052399

Uggenti, C., & Crow, Y. J. (2018). Taking the STING out of inflammation. *Nat Rev Rheumatol, 14*(9), 508-509. doi:10.1038/s41584-018-0071-z

Ungaro, F., d'Angelo, I., Coletta, C., d'Emmanuele di Villa Bianca, R., Sorrentino, R., Perfetto, B., . . . Quaglia, F. (2012). Dry powders based on PLGA nanoparticles for pulmonary delivery of antibiotics: modulation of encapsulation efficiency, release rate and lung deposition pattern by hydrophilic polymers. *J Control Release, 157*(1), 149-159. doi:10.1016/j.jconrel.2011.08.010

Uzaslan, E., Mahboub, B., Beji, M., Nejjari, C., Tageldin, M. A., Khan, J. A., . . . Group, B. S. (2012). The burden of chronic obstructive pulmonary disease in the Middle

East and North Africa: results of the BREATHE study. *Respir Med, 106 Suppl 2*, S45-59. doi:10.1016/S0954-6111(12)70014-8

Vazquez-Tello, A., Halwani, R., Hamid, Q., & Al-Muhsen, S. (2013). Glucocorticoid receptor-beta up-regulation and steroid resistance induction by IL-17 and IL-23 cytokine stimulation in peripheral mononuclear cells. *J Clin Immunol, 33*(2), 466-478. doi:10.1007/s10875-012-9828-3

Vestbo, J. (2014). COPD: definition and phenotypes. *Clin Chest Med, 35*(1), 1-6. doi:10.1016/j.ccm.2013.10.010

Wang, J., Li, R., Lin, H., Qiu, Q., Lao, M., Zeng, S., . . . Xiao, Y. (2019). Accumulation of cytosolic dsDNA contributes to fibroblast-like synoviocytes-mediated rheumatoid arthritis synovial inflammation. *Int Immunopharmacol, 76*, 105791. doi:10.1016/j.intimp.2019.105791

Wang, J., Wang, R., Yang, J., Yang, X., Hu, S., Wang, H., . . . Ma, L. (2017). Glucocorticoids differentially regulate the innate immune responses of TLR4 and the cytosolic DNA sensing pathway. *International Immunopharmacology, 47*, 190-198. doi:10.1016/j.intimp.2017.03.022

Wang, Y., Chen, J., Chen, W., Liu, L., Dong, M., Ji, J., . . . Zhang, N. (2020). LINC00987 Ameliorates COPD by Regulating LPS-Induced Cell Apoptosis, Oxidative Stress, Inflammation and Autophagy Through Let-7b-5p/SIRT1 Axis. *Int J Chron Obstruct Pulmon Dis, 15*, 3213-3225. doi:10.2147/COPD.S276429

Wang, Y., Lin, J., Shu, J., Li, H., & Ren, Z. (2018a). Oxidative damage and DNA damage in lungs of an ovalbumin-induced asthmatic murine model. *J Thorac Dis, 10*(8), 4819-4830. doi:10.21037/jtd.2018.07.74

Wang, Y., Xu, J., Meng, Y., Adcock, I. M., & Yao, X. (2018b). Role of inflammatory cells in airway remodeling in COPD. *Int J Chron Obstruct Pulmon Dis, 13*, 3341-3348. doi:10.2147/COPD.S176122

Wenzel, S. E. (2012). Asthma phenotypes: the evolution from clinical to molecular approaches. *Nat Med, 18*(5), 716-725. doi:10.1038/nm.2678

WHO. (2007). *Global surveillance, prevention and control of chronic respiratory diseases: a comprehensive approach*. Geneva: World Health Organization.

WHO. (2022a). Asthma. Retrieved from https://www.who.int/news-room/fact-sheets/detail/asthma

WHO. (2022b). Chronic obstructive pulmonary disease (COPD). Retrieved from https://www.who.int/news-room/fact-sheets/detail/chronic-obstructive-pulmonary-disease-(copd)

Wiese, A. V., Duhn, J., Korkmaz, R. U., Quell, K. M., Osman, I., Ender, F., . . . Laumonnier, Y. (2023). C5aR1 activation in mice controls inflammatory eosinophil recruitment and functions in allergic asthma. *Allergy*. doi:10.1111/all.15670

Woodruff, P. G., Modrek, B., Choy, D. F., Jia, G., Abbas, A. R., Ellwanger, A., . . . Fahy, J. V. (2009). T-helper type 2-driven inflammation defines major subphenotypes of asthma. *Am J Respir Crit Care Med, 180*(5), 388-395. doi:10.1164/rccm.200903-0392OC

Wu, B., Xu, M. M., Fan, C., Feng, C. L., Lu, Q. K., Lu, H. M., . . . Tang, W. (2021). STING inhibitor ameliorates LPS-induced ALI by preventing vascular endothelial cells-mediated immune cells chemotaxis and adhesion. *Acta Pharmacol Sin*. doi:10.1038/s41401-021-00813-2

Wu, B., Xu, M. M., Fan, C., Feng, C. L., Lu, Q. K., Lu, H. M., . . . Tang, W. (2022a). STING inhibitor ameliorates LPS-induced ALI by preventing vascular endothelial cells-mediated immune cells chemotaxis and adhesion. *Acta Pharmacol Sin, 43*(8), 2055-2066. doi:10.1038/s41401-021-00813-2

Wu, G., Zhu, Q., Zeng, J., Gu, X., Miao, Y., Xu, W., . . . Song, Y. (2019). Extracellular mitochondrial DNA promote NLRP3 inflammasome activation and induce acute lung injury through TLR9 and NF-kappaB. *J Thorac Dis, 11*(11), 4816-4828. doi:10.21037/jtd.2019.10.26

Wu, J., Zhai, T., Sun, J., Yu, Q., Feng, Y., Li, R., . . . Wang, F. (2022b). Mucus-permeable polymyxin B-hyaluronic acid/ poly (lactic-co-glycolic acid) nanoparticle platform for the nebulized treatment of lung infections. *J Colloid Interface Sci, 624*, 307-319. doi:10.1016/j.jcis.2022.05.121

Yun, J. H., Lee, S., Chase, R., Saferali, A., Morrow, J., Bowler, R. P., . . . Hersh, C. P. (2020). *An Interferon Inducible Signature of Airway Disease from Gene Expression Profiling of Peripheral Blood from COPDGene*. Paper presented at the American Thoracic Society 2020 International Conference. Abstract retrieved from

Yun, J. H., Lee, S., Srinivasa, P., Morrow, J., Chase, R., Saferali, A., . . . Hersh, C. P. (2022). An interferon-inducible signature of airway disease from blood gene expression profiling. *Eur Respir J, 59*(5). doi:10.1183/13993003.00569-2021

Zhang, D., Liu, Y., Zhu, Y., Zhang, Q., Guan, H., Liu, S., . . . Xu, P. (2022). A non-canonical cGAS–STING–PERK pathway facilitates the translational program critical for senescence and organ fibrosis. *Nature Cell Biology, 24*(5), 766-782. doi:10.1038/s41556-022-00894-z

Zhang, Y., Chen, W., & Wang, Y. (2020). STING is an essential regulator of heart inflammation and fibrosis in mice with pathological cardiac hypertrophy via endoplasmic reticulum (ER) stress. *Biomedicine & Pharmacotherapy, 125*, 110022. doi:10.1016/j.biopha.2020.110022

Zhao, C., & Zhao, W. (2020). NLRP3 Inflammasome-A Key Player in Antiviral Responses. *Front Immunol, 11*, 211. doi:10.3389/fimmu.2020.00211

Zhong, Z., Liang, S., Sanchez-Lopez, E., He, F., Shalapour, S., Lin, X. J., . . . Karin, M. (2018). New mitochondrial DNA synthesis enables NLRP3 inflammasome activation. *Nature, 560*(7717), 198-203. doi:10.1038/s41586-018-0372-z

Chapter VI.
Appendix

6.1. Introduction

6.1.1. COPD

6.1.1.1. Definition

The largest contributor to CRDs burden is chronic obstructive pulmonary disease (COPD) (GBD, 2020). Over the years, COPD has emerged as a major health burden and cause of mortality and morbidity worldwide (Pauwels et al., 2004). COPD is shortly defined as a progressive and irreversible chronic inflammatory disease of the lung (Barnes, 2019; Wang et al., 2018b). Recently, COPD has been defined by Global Initiative for Chronic Obstructive Lung Disease (GOLD) in the 2022 update of the Global Strategy for the Diagnosis, Management, and Prevention of COPD as: "Chronic obstructive pulmonary disease (COPD) is a common preventable, treatable disease that is characterized by persistent respiratory symptoms and airflow limitation due to airway and/or alveolar abnormalities usually caused by significant exposure to noxious particles or gases (GOLD, 2022)."

The main respiratory symptoms that COPD patients usually present with are cough, dyspnea, and high sputum production (GOLD, 2022). There is no cure for COPD, nonetheless early diagnosis and treatment are essential to slow disease progression and reduce the risk of exacerbations. Based on the severity of airway limitation, COPD is classified into 4 categories, from low severity to high severity, GOLD1 (mild), GOLD2 (moderate), GOLD3 (severe), and GOLD 4 (very severe).

The main etiology of COPD is cigarette smoke, including tobacco (e.g., cigar, and pipe) and marijuana (GOLD, 2022). The second-hand smoke exposure, the passive exposure to cigarette smoke, is also one of the risk factors associated with COPD. Other risk factors for COPD are occupational exposure to dust, and chemical fumes. Other environmental exposures such as fuel exposure, air pollution, and biomass, may also contribute to COPD. Further, different host factors such as abnormal lung development and genetic abnormalities also contribute to COPD development.

6.1.1.2. Epidemiology

COPD is the third leading cause of death worldwide; resulting in 6% or more than 3 million of deaths in 2019 (WHO, 2022b), and 74·4 million DALYs globally. COPD represented 71·9% of total CRDs DALYs in 2019 which made it the largest contributor to CRDs worldwide burden (GBD, 2020) (**Fig. 6.1.1**). Further, COPD is the major leading cause for hospitalizations and emergency department visits (Pfuntner et al., 2006). Therefore, Better Respiratory Education and Treatment Help Empower (BREATHE) study was conducted to help hospitalized COPD patients and their caregivers to improve their quality of life by preparing them for the post-discharge period and self-management of COPD (Aboumatar et al., 2022; Aboumatar et al., 2017; Aboumatar et al., 2020).

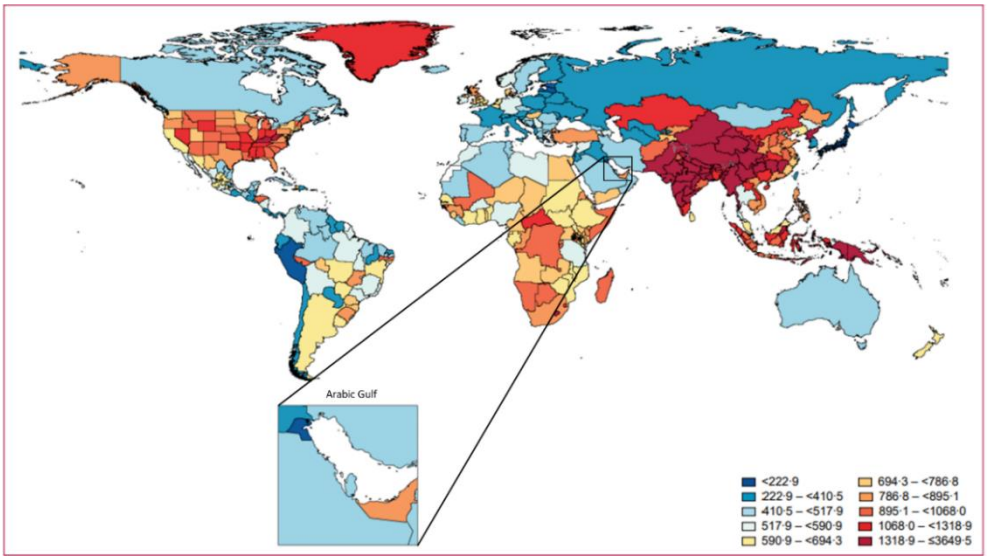

Appendix 6.1.1. COPD age-standardized DALYs rates (per 100000) by location, both sexes combined, 2019 (GBD, 2020).

The epidemiology of COPD in UAE is poorly characterized. Although a few studies were found, they were conducted a decade ago. In 2011, UAE was a part of the ten countries in the BREATHE study on Middle East and North Africa (MENA) region, which also included: Algeria, Egypt, Jordan, Lebanon, Morocco, Saudi Arabia, Syria, Tunisia, and Turkey , together with Pakistan (El Hasnaoui et al., 2012). The prevalence of COPD in UAE was 1.9% which accounted for the lowest prevalence among the rest of MENA region (Tageldin et al., 2012). Overall, MENA region showed low prevalence at an estimated 3.6%, in comparison to

developed countries. This could be because of under-reporting and/or underdiagnosed/misdiagnosed cases in this region. The frequency of symptoms was associated highly with those using cigarettes and waterpipe. COPD was more frequent in men in comparison to women. Around 50% of COPD patients reported exacerbation of their respiratory condition, and 50% of severe cases have been hospitalized (Uzaslan et al., 2012). In another study, case-finding strategy was performed to screen for COPD in Dubai in 2012, and the prevalence of COPD was 12.8% and significantly higher in elderly, 50 years old and above. COPD was significantly associated with occupational exposure to dust (Mahboub et al., 2014; Salameh et al., 2013). Further, COPD prevalence in Abu Dhabi was 3.7% and only significant in elderly (above 70 years old) (Al Zaabi et al., 2011). Interestingly, there was no significant difference in the COPD prevalence according to gender. Recently, the estimated prevalence and mortality rate of COPD in UAE was the highest among GCC countries; with an estimated mortality rate of 11.8 deaths per 100,000 population and 2.1% estimated prevalence (Finkelstein et al., 2021). COPD was the second leading cause of estimated annual direct medical costs among the GCC countries, which was 577 million of 2019 international dollars.

6.1.1.3. Pathophysiology of COPD

The GOLD definition of COPD illustrated the two major COPD phenotypes, chronic bronchitis and emphysema, that are distinguishable using computerized tomography scans (Barnes, 2019), in particular, “the airway limitation is due to airway and/or alveolar abnormalities (GOLD, 2022)”. Chronic bronchitis is the inflammation of the bronchi that is characterized by cough and sputum production at least for 3 months per year, in 2 consecutive years (GOLD, 2022). Emphysema is the destruction of alveoli walls that result in loss of alveolar elasticity and hyperinflation (GOLD, 2022; Vestbo, 2014). Other, phenotypes are frequent exacerbator, and asthma and COPD overlap. Exacerbation is considered frequent when the patients suffer from 2 or more exacerbations per year (Mirza et al., 2017; Vestbo, 2014), which may be because of bacterial, viral infection, eosinophilic, or pauci-inflammation (Celebioglu, 2020). Asthma and COPD overlap is the increased airflow variability with incompletely reversible airway obstruction (Barnes, 2019; Mirza et al., 2017).

6.1.2. Objective

Indeed, the role of STING pathway and the effect of steroids on this pathway has not yet been explored in COPD. Therefore, in this study, using fibroblasts from smoker COPD

patients and healthy subjects, we investigated the activation status of STING/IFN-I pathway and the rationale behind using pharmacological inhibition of STING as a potential adjuvant to enhance the anti-inflammatory effects of commonly used corticosteroids.

6.1.3. Aims

Aim 1: Examine STING activation in COPD fibroblasts and in response to cigarette smoke.

Aim 2: Evaluate the resistance of STING activity in COPD fibroblasts to dexamethasone monotherapy and its response to combination therapy of STING inhibitor and dexamethasone.

Aim 3: Assess the ability of H151 to alleviate fibrosis and augment steroid responsiveness in COPD fibroblasts by upregulating HDAC2 levels.

6.2. Methodology

6.2.1. Fibroblast cell culture

As has been discussed previously in **Method 2.2**, Briefly, human primary bronchial fibroblasts were isolated from endobronchial tissue biopsies of healthy nonsmoker (n = 4), healthy smoker (n = 3), and smoker COPD patients (n = 4) with forced expiratory volume in 1 s (FEV1)/forced vital capacity (FVC) of 56.7 % ± 9.35 and predicted FEV1 is 61.5 % ± 10.6.

6.2.2. Cigarette smoke extract (CSE)

Marlboro Red cigarettes (Philip Morris, Victoria, Australia) has been used; each cigarette contained 1.1 mg of nicotine, 15 mg of tar, and 15 mg of carbon monoxide (Chen et al., 2014). CSE was prepared by bubbling one Marlboro cigarette through 5 mL of PBS at a constant rate and this solution was considered as 100% concentration CSE.

6.2.3. Cell Treatment

The non-smoker healthy, and smoker COPD fibroblasts were seeded in 6- or 12-well-plates for experiments, and at ~70% confluency, they were serum-starved in 1% FBS supplemented DMEM for 16 hours (h). Then, the cells were stimulated with 5% of CSE for 8 h or 12 h, or 10 µg/ml 2′,3′-cyclic guanosine monophosphate–adenosine monophosphate (2′,3′-cyclic GMP-AMP, cGAMP) (invivogen, USA) for 8 h, or with 10 µg/ml pseudomonas

aeruginosa lipopolysaccharide (LPS) (Sigma-Aldrich, Germany) for 4 h, 8 h, or 24 h. For drug treatment, cells were stimulated with LPS (10 µg/ml) for 1 h then treated with dexamethasone (10nM) and/or STING antagonist, H151 (1µM), for the rest of the incubation period. LPS used as a model for COPD exacerbation (Nachmias et al., 2019; Wang et al., 2020).

6.2.4. Quantitative Real Time-Polymerase Chain Reaction (qRT-PCR)

qRT-PCR has performed to study the gene expression as has been described in **Method 2.8**. The primers used in this set of experiments are listed in **Table 5**.

Table 5. List of human (h) primer sequences used in qRT-PCR.

Genes	Forward Primer Sequence (5′-3′)	Reverse Primer Sequence (5′-3′)
h-STING	GTACCTGGTGCTCCACCTAGCC	CCCGGTACCTGGAGTGGATGTG
h-TBK1	TTGCGAGATGTGGTGGGTGG	ACACAGACTGTCCATCTTCCCCT
h-IFN-β	CCTGTGGCAATTGAATGGGAGGC	AGATGGTCAATGCGGCGTCCTC
h-IL-6	GAAAGCAGCAAAGAGGCAC	GCACAGCTCTGGCTTGTTCC
h-TGF-β	AAATTGAGGGCTTTCGCCTTA	GAACCCGTTGATGTCCACTTG
h-COL1A1	GATTGACCCCAACCAAGGCTG	GCCGAACCAGACATGCCTC
h-COL3A1	GATCAGGCCAGTGGAAATG	GTGTGTTTCGTGCAACCATC
h-HDAC2	CACCTGGTGTCCAGATGCAA	GCTATCCGCTTGTCTGATGCT
h-18s	CTACCACATCCAAGGAAGCA	TTTTTCGTCACTACCTCCCCG

6.2.5. Western blot

The protein levels were studied by performing western as has been discussed in **Method 2.9**. The antibodies used in this set of experiments are listed in **Table 6**.

Table 6. List of human (H) antibodies used in western blot.

Antibodies	Reactivity	Source	Dilution
anti-phospho-STING (Ser365) Rabbit mAb	H	CST (#72971)	1:500
anti-STING Rabbit mAb	H	CST (#13647)	1:1000
anti-phospho-TBK1/NAK (Ser172) Rabbit mAb	H M	CST (#5483)	1:500
anti-TBK1/NAK Rabbit mAb	H M	CST (#3504)	1:1000
anti-phospho-IRF3 (Ser396) Rabbit mAb	H M	CST (#29047)	1:500

anti-IRF3 Rabbit mAb	H M	CST (#4302)	1:1000
anti-COL1A1 Rabbit mAb	H	CST (#66948)	1:500
anti-alpha smooth muscle actin mouse mAb	H	Sigma (#A5228)	1:1000
anti-β-actin Rabbit mAb	H M	CST (#4970)	1:1000

6.2.6. Enzyme-linked immunosorbent assay (ELISA)

Fibroblast cell culture supernatant was collected at 24 h of stimulation to determine the levels of IFN-β and TGF-β1 using standard ELISA kits according to the manufacturer's instructions (Abcam, and R&D systems, respectively).

6.2.7. Statistical analysis

The results are presented as mean ± standard error of the mean (SEM) *via* GraphPad Prism software, version 8.00 (GraphPad Software, Inc. La Jolla, CA, USA). Statistical comparisons were performed using unpaired independent student's t-test for baseline expression comparison, and one-way ANOVA followed by the post hoc Bonferroni test for multiple comparisons among different groups. Statistical significance was accepted at a level of $p < 0.05$.

6.3. Results

6.3.1. Elevated STING activation in COPD fibroblasts.

To examine the baseline profile of the STING pathway in COPD human lung fibroblasts, the mRNA and protein expression levels of intermediates in the STING pathway, such as STING, TBK1 and interferon type I (IFN-β), were examined in fibroblasts from healthy non-smokers, healthy smokers, and smoker COPD patients. At baseline, in comparison to healthy non-smoker fibroblasts, STING gene expression was higher in healthy smokers with a 2.2 fold increase ($p<0.01$) and in smoker COPD with a 6.9 fold increase ($p<0.001$) as shown in **figure 6.3.1.A**. The baseline expression of TBK1 gene was elevated in healthy smoker by 3.4 fold ($p<0.01$) and in smoker COPD by 4.5 fold ($p<0.01$) (**Fig. 6.3.1.B**). Similarly, IFN-β gene expression was increased in healthy smoker and to higher extent in smoker COPD, by 2.6 fold ($p<0.001$) and 5.8 fold ($p<0.001$), respectively (**Fig. 6.3.1.C**). At baseline, in comparison to healthy smoker, the gene expression of STING, TBK1, and IFN-β were also significantly

higher in smoker COPD by 4.7 fold ($p<0.01$), 1.2 fold, and 3.2 fold ($p<0.01$), respectively (**Fig. 6.3.1.A-C**).

We next investigated the protein expression of STING, TBK1, and IRF3 in these fibroblasts. STING protein level was elevated in healthy smoker by 1.7 fold ($p<0.05$), and in smoker COPD by 8.0 fold ($p<0.01$) when compared to healthy non-smoker fibroblasts (**Fig. 6.3.1.D**). Further, TBK1 protein level was higher in healthy smoker by 1.28 fold and in smoker COPD by 3.8 fold ($p<0.05$) (**Fig. 6.3.1.E**). In smoker COPD, the protein level of IRF3 was increased by 9.1 fold ($p<0.05$) and in healthy smoker by 5.2 fold in comparison to healthy non-smokers (**Fig. 6.3.1.F**). Similarly, STING, TBK1, and IRF3 protein levels were elevated in smoker COPD in comparison to healthy smoker fibroblasts by 6.3 fold ($p<0.01$), 2.0 fold, and 3.9 fold, respectively (**Fig. 6.3.1.D-F**).

These results suggest that STING pathway is elevated in COPD fibroblasts.

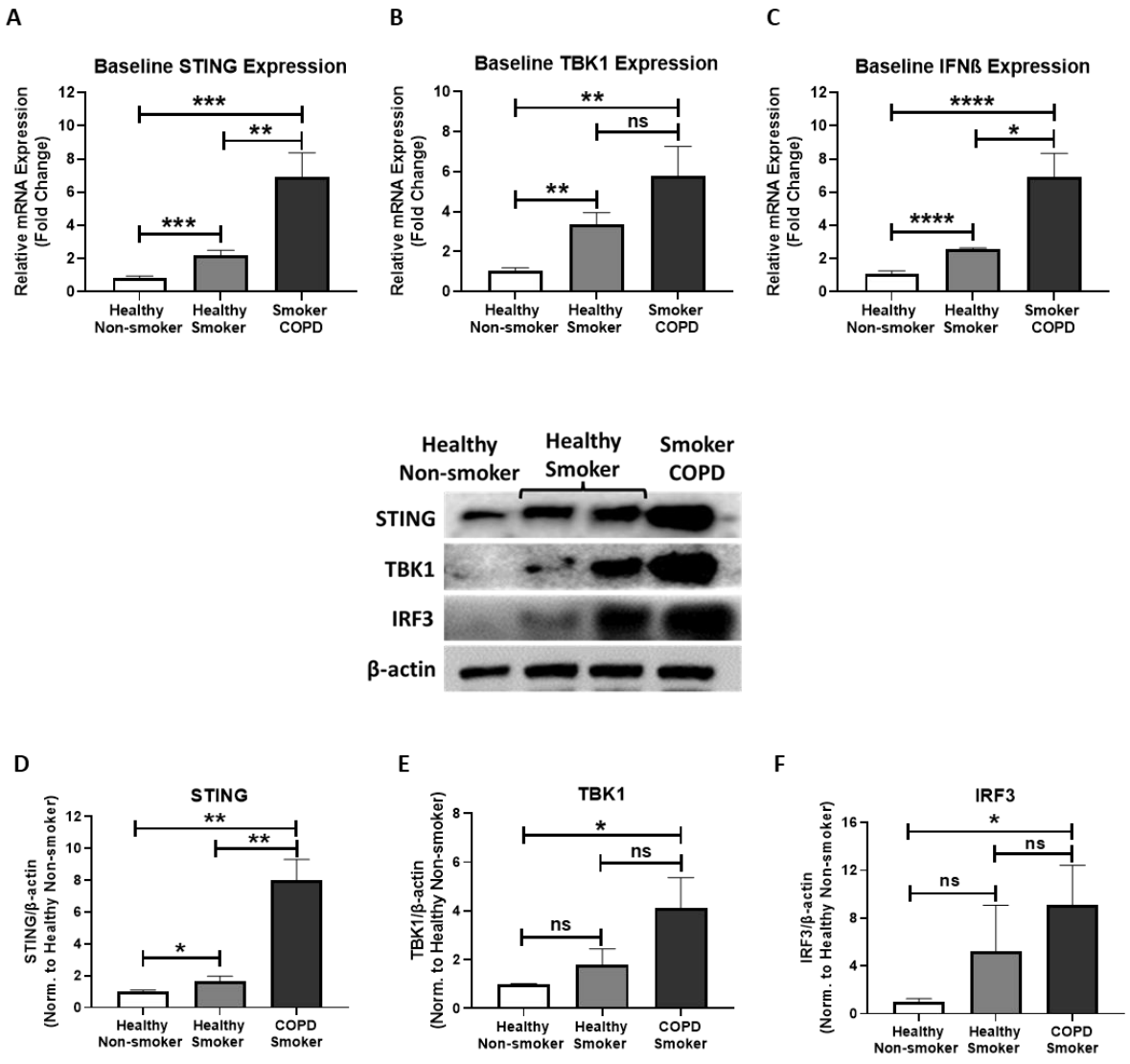

Appendix 6.3.1. Elevated STING activation in COPD fibroblasts.

The baseline gene expression of STING **(A)**, TBK1 **(B)**, and IFN-β **(C)** in healthy non-smoker, healthy smoker, and smoker COPD fibroblasts. Data representative of 3-6 independent experiments from 3-4 unique donors in each group. Representative western blots of STING pathway in healthy non-smoker, healthy smoker, and smoker COPD fibroblasts. Densitometric analysis of immunoblots depicting expression of STING **(D)**, TBK1 **(E)**, and IRF3 **(F)**. β-actin was used as a loading control. Data representative of 2-3 independent experiments from 2-3 unique donors in each group. Results are presented as mean (± SEM) and relative to healthy non-smoker fibroblasts. The values were compared across the different groups using one-way ANOVA followed by post hoc Bonferroni test for multiple comparisons. $*p < 0.05$, $**p < 0.01$, $***p < 0.001$, $****p < 0.0001$.

6.3.2. STING pathway is suppressed by dexamethasone in healthy non-smoker fibroblasts and STING inhibitor induced an additive effect.

Healthy non-smoker fibroblasts were first stimulated with CSE, since STING expression was higher at baseline in healthy smoker individuals (**Fig. 6.3.1**). Upon CSE stimulation for 12 h, STING, and IFN-β gene expression levels were upregulated by 1.4 fold ($p<0.01$), and 2.4 fold ($p<0.05$), respectively in comparison to unstimulated control, as shown in **figure 6.3.2.A and B**. The effects of CSE stimulation on the expression and activity at the protein level was examined by western blot analysis. STING, and IRF3 was activated by phosphorylation upon CSE stimulation for 12 h by 2.0 fold ($p<0.05$), and 2.8 fold ($p<0.05$), respectively, relative to unstimulated control (**Fig. 6.3.2.C-F**). IFN-β secretion upon stimulation with CSE was also increased by 78 % ($p<0.05$) after 24 h stimulation compared with dexamethasone single treatment (**Fig. 6.3.2.G**).

Moreover, healthy non-smoker fibroblasts were stimulated with LPS from *pseudomonas aeruginosa* as LPS is known to activate the STING pathway (Ning et al., 2020). Upon LPS stimulation for 4 h, STING, TBK1, IFN-β, and IL-6 gene expression levels were upregulated by 2.3 fold ($p<0.01$), 3.3 fold ($p<0.0001$), 2.5 fold ($p<0.001$), and 2.8 fold ($p<0.0001$), respectively in comparison to unstimulated control, as shown in **figure 6.3.3.A-D**. The upregulated STING, TBK1, IFN-β and IL-6 were significantly decreased upon dexamethasone treatment by 1.0 fold ($p<0.001$), 0.8 fold ($p<0.0001$), 2.2 fold ($p<0.05$), and 0.3 fold ($p<0.0001$), respectively in comparison to LPS stimulation (**Fig. 6.3.3.A-D**). We next proposed the use of dexamethasone in combination with STING inhibitor (H151); where H151 is a recently discovered potent, irreversible, and selective inhibitor of STING (Haag et al., 2018). The mRNA levels of STING, and IFN-β were significantly downregulated by 0.6 fold ($p<0.0001$), and 1.4 fold ($p<0.01$), respectively, upon the combination treatment when compared to dexamethasone single treatment (**Fig. 6.3.3.A and C**).

The effect of the proposed treatment was also confirmed at the protein level by western blot analysis. The activation of STING, TBK1, and IRF3 by phosphorylation was induced upon LPS stimulation for 8 h by 3.6 fold ($p<0.001$), 2.4 fold ($p<0.01$), and 4.0 fold ($p<0.001$), respectively, relative to unstimulated control. The induced activity and expression of these proteins, STING, TBK1, and IRF3, were significantly inhibited when treated with dexamethasone in comparison to LPS stimulation by 1.1 fold ($p<0.001$), 1.5 fold ($p<0.05$), 1.2 fold ($p<0.001$), respectively. Then, the proposed dexamethasone and H151 combination inhibited the phosphorylation of STING, TBK1, and IRF3 by 1.0 fold ($p<0.05$), 1.5 fold

(p<0.01), and 0.9 fold (p<0.05), respectively in comparison to dexamethasone treatment (**Fig. 6.3.3.E-J**). The combination treatment further suppressed IFN-β secretion by 9.8% (p<0.05) after 24 h stimulation compared with dexamethasone treatment alone (**Fig. 6.3.3.K**).

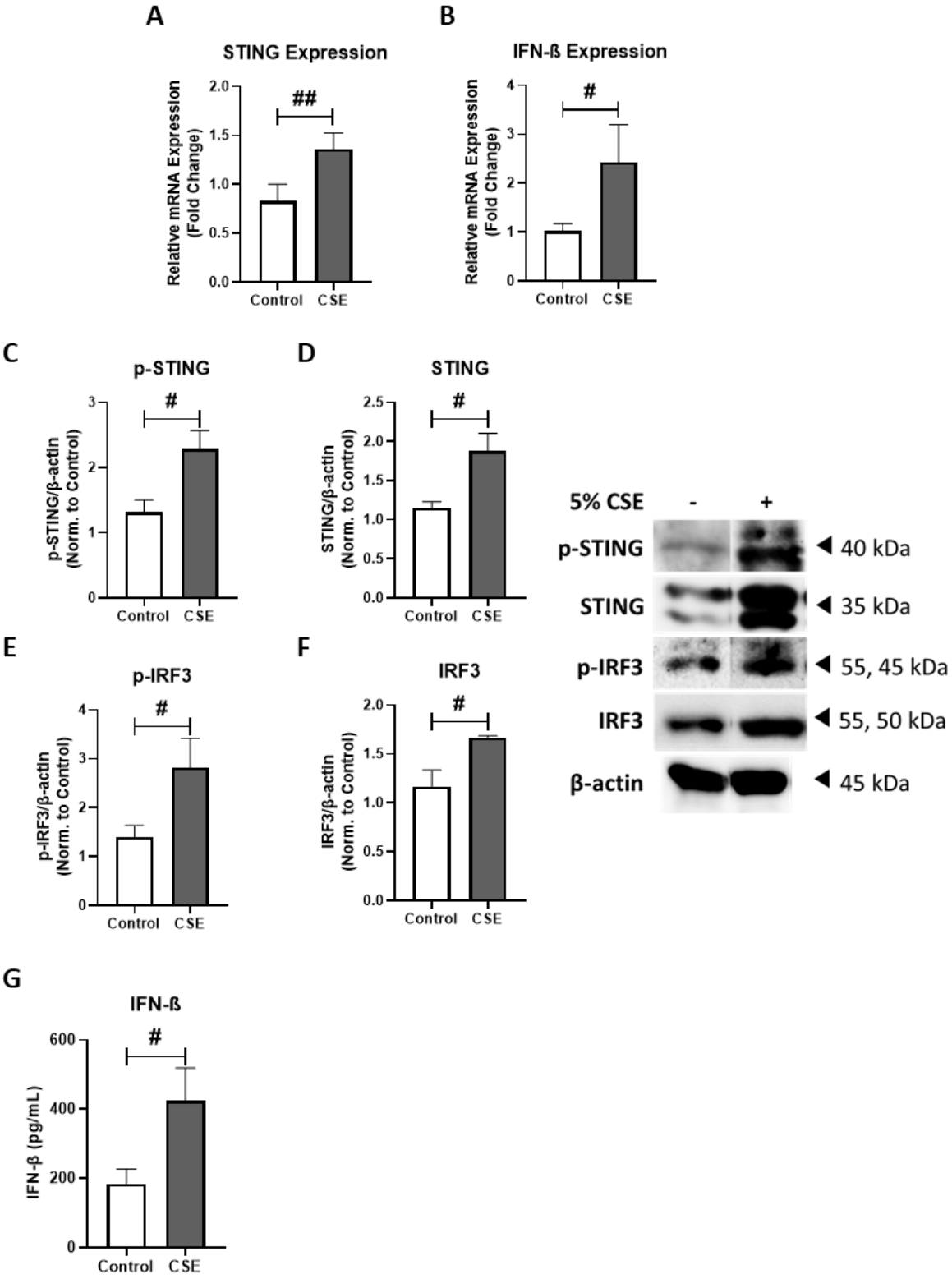

Appendix 6.3.2. Stimulation of STING pathway by cigarette smoke in healthy non-smoker fibroblasts.

The gene expression of STING **(A)**, and IFN-β **(B)** was compared upon stimulation with CSE for 12 h in healthy non-smoker fibroblasts. At indicated concentration of the stimulant for 12 h, representative western blots and densitometric analysis of immunoblots depicting the expression of STING pathway members **(C-F)**. β-actin was used as a loading control. Concentration of type I IFN (IFN-β) in the culture media upon 24 h stimulation was analyzed by ELISA **(K)**. Data representative of two independent experiments. Results are presented as mean (± SEM) and relative to unstimulated control. The values were compared across the different groups using independent student's t-test between the groups. #$p < 0.05$ vs. unstimulated control.

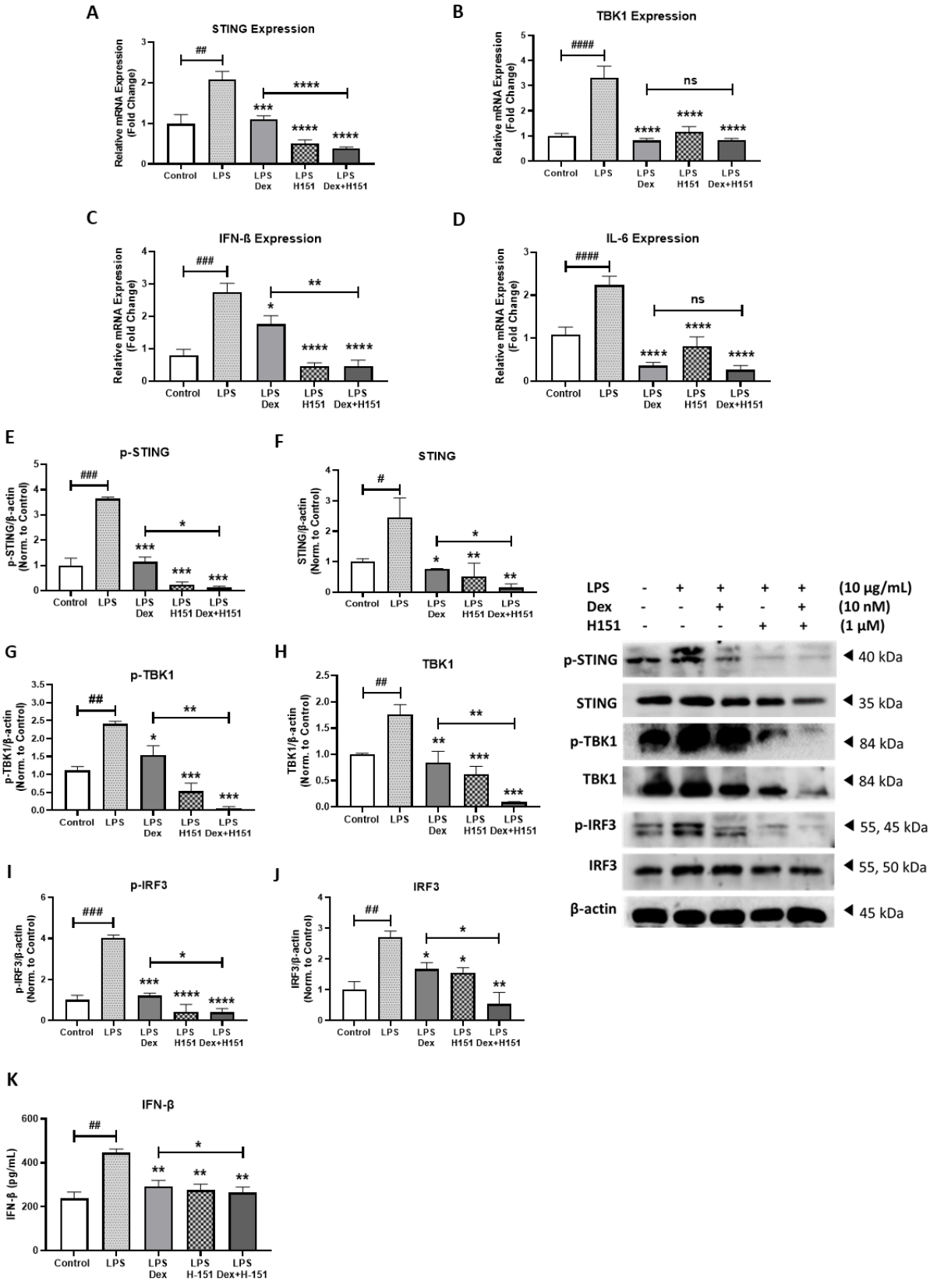
A
STING Expression
Relative mRNA Expression (Fold Change)
B
TBK1 Expression
C
IFN-ß Expression
D
IL-6 Expression
E
p-STING
p-STING/β-actin (Norm. to Control)
F
STING
STING/β-actin (Norm. to Control)
G
p-TBK1
p-TBK1/β-actin (Norm. to Control)
H
TBK1
TBK1/β-actin (Norm. to Control)
I
p-IRF3
p-IRF3/β-actin (Norm. to Control)
J
IRF3
IRF3/β-actin (Norm. to Control)
K
IFN-β
IFN-β (pg/mL)
Control
LPS
LPS Dex
LPS H151
LPS Dex+H151
LPS H-151
LPS Dex+H-151
LPS - + + + + (10 µg/mL)
Dex - - + - + (10 nM)
H151 - - - + + (1 µM)
p-STING ◀ 40 kDa
STING ◀ 35 kDa
p-TBK1 ◀ 84 kDa
TBK1 ◀ 84 kDa
p-IRF3 ◀ 55, 45 kDa
IRF3 ◀ 55, 50 kDa
β-actin ◀ 45 kDa

Appendix 6.3.3. STING pathway is suppressed by dexamethasone in healthy non-smoker fibroblasts and STING inhibitor induced an additive effect.

The gene expression of STING **(A)**, TBK1 **(B)**, IFN-β **(C),** and IL-6 (**D**) was compared upon stimulation with LPS for 4 h, then treatment with dexamethasone (Dex), and STING inhibitor (H151) either alone or in combination in healthy non-smoker fibroblasts. Data representative of 2-3 independent experiments from 4 unique donors. At indicated concentration of the stimulant and treatment for 8 h, representative western blots and densitometric analysis of immunoblots depicting the expression of STING pathway members **(E-J)**. Data representative from two unique donors. β-actin was used as a loading control. Concentration of type I IFN (IFN-β) in the culture media upon 24 h stimulation was analyzed by ELISA **(K)**. Data representative from two unique donors. Results are presented as mean (± SEM) and relative to unstimulated control. The values were compared across the different groups using one-way ANOVA followed by post hoc Bonferroni test for multiple comparisons. ∗p < 0.05, ∗∗p < 0.01, ∗∗∗p < 0.001, ∗∗∗∗p < 0.0001 vs. LPS stimulation. #p < 0.05, ##p < 0.01, ###p < 0.001, ####p < 0.0001 vs. unstimulated control.

6.3.3. STING activity in COPD fibroblasts is resistant to dexamethasone monotherapy but responsive to combination therapy of STING inhibitor and dexamethasone.

Since STING pathway was activated in smoker COPD fibroblasts (**Fig. 6.3.1**), we first stimulated with CSE to aggravate the in-vitro model for COPD (Nachmias et al., 2019). STING, and IRF3 was further activated by phosphorylation upon CSE stimulation for 12 h by 2.3 fold ($p<0.05$), and 1.8 fold ($p<0.05$), respectively, relative to unstimulated control (**Fig. 6.3.4.A-D**).

We next investigated whether the commonly used steroid treatment, dexamethasone, inhibits STING pathway in in-vitro model of COPD exacerbation using *pseudomonas aeruginosa* LPS stimulation (Nachmias et al., 2019; Wang et al., 2020). First, smoker COPD fibroblasts were stimulated for 4 h with *pseudomonas aeruginosa* LPS, then treated with dexamethasone. The expression of STING, TBK1, and IFN-β genes were upregulated upon LPS stimulation with 4.1 fold ($p<0.01$), 3.4 fold ($p<0.0001$), and 3.7 fold ($p<0.01$), respectively in comparison to unstimulated control. However, upon dexamethasone treatment, the increased mRNA levels of STING, TBK1, and IFN-β specifically were not significantly reduced when compared to LPS stimulation. Interestingly, combination treatment of dexamethasone and H151 showed a significant reduction in the gene expression of STING, TBK1, and IFN-β by

1.8 fold ($p<0.01$), 2.0 fold ($p<0.0001$), and 1.5 fold ($p<0.001$), respectively, when compared to dexamethasone treatment as presented in **figure 6.3.5.A-C**.

In smoker COPD fibroblasts, both the expression on protein level and the activity were affected as per the proposed treatment plan. Upon LPS stimulation for 8 h, the phosphorylation of STING, TBK1, and IRF3 was increased by 1.9 fold ($p<0.05$), 1.7 fold ($p<0.05$), and 2.6 fold ($p<0.05$), respectively. Then, the expression of these proteins, STING, TBK1, and IRF3, were not significantly inhibited when treated with dexamethasone in comparison to LPS stimulation. The combination treatment of dexamethasone and H151 decreased the phosphorylation levels of STING, TBK1, and IRF3 when compared to dexamethasone treatment by 1.2 fold ($p<0.05$), 0.8 fold ($p<0.05$), and 1.2 fold ($p<0.05$), respectively (**Fig. 6.3.5.D-I**). Further, we investigated the effect of combination treatment on LPS-induced type I IFN secretion. Combination treatment caused 25.3% ($p<0.05$) reduction in IFN-β level after 24 h stimulation compared with dexamethasone treatment (**Fig. 6.3.5.J**).

Altogether, these results demonstrate that the inhibition of the STING pathway enhanced the steroid responsiveness of COPD fibroblasts.

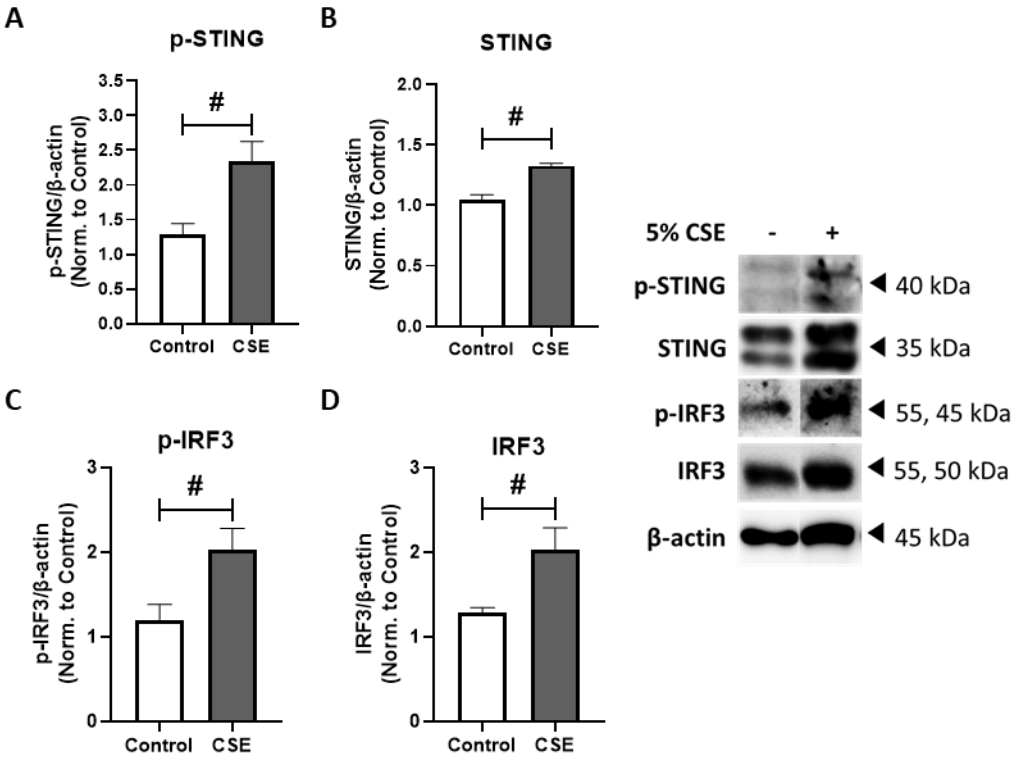

Appendix 6.3.4. Stimulation of STING pathway by cigarette smoke in COPD fibroblasts.

At indicated concentration of CSE stimulation for 12 h in COPD fibroblasts, representative western blots and densitometric analysis of immunoblots depicting the expression of STING pathway members **(A-D)**. β-actin was used as a loading control. Data representative of two independent experiments. Results are presented as mean (± SEM) and relative to unstimulated control. The values were compared across the different groups using independent student's t-test between the groups. #$p < 0.05$ vs. unstimulated control.

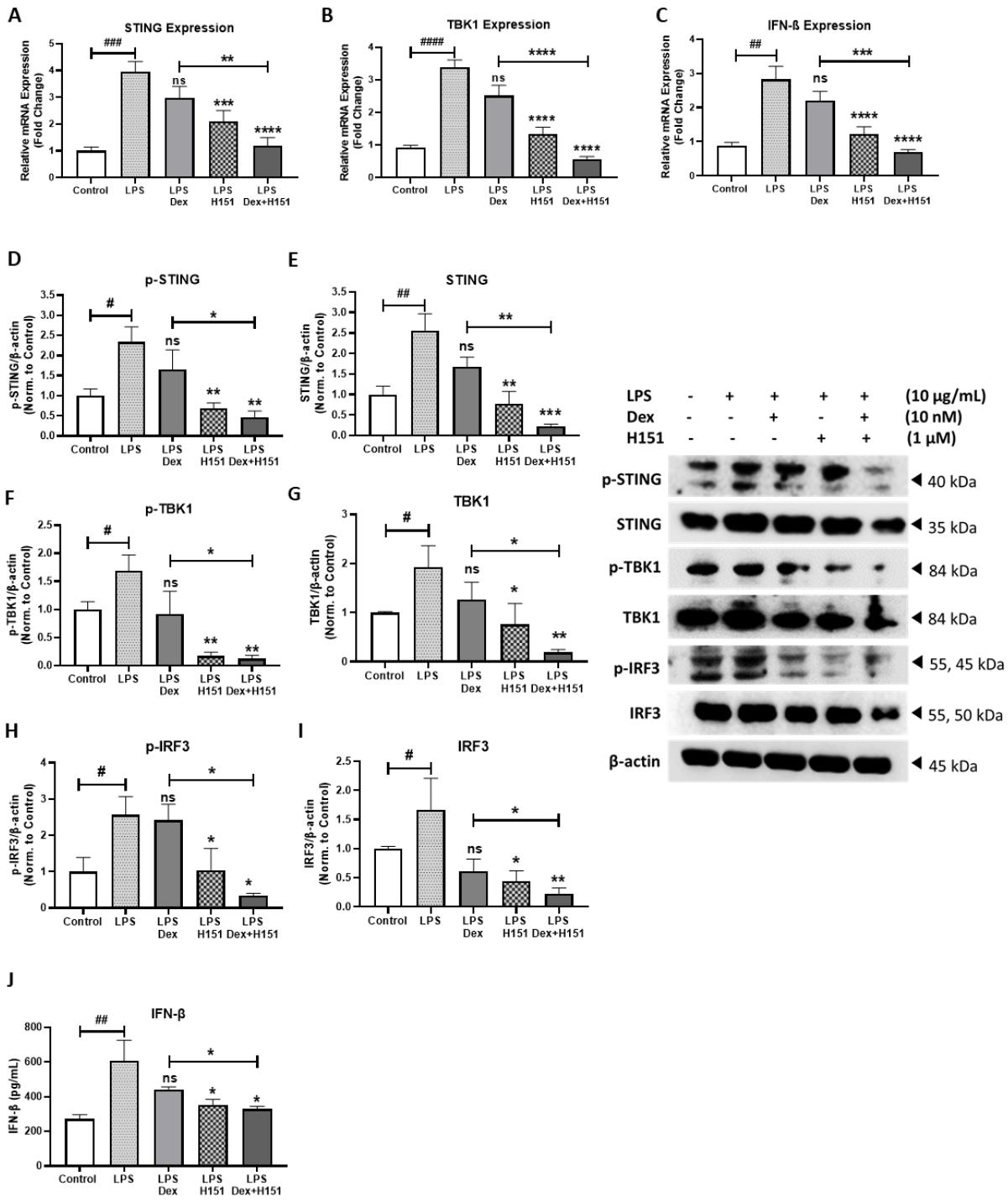

Appendix 6.3.5. STING activity in COPD fibroblasts is resistant to dexamethasone monotherapy but responsive to combination therapy of STING inhibitor and dexamethasone.

The gene expression of STING **(A)**, TBK1 **(B)**, and IFN-β **(C)** was compared upon stimulation for 4 h with LPS, then treatment with Dex, H151 and combination in smoker COPD fibroblasts. Data representative of 2-3 independent experiments from 4 unique donors. Representative western blots and densitometric analysis of STING pathway members in smoker COPD fibroblasts at indicated

concentration of the stimulant and treatment for 8 h **(D-I)**. β-actin was used as a loading control. Data representative from three unique donors. Concentration of IFN-β in the culture media after 24 h of stimulation was analyzed by ELISA **(J)**. Data representative from two unique donors. Results are presented as mean (± SEM) and relative to unstimulated control. The values were compared across the different groups using one-way ANOVA followed by post hoc Bonferroni test for multiple comparisons. ∗p < 0.05, ∗∗p < 0.01, ∗∗∗p < 0.001, ∗∗∗∗p < 0.0001 vs. LPS stimulation. #p < 0.05, ##p < 0.01, ###p < 0.001, ####p < 0.0001 vs. unstimulated control.

6.3.4. Inhibition of STING pathway augments steroid responsiveness in COPD fibroblasts by upregulating HDAC2 levels.

Corticosteroid treatment hyporesponsiveness is one of the key characteristic features of COPD; which is associated with decrease in activity and expression of histone deacetylase 2 (HDAC2) (Barnes, 2009). Here, the mRNA baseline expression levels of HDAC2 in smoker COPD human lung fibroblasts was examined in comparison to healthy non-smokers, and healthy smokers. HDAC2 gene expression was lower in healthy smokers by 0.8 fold ($p<0.05$) and to a lower extent in smoker COPD by 0.6 fold ($p<0.01$) as shown in **figure 6.3.6.A**. Healthy non-smoker fibroblasts stimulated with mammalian STING ligand, cGAMP (2'-3'-cyclic GMP-AMP), for 8 h inhibited HDAC2 gene expression by almost 1.0 fold ($p<0.0001$), when compared to unstimulated control. Interestingly, cGAMP stimulation significantly inhibited HDAC2 expression to higher extent ($p<0.01$) in comparison to CSE (**Fig. 6.3.6.B**). LPS stimulation in smoker COPD fibroblasts for 4 h reduced HDAC2 mRNA level by 0.4 fold ($p<0.001$), relative to unstimulated control. The expression of HDAC2 was not significantly induced upon treatment with dexamethasone when compared to LPS stimulation. However, the combination treatment of dexamethasone and STING inhibitor (H151) showed a significant induction in HDAC2 gene expression by 6.5 fold increase ($p<0.0001$), in comparison to dexamethasone single treatment (**Fig. 6.3.6.C**). This indicated that the proposed combination therapy may improve steroid responsiveness in COPD by enhancing HDAC2 expression.

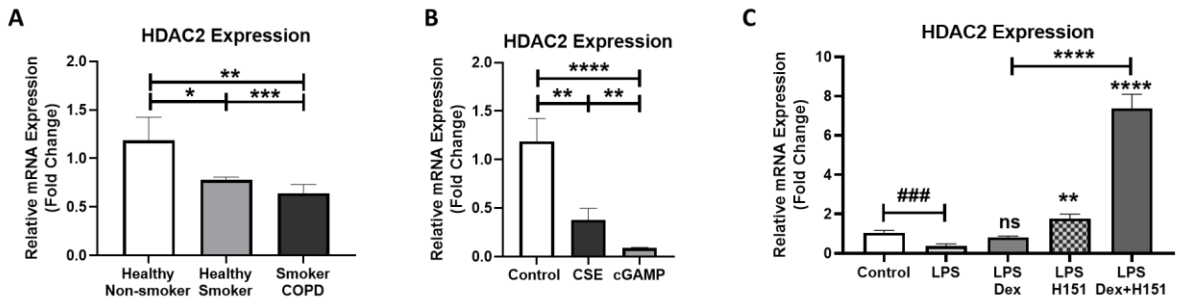

Appendix 6.3.6. The combination of STING inhibitor and dexamethasone augments steroid responsiveness in COPD fibroblasts by upregulating HDAC2.

(A) The baseline gene expression of HDAC2 in healthy non-smoker, healthy smoker, and smoker COPD fibroblasts. Data representative of 2-4 independent experiments from 2-3 unique donors in each group. **(B)** In healthy non-smoker fibroblasts, comparison of HDAC2 gene expression upon stimulation for 8 h with CSE, and 2'3'-cGAMP. Data representative of 2-3 independent experiments from 2 unique donors. **(C)** In smoker COPD fibroblasts, comparison of HDAC2 gene expression upon stimulation for 4 h with LPS, then treatment with Dex, H151 and combination. Data representative from 4 unique donors. Results are presented as mean (± SEM) and relative to unstimulated control. The values were compared across the different groups using one-way ANOVA followed by post hoc Bonferroni test for multiple comparisons. ∗p < 0.05, ∗∗p < 0.01, ∗∗∗p < 0.001, ∗∗∗∗p < 0.0001 vs. LPS stimulation. ###p < 0.001, ####p < 0.0001 vs. unstimulated control.

6.3.5. STING inhibitor in combination with dexamethasone alleviates fibrosis in steroid resistant COPD fibroblasts.

STING pathway plays an essential role in inducing pulmonary fibrosis via stimulating the expression of fibrotic hallmarks, such as collagen I (COL1A1), collagen III (COL3A1), and TGF-β1 (Nascimento et al., 2019). Further, our group recently published that LPS induced pro-fibrotic signalling in severe asthmatic bronchial fibroblasts (Ramakrishnan et al., 2022). Therefore, LPS was used as stimulated for fibrosis in smoker COPD fibroblasts. Here, stimulating smoker COPD fibroblasts with LPS for 4 h induced the gene expression of TGF-β1, COL1A1, and COL3A1 by 5.5 fold ($p<0.0001$), 4.9 fold ($p<0.05$), and 5.5 fold ($p<0.01$), respectively, relative to unstimulated control. Upon treatment with dexamethasone, the expression of these fibrotic markers was not significantly reduced when compared to LPS stimulation. Treatment with dexamethasone in combination with STING inhibitor (H151)

showed a significant reduction in the mRNA levels of TGF-β1, COL1A1, and COL3A1 by 2.7 fold ($p<0.0001$), 1.4 fold ($p<0.01$), and 2.5 fold ($p<0.05$), respectively, when compared to dexamethasone single treatment (**Fig. 6.3.7.A-C**).

In parallel, the COL1A1 and α-SMA protein levels were increased upon LPS stimulation for 24 h by 2.8 fold and 1.3 fold ($p<0.05$), respectively, in comparison to unstimulated control. The elevated proteins, COL1A1 and α-SMA, were not significantly inhibited when treated with dexamethasone compared to LPS stimulation. Interestingly, the combination treatment decreased the protein level of COL1A1 and α-SMA by 0.3 fold, 0.6 fold ($p<0.05$), respectively, when compared to dexamethasone treatment (**Fig. 6.3.7.D**). In addition, the combination treatment suppressed TGF-β1 levels by 23.3% ($p<0.0001$) after 24 h stimulation when compared with dexamethasone treatment alone (**Fig. 6.3.7.E**). Altogether these results indicate that STING inhibitor augmented the effect of steroids in inhibiting fibrosis in COPD.

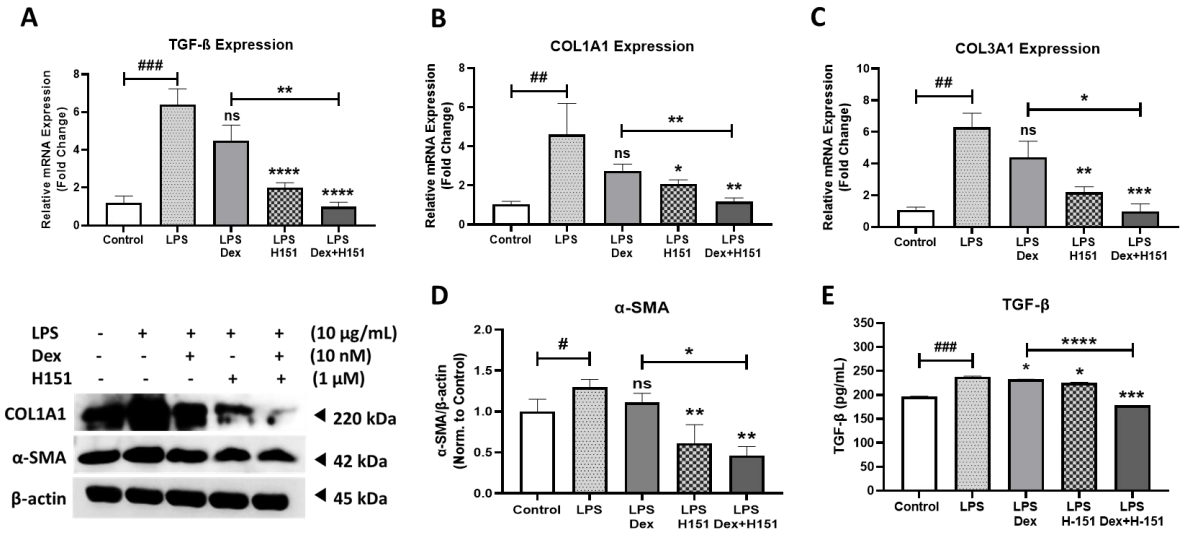

Appendix 6.3.7. STING inhibitor in combination with dexamethasone alleviates fibrosis in steroid resistant COPD fibroblasts.

Comparison of COL1A1 **(A)**, COL3A1 **(B)**, and TGF-β **(C)** gene expression upon stimulation for 4 h with LPS, then treatment with Dex, H151 and combination in smoker COPD fibroblasts. Data representative of 2 independent experiments from 4 unique donors. **(D)** Representative western blot analysis of fibrotic mediators in smoker COPD fibroblasts at indicated concentration of the stimulant and treatment for 24 h. β-actin was used as a loading control. Data representative from three unique donors. **(E)** TGF-β concentration in the culture media after 24 h of LPS stimulation was analyzed by ELISA. Data representative of 2 independent experiments. Results are presented as mean (± SEM) and

relative to unstimulated control. The values were compared across the different groups using one-way ANOVA followed by the post hoc Bonferroni test for multiple comparisons. $*p < 0.05$, $**p < 0.01$, $***p < 0.001$, $****p < 0.0001$ vs. LPS stimulation. ###p < 0.001, ####p < 0.0001 vs. unstimulated control.

6.4. Discussion

The respiratory barrier damage upon cigarette smoke exposure triggers cell-free DNA and oxidative DNA damage (Nascimento et al., 2019; Paschalaki et al., 2013; Pouwels et al., 2017), that could be detected in the peripheral blood of COPD patients (Avriel et al., 2016; Maluf et al., 2007). Thus, the released self-dsDNA triggers DNA sensor cGAS-STING pathway, inducing IFN I-dependent lung inflammation (Nascimento et al., 2019). In peripheral blood and bronchial brushings from COPD patients, the gene expression signature of IFN signaling, particularly, ISGs, positively correlated with exacerbations, airway remodeling and impaired lung function (Yun et al., 2020; Yun et al., 2022). In addition, IFN-β and -λ were found to be higher in sputum from COPD patients compared to healthy volunteers, which positively correlated with sputum neutrophil count, one of the key features of COPD (Hilzendeger et al., 2016). Further, using nontypeable *Haemophilus influenzae* as a model for COPD exacerbation, STING played an essential role in IFN-β expression (Lu et al., 2018). Following the previous findings, we have shown substantial enrichment of the baseline STING profile in COPD fibroblasts (**Fig. 6.3.1**), which was further elevated upon CSE and LPS stimulation at both mRNA and protein levels (**Fig. 6.3.4 and Fig. 6.3.5**).

Glucocorticoids differentially affected the innate immune responses via the cytosolic DNA sensing pathway (Wang et al., 2017). For instance, in LPS stimulated primary macrophages, dexamethasone treatment suppressed TBK1 activation; inhibiting IRF3 phosphorylation (McCoy et al., 2008), disrupting IRF3-glucocorticoid receptor protein complex (Reily et al., 2006), and decreasing IFN-I secretion (Flammer et al., 2010; Wang et al., 2017). In the line with these findings, we showed that STING/IFN-β was sensitive to dexamethasone in healthy non-smoker fibroblasts (**Fig. 6.3.3**). However, dexamethasone did not significantly affect the activation of this pathway in COPD fibroblasts (**Fig. 6.3.5**), while STING inhibitor had an additive anti-inflammatory effect to steroid upon combination of STING inhibitor and commonly used steroid treatment, dexamethasone (**Fig. 6.3.3 and Fig. 6.3.5**).

Corticosteroids utilize HDACs to suppress inflammatory gene expression (Barnes, 2009). In COPD, oxidative stress and smoking suppress HDAC2 expression and activity and result in steroid hyporesponsiveness (Barnes, 2009). Likewise, our results showed that HDAC2 expression was lower in COPD fibroblasts (**Fig. 6.3.6.A**). While, selective STING stimulant, 2',3'-cGAMP, significantly reduced HDAC2 expression in healthy fibroblasts in comparison to CSE (**Fig. 6.3.6.B**), the combination of STING inhibitor and dexamethasone in COPD fibroblasts reversed the steroid hyporesponsiveness through upregulation of HDAC2 (**Fig. 6.3.6.C**). To the best of our knowledge, this is the first study to associate the HDAC2 attenuation to the DNA damage and STING upregulation. The link between STING signaling and HDAC2 expression is not well investigated and requires further evaluation.

Recently, STING signaling was reported to induce fibrosis in cardiac (Zhang et al., 2020), hepatic (Luo et al., 2018), renal (Chung et al., 2019), and pulmonary inflammation (Sun et al., 2020); via the upregulation of fibrotic hallmarks, TGF-β, and collagen I (COL1A1) (Chung et al., 2019; Luo et al., 2018; Sun et al., 2020; Zhang et al., 2020). From a mechanistic perspective, the binding of cGAMP to STING on endoplasmic reticulum (ER), directly activates the ER-located kinase phospho-protein kinase RNA-like endoplasmic reticulum kinase (PERK). The activated PERK phosphorylates phospho-eukaryotic initiation factor 2 alpha (eIF2α); this STING–PERK–eIF2α pathway is physiologically essential to senescence and fibrosis (Zhang et al., 2022). Further, genetic depletion of STING restrains ER stress, decreasing the activation of PERK–eIF2α pathway (Zhang et al., 2020). Therefore, STING could be a therapeutic target for lung fibrosis. Our data in the line with the previous findings, where STING stimulation in COPD fibroblasts triggered significant increase in fibrotic markers, TGF-β, alpha-smooth muscle actin (α-SMA), COL1A1 and collagen III (COL3A1), while treatment with STING inhibitor, H151, in combination with dexamethasone reduced them (**Fig. 6.3.7**).

6.5. Conclusion

The current work highlights the important effects of STING pathway in COPD pathogenesis through inducing IFN-I secretion, pulmonary inflammation, and fibrosis. STING inhibitor, therefore, might represent a potential therapeutic adjuvant in combination with routine steroid treatment to enhance steroid sensitivity and to control lung inflammation and fibrosis, thereby preventing COPD progression.

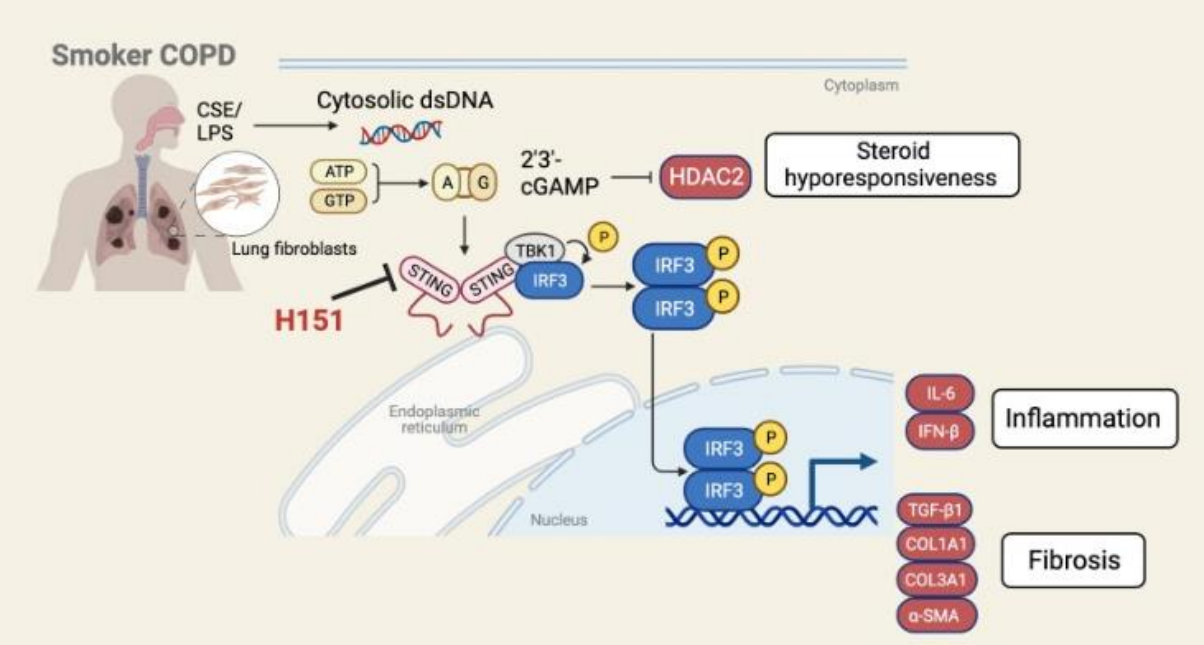

Appendix 6.5.1. Schematic representation of STING activation in smoker COPD.

STING pathway could play important roles in COPD pathogenesis, via inducing IFN-I secretion, steroid resistance, pulmonary inflammation, and fibrosis. Fibroblasts were isolated from smoker COPD patients and had an elevation in the baseline expression of STING pathway. Further, stimulating COPD fibroblasts with CSE or LPS activated STING, TBK1, and IRF3 by phosphorylation, which in turn resulted in type I interferon response. Interestingly, STING pathway was resistant to dexamethasone therapy but sensitive to combination of STING inhibitor and dexamethasone in COPD fibroblasts. Moreover, STING stimulation triggered a significant increase in fibrotic markers and a reduction in HDAC2 expression. Interestingly, treating COPD fibroblasts with the combination of STING inhibitor and dexamethasone alleviated fibrosis and reversed steroid hyporesponsiveness through an upregulation of HDAC2.

Acknowledgments

With special regards to His Highness Sheikh Dr. Sultan bin Muhammad Al Qassimi, a member of the Supreme Council of the United Arab Emirates, the Ruler of Sharjah, and founder of the University of Sharjah, and His Highness Sheikh Sultan bin Ahmed bin Sultan Al Qasimi, Deputy Ruler of Sharjah, and President of the University of Sharjah, for supporting my PhD journey through the generous scholarship.

First and foremost, I would like to express my sincere gratitude to my esteemed supervisor, Prof. Rabih Halwani, Director of Research Institute of Medical & Health Sciences, for his invaluable supervision, continuous support, patience, and tutelage during my PhD degree. Further, I am deeply grateful to my co-supervisor, Prof. Qutayba Hamid, Vice Chancellor for Colleges of Medicine & Health Sciences and Dean of College of Medicine, for his motivation, and immense knowledge. Their knowledge and plentiful experience have encouraged me in all the time of my academic research. I would like also to express my deepest appreciation to my Lubeck supervisor, Dr. Yves Laumonnier, who generously provided knowledge, expertise, and invaluable feedback.

My sincere thanks also go to Dr. Mutasem (Mark) Rawas-Qalaji, Head of Department of Pharmaceutics & Pharmaceutical Technology in College of Pharmacy, for his mentorship, and treasured support, which was really influential in nanoparticle work, as well as, his post-doctorate research associate, Dr. Roberta Cagliani. Further, I would like to extend my special thanks to Dr Ibrahim Hachim for his help in histological analysis, Dr Narjes Saheb Sharif-Askari for her help in in-silico analysis, and Dr Khuloud Bajbouj for her help with fibroblasts, advice, and support.

In addition, I express my indebtedness to the Tissue Injury and Repair Group in Sharjah Institute for Medical Research at University of Sharjah. My appreciation goes to Dr. Narjes Saheb Sharif-Askari, and Dr. Fatemeh Saheb Sharif-Askari, and post-doctorate research associate, Dr Rakhee Kizhuvappat Ramakrishnan, for their assistance at every stage of the research project, insightful comments and suggestions, and reviewing my manuscripts and PhD thesis. I also want to extend my gratitude to my fellow labmates, Mrs. Baraa Khalid, Mrs. Shirin Hafezi, Miss Zaina Kalaji, Mrs. Bariaa Khalil, Mrs. Mariam Wed, and Miss Sara Tilal for the stimulating discussions, for the sleepless nights we were working, and for all the fun

we have had in the last four years. Also, my special thanks go to Dr. Laumonnier PhD student, Mrs. Rabia Ülkü Korkmaz, for her continuous help and support in and out.

I would like to thank my colleagues in dual-degree program between University of Sharjah and University of Lubeck, Miss Alya Al Nuaimi, Mrs. Lama Lozon, Miss Sarah Daiban, and Miss Wafaa Abumustafa, who made travel to Germany easy and fun.

Finally, my heartfelt gratitude and thankfulness is extended to my beloved family, my parents, sisters, and brother, for their patience, and support throughout my research and years of study.

- **Thanks to all funding sources**
  1. PhD student fund from College of Graduate Studies.
  2. Collaborative research grant (Grant code: 2001090278), University of Sharjah, UAE.
- **Ethical approval**
  1. Human primary bronchial fibroblasts were isolated from endobronchial tissue biopsies and obtained from the Quebec Respiratory Health Research Network Tissue Bank (McGill University Health Centre (MUHC)/ Meakins-Christie Laboratories Tissue Bank, Montreal, Canada). The original study was approved by the MUHC Research Ethics Board (2003–1879).
  2. Mouse care and experimental procedures were performed following approval from Animal Care and Use Committee of University of Sharjah (agreement number: ACUC-20–02-11–01).
  3. Mouse experimental procedures was approved by the Schleswig-Holstein state authorities (56-5/16, 86-7/17 and 44-5/18). Animal care was provided in accordance with German rights.

Publications associated with this research

1. **Bushra Mdkhana**, Narjes Saheb Sharif-Askari, Rakhee K Ramakrishnan, Swati Goel, Qutayba Hamid, Rabih Halwani. Nucleic Acid-Sensing Pathways During SARS-CoV-2 Infection: Expectations versus Reality. **J Inflamm Res.** 2021; 14:199-216. DOI: 10.2147/JIR.S277716.

2. **Bushra Mdkhana**, Narjes Saheb Sharif-Askari, Rakhee K. Ramakrishnan, Baraa Khalid Al-Sheakly, Fatemeh Saheb Sharif-Askari, Khuloud Bajbouj, Qutayba Hamid, and Rabih Halwani. Nucleic Acid Sensor STING Drives Fibrosis and its Inhibition Enhances Steroid Responsiveness in Chronic Obstructive Pulmonary Disease. **Submitted to PLOS ONE.**

3. **Bushra Mdkhana**, Narjes Saheb Sharif-Askari, Roberta Cagliani, Rakhee K. Ramakrishnan, Baraa Khalid Al-Sheakly, Bariaa A. Khalil, Shirin Hafezi, Fatemeh Saheb Sharif-Askari, Zaina Kalaji, Ibrahim Hachim, Mutasem Rawas-Qalaji, Qutayba Hamid, and Rabih Halwani. Inhibiting DNA Sensing Pathway to Control Steroid Resistant Lung Inflammation. **In preparation.**

4. Katharina M. Quell*, **Bushra Mdkhana**X, Rabia Ü. Korkmaz*, Kuheli Dutta*, Peter König†‡, Ian Lewkowich§, George S. Deepe, Jrß, Rabih HalwaniX, Christian Sina&, Jörg Köhl*§‡, Yves Laumonnier*‡&. De novo expression of C3aR by alveolar macrophages regulates the production of AM-dependent IFNa in an experimental model of allergic asthma. **In preparation.**

Author's Biographical Sketch

Bushra Ahmed Mdkhana

Ph.D. candidate in Molecular Medicine and Translational Research dual-degree program between University of Sharjah and University of Lubeck.

+971529626246

bmdkhana@sharjah.ac.ae

Education

September 2019 - present	Ph.D. candidate in Molecular Medicine and Translational Research dual-degree program between University of Sharjah in United Arab Emirate and University of Lubeck in Germany. **Thesis Title:** Inhibiting DNA Sensing Pathway to Control Steroid Resistant Lung Inflammation.
September 2017 - May 2019	M.Sc. in Molecular Medicine and Translational Research, College of Medicine, University of Sharjah, Sharjah, United Arab Emirate. **Thesis Title:** Sensitizing Breast Cancer to Energy Restriction Using Potential Synergistic Combinations.
September 2012 - May 2017	B.Sc. in Pharmacy, College of Pharmacy, University of Sharjah, Sharjah, United Arab Emirates. **Project Title:** Development and validation of ultra-performance liquid chromatographic method with tandem mass spectrometry for determination of Doxorubicin human plasma.

Professional Experience

- Research Assistant PhD scholarship in **Tissue Injury and Repair Group** in Research Institute of Medical & Health Sciences (RIHMS) at University of Sharjah, Sharjah, United Arab Emirates – September 2019 to present.
- Research Assistant M.Sc. scholarship in **Drug Design and Discovery Group** in Research Institute of Medical & Health Sciences (RIHMS) at University of Sharjah, Sharjah, United Arab Emirates – September 2018 to August 2019

Experimental/Research Skills

- Inflammatory mouse models: HDM/cdiGMP, and Ova mice models.
- Routes of administration in mouse: intraperitoneal injection (i.p.), intranasal drops (i.n.) and nebulization.
- Euthanize mouse: Cervical dislocation, cardiac puncture, and CO_2 exposure.
- Assessment of airway function: FlexiVent (SCIREQ, Montreal, Quebec, Canada).
- 2D Cell Culturing: primary cells (patient derived bronchial fibroblasts and murine alveolar macrophages) and cancerous cells (breast cancer cells)
- Knockdown techniques: small interference RNA (siRNA) technique.
- Protein and RNA techniques: Western blot, PCR, and qRT-PCR.
- Extraction techniques: RNA extraction, and protein extraction.
- Luminescence techniques: ROS assay, and CellTiter-Glo
- Functional assay: MTT assay
- Invasion assay: Wound healing assay
- Flow cytometry techniques: Cell cycle, Annexin/PI assays, cell sorting and flow.
- Tissue stains: Hematoxylin and eosin (H&E) stain and Periodic Acid-Schiff (PAS) stain
- Imaging techniques: Confocal microcopy, and immunofluorescence.
- Drug delivery: Polymeric nano-particles fabrication and characterization.
- Experienced in Graph Pad Prism, CalcuSyn, Image lab, FlowJo and Image J programs.

Certificates

o MOH licensed Pharmacist.

o Dean's list for academic excellence during bachelor's degree (2013 - 2017), and master's degree (2018 – 2019) at University of Sharjah, Sharjah, United Arab Emirates.

o SANID (Arabic for 'Support' is National Emergency Response Volunteer Program of the UAE): 1st, 2nd, 3rd levels and children safety in 2015.

Poster Presentation

- **Bushra Mdkhana,** Narjes Saheb Sharif-Askari, Rakhee K. Ramakrishnan, Baraa Khalid Al-Sheakly, Fatemeh Saheb Sharif-Askari, Khuloud Bajbouj, Qutayba Hamid, Rabih Halwani. Nucleic Acid Sensor STING Drives Fibrosis and its Inhibition Enhances Steroid Responsiveness in Chronic Obstructive Pulmonary Disease. **Your Gateway to Research**. University of Sharjah, Sharjah, United Arab Emirates. 2022.
- **Bushra Mdkhana**, Ruba Zenati, Omayma Hawari, Shirin Audeh. Diet pills losing health and weight. **First future pharmacist day**. University of Sharjah, Sharjah, United Arab Emirates. 2017- Award 2nd best poster presentation.

- **Bushra Mdkhana**, Ruba Zenati, Omayma Hawari, Shirin Audeh. Diet pills losing health and weight. **DUPHAT**: Dubai International Pharmaceuticals & Technologies. Dubai, United Arab Emirates. 2017.
- **Bushra Mdkhana**, Ruba Zenati, Omayma Hawari, Shirin Audeh. General awareness. **Scientific day**. University of Sharjah, Sharjah, United Arab Emirates. 2015.

Conference Presentation

- **Bushra Mdkhana,** Narjes Saheb Sharif-Askari, Rakhee K. Ramakrishnan, Baraa Khalid Al-Sheakly, Fatemeh Saheb Sharif-Askari, Khuloud Bajbouj, Qutayba Hamid, Rabih Halwani. Nucleic Acid Sensor STING Drives Fibrosis and its Inhibition Enhances Steroid Responsiveness in Chronic Obstructive Pulmonary Disease. **DUPHAT**: Dubai International Pharmaceuticals & Technologies. Dubai, United Arab Emirates. 2022.
- **Bushra Mdkhana,** Narjes Saheb Sharif-Askari, Rakhee K. Ramakrishnan, Baraa Khalid Al-Sheakly, Fatemeh Saheb Sharif-Askari, Khuloud Bajbouj, Qutayba Hamid, Rabih Halwani. Nucleic Acid Sensor STING Drives Fibrosis and its Inhibition Enhances Steroid Responsiveness in Chronic Obstructive Pulmonary Disease. **The 9th Emirati German Congress of Medicine and Dental Medicine.** University of Sharjah, Sharjah, United Arab Emirates. 2022.

Publication

1. **Bushra Mdkhana**, Narjes Saheb Sharif-Askari, Rakhee K Ramakrishnan, Swati Goel, Qutayba Hamid, Rabih Halwani. Nucleic Acid-Sensing Pathways During SARS-CoV-2 Infection: Expectations versus Reality. **J Inflamm Res.** 2021; 14:199-216. DOI: 10.2147/JIR.S277716.
2. **Bushra Mdkhana**, Swati Goel, Mohamed A Saleh, Ruqaiyyah Siddiqui, Naveed Ahmed Khan, Adel B Elmoselhi. Role of oxidative stress in angiogenesis and the therapeutic potential of antioxidants in breast cancer. **Eur Rev Med Pharmacol Sci.** 2022; 26(13):4677-92. DOI: 10.26355/eurrev_202207_29192.
3. **Bushra Mdkhana**, Dana M. Zaher, Shifaa M. Abdin, Hany A. Omar. Tangeretin boosts the anticancer activity of metformin in breast cancer cells via curbing the energy production. **Phytomedicine.** 2021; 83:153470. DOI: 10.1016/j.phymed.2021.153470.
4. Narjes Saheb Sharif-Askari, Mashael Alabed, Balachandar Selvakumar, **Bushra Mdkhana**, Ola Salam Bayram, Zaina Kalaji, Shirin Hafezi, Noha M Elemam, Fatemeh Saheb Sharif-Askari, Rabih Halwani. Simvastatin reduced infiltration of memory subsets of T lymphocytes in the lung tissue during Th2 allergic inflammation. **International Immunopharmacology.** 2022, 113: 109347. DOI: 10.1016/j.intimp.2022.109347

5. Fatemeh Saheb Sharif-Askari, Shirin Hafezi, Narjes Saheb Sharif-Askaria, Hawra Ali Hussain Alsayed, **Bushra Mdkhana,** Balachandar Selvakumara, Mohamad-Hani Temsah Basema Saddik, Fatme Al Anouti, Rabih Halwani. Vitamin D modulates systemic inflammation in patients with severe COVID-19. **Life Sciences.** 2022; 307:120909. DOI: 10.1016/j.lfs.2022.120909

6. Fatemeh Saheb Sharif-Askari, Narjes Saheb Sharif-Askari, Shirin Hafezi, **Bushra Mdkhana,** Hawra Ali Hussain Alsayed, Abdul Wahid Ansari, Bassam Mahboub, Adel M Zakeri, Mohamad-Hani Temsah, Walid Zahir, Qutayba Hamid, Rabih Halwani. Interleukin-17, a salivary biomarker for COVID-19 severity. **PloS one.** 2022; 17(9): e0274841. DOI: 10.1371/journal.pone.0274841.

7. Bariaa A. Khalil, Sarra B. Shakartalla, Swati Goel, **Bushra Madkhana,** Rabih Halwani, Azzam A. Maghazachi, Habiba AlSafar, Basem Al-Omari, Mohammad T. Al Bataineh. Immune Profiling of COVID-19 in Correlation with SARS and MERS. **Viruses.** 2022; 14(1):164. DOI: 10.3390/v14010164.

8. Mashael Alabed, Asma Sultana Shaik, Narjes Saheb Sharif-Askari, Fatemeh Saheb Sharif-Askari, Shirin Hafezi, **Bushra Mdkhana,** Elaref Ratemi, Saleh Al-Muhsen, Qutayba Hamid, Rabih Halwani. Enhanced Infiltration of Central Memory T Cells to the Lung Tissue during Allergic Lung Inflammation. **Int Arch Allergy Immunol.** 2021; 1-15. DOI: 10.1159/000518835.

9. Narjes Saheb Sharif-Askari, Fatemeh Saheb Sharif-Askari, **Bushra Mdkhana,** Hawra Ali Hussain Alsayed, Habiba Alsafar, Zeyad Faoor Alrais, Qutayba Hamid, Rabih Halwani. Upregulation of oxidative stress gene markers during SARS-COV-2 viral infection. **Free Radic Biol Med.** 2021; 172:688-698. DOI: 10.1016/j.freeradbiomed.2021.06.018.

10. Narjes Saheb Sharif-Askari, Fatemeh Saheb Sharif-Askari, **Bushra Mdkhana,** Saba Al Heialy, Habiba S. Alsafar, Rifat Hamoudi, Qutayba Hamid, Rabih Halwani. Enhanced expression of immune checkpoint receptors during SARS-CoV-2 viral infection. **Molecular Therapy - Methods & Clinical Development.** 2021; 20:109-21. DOI: 10.1016/j.omtm.2020.11.002.

11. Swati Goel, Fatemeh Saheb Sharif-Askari, Narjes Saheb Sharif-Askari, **Bushra Madkhana,** Bassam Mahboub, Adel M. Zakri, Elaref Ratemi, Qutayba Hamid, and Rabih Halwani. SARS-CoV-2 Switches 'on' MAPK and NFkB signaling via the reduction of nuclear DUSP1 and DUSP5 expression. **Frontiers in pharmacology.** 2021; 12:404. DOI: 10.3389/fphar.2021.631879.

12. Narjes Saheb Sharif-Askari, Fatemeh Saheb Sharif-Askari, **Bushra Mdkhana,** Saba Al Heialy, Elaref Ratemi, Malak Alghamdi, Salah Abusnana, Tarek Kashour, Qutayba Hamid, Rabih Halwani. Effect of common medications on the expression of SARS-CoV-2 entry receptors in liver tissue. **Archives of Toxicology.** 2020; 94(12):4037-41. DOI: 10.1007/s00204-020-02869-1.